Charles University in Prague
2nd Faculty of Medicine

Field of study: Medical Biophysics

Mgr. Eva Prosecká

Development of Scaffolds for Bone Defects Regeneration

Vývoj scaffoldů pro regeneraci kostních defektů

PhD Thesis

Supervisor: Prof. RNDr. Evžen Amler, CSc.

Prague, 2014

Statement of originality:

I hereby declare that this thesis and the work reported herein was composed by and originated entirely from me. This thesis has not been submitted for any degree or other purposes. Information derived from the published and unpublished work of others has been acknowledged in the text and references are given in the list of sources.

I agree with prolonged accumulation of an electronic version of my work in the Theses.cz interuniversity database system project for the purposes of systematic checks on similarities among theses.

Prague

Eva Prosecká

Identifikační záznam:

PROSECKÁ, Eva. *Vývoj scaffoldů pro regeneraci kostních defektů (Development of Scaffolds for Bone Defects Regeneration).* Praha, 2014, 116 S., 3 příl. Disertační práce (Ph.D.). Univerzita Karlova v Praze, 2. Lékařská fakulta, Ústav biofyziky. Vedoucí práce Amler, Evžen.

Key words: Bone Tissue Engineering, Collagen/Hydroxyapatite 3D scaffold, Mesenchymal stem cells, Pore size, Nanofibers, Platelet Rich Plasma, Drug delivery.

Klíčová slova: Kostní tkáňové inženýrství, Kolagen/hydroxyapatitový 3D scaffold, Mesenchymální kmenové buňky, Velikost pórů, Nanovlákna, Plasma bohatá na trombocyty, Dodávání léčiv/bioaktivních molekul.

First of all, I would like to express my gratitude to my supervisor, Prof. RNDr. Evžen Amler, CSc., for his kind and valuable advice and for many suggestions concerning my experimental work and the writing of this manuscript.

I would like to thank the Institute of Biophysics, 2nd Faculty of Medicine, Charles University in Prague and the Institute of Experimental Medicine of the Academy of Sciences of the Czech Republic (IEM ASCR), with whose support and under whose supervision it was possible to carry out all the experiments that have formed a central part of this doctoral thesis.

I appreciate the kind help of my colleagues from (IEM ASCR), Mgr. Michala Rampichová, PhD, Mgr. Eva Filová, PhD, Mgr. Martin Plencner, Mgr. Andrea Míčková, MUDr. Ing. Karolína Vocetková, Mgr. Jana Benešová, Mgr. Věra Sovková and Mgr. Matej Buzgo. My thanks also belong to Ing. Lucy Vojtová, PhD for preparing the collagen/ hydroxyapatite scaffolds and to MVDr. Andrej Litvinec, PhD for the operations on animals, Doc. MUDr. Mgr. Zbyněk Tonar, PhD and Doc. MUDr. Milena Králíčková, PhD for their great work in the histological analyses, and to Ing. Petra Kochová, PhD for finding appropriate methods for measuring the mechanical properties of the scaffolds. I would also like to thank MVDr. Jana Hlučilová, PhD and all of the researchers at the Institute of Animal Physiology and Genetics ASCR in Liběchov for their kindness in harvesting mesenchymal stem cells.

I am grateful to my reviewers and opponents for revising my thesis and for their comments.

I owe a great debt of gratitude to my family and friends for their support throughout all my studies.

List of Abbreviations

2D	2- dimensional
3D	3- dimensional
BCECF-AM	Bis(2-carboxyethyl)-5(6)-carboxyfluorescein acetoxymethyl ester
bFGF	Basic fibroblast growth factor
BMP	Bone morphogenic protein
Cbfa1	Core binding factor alpha 1
Col 0.5/ HA 70	70% HA with 0.5% collagen (1:1 wt%)
Col 0.5/HA 40	40% HA with 0.5% collagen (1:1 wt%)
Col 0.5/HA 50	50% HA with 0.5% collagen (1:1 wt%)
Col 0.5/HA 60	60% HA with 0.5% collagen (1:1 wt%)
Col 1.0/HA 50	50% HA with 1.0% collagen (1:1 wt%)
Col 1.5/HA 50	50% HA with 1.5% collagen (1:1 wt%)
Col 2.0/HA 50	50% HA with 2.0% collagen (1:1 wt%)
Coll/HA	50% HA with 0.5% collagen (1:1 wt%)
Coll/HA/PCL	50% HA with 0.5% collagen (1:1 wt%) + Polycaprolactone nanofibers
CT	Computer-aided tomography
CTGF	Connective tissue growth factor
DBM	Demineralized bone matrix
DiOC6	3,3-diethyloxacarbocyanine iodide
ECM	Extracellular matrix
EDC	N-(3-dimethylamino propyl)-N’-ethylcarbodiimide hydrochloride
EGF	Epidermal growth factor
FBS	Fetal bovine serum
FEA	Finite Element Analysis

FGF	Fibroblast growth factor
HA	Hydroxyapatite
ID	Inhibitor of DNA binding
IGF	Insulin-like growth factor
IL-1	Interleukin-1
IL-8	Interleukin-8
MEM	Minimum Essential Media
MSCs	Mesenchymal stem cells
MTT	[3-(4,5- dimethylthiazol-2-yl)-2,5-diphenyl-2H-tetrazolium bromide]
NHS	N-hydroxysuccinimide
PBS	Phosphate-buffered saline
PCL	Poly(ε-caprolactone)
PCL/PVA	Polycaprolactone/Polyvinyl alcohol core-shell nanofibers
PCL/PVA200HA	Polycaprolactone/Polyvinyl alcohol core-shell nanofibers with 200 um Hydroxyapatite films
PCL/PVA400HA	Polycaprolactone/Polyvinyl alcohol core-shell nanofibers with 400 um Hydroxyapatite films
PCL/PVA800HA	Polycaprolactone/Polyvinyl alcohol core-shell nanofibers with 800 um Hydroxyapatite films
real- time PCR	Quantitative real- time polymerase chain reaction
PDGF	Platelet-derived growth factor
PGK	Phosphogycerate kinase
PGK	Phosphogycerate kinase
PLA	Poly (lactic acid)
PLCL	Poly(L-lactide-co-ε-caprolactone)
PLD	Pulsed laser deposition
PLGA	Polylactide-co-glycolide

PPF	Poly(propylene fumarate)
PRP	Platelet-rich plasma
PVA	Polyvinyl alcohol
RunX2	Runt related transcription factor 2
SD	Mean/standard deviation
SDS	Sodium dodecyl sulfate
SEM	Scanning electron microscope
TGF-β	Transforming growth factor β
TGF-β1	Transforming growth factor-β1
TGF-β2	Transforming growth factor-β2
TRS	Thrombocyte-rich solution
VEGF	Vascular endothelial growth factor

Contents

1. Introduction

In comparison with other tissues, bone has a robust healing capacity. However, large bone defects regenerate only to a limited extent, and it remains a substantial therapeutic challenge to deal with this issue (Zhang *et al.* 2012). Critical bone defects observed in a variety of conditions, e.g. acute injuries, major fractures, hip implant revision, fall fractures in osteoporotic patients, and tumours all require resection of the affected bone. After removal of the bone, autograft or allograft bone tissue and prosthetic implants are commonly implanted. However, these methods have several limitations, including patient pain, the risk of an immune reaction, disease transmission, and a non-optimal interaction between the body and the implanted materials (Pearce *et al.* 2007; Tu *et al.* 2009). Bone tissue engineering is a promising novel discipline dealing with ways to bridge a bone defect with healing procedures that are stable and durable, and that do not introduce any new problems or complications (Bose *et al.* 2012; Hutmacher 2000).

1.1. Bone composition

Bone is a composite material consisting of collagen (17–20 wt.%) stiffened by an extremely dense filling and surrounded by calcium phosphate $Ca_{10}(PO_4)_6(OH)_2$ crystals of hydroxyapatite (HA) (69–80 wt%), and other components, notably water, proteins and polysaccharides, living cells and blood vessels (Currey 2012; Ferreira *et al.* 2012; Marks and Odgren 2002). HA crystals are precipitated on the surface of the nanofibrils of type I collagen (Currey 2012). Apatite compounds in natural bone are needle-like or rod-like in shape, 40–60 nm in length, 10–20 nm in width, and 1–3 nm

in thickness (Abdal-hay *et al.* 2013). The outer surface of the bone is organized into a dense fibrous layer called the periosteum. The inner surface of the bone, including the inner surface of the trabeculae of cancellous bone, is lined with a delicate layer called endosteum. Cells of a different type are found in periosteum and in endosteum. All of them play an important role in the formation of bone tissue. The main types of cells include osteoblasts, osteocytes and osteoclasts. Osteoblasts are derived from osteoprogenitor cells. These cells are originated from mesenchymal stem cells (MSCs). Osteoblasts secrete type I collagen and some non-collagenous proteins, such as osteocalcin (OC), bone sialoprotein and osteopontin. Osteoblasts also promote the process of mineralization, which is thought to be initiated by the matrix vesicles that build from the plasma membrane of osteoblasts to create an environment for the concentration of calcium and phosphate, allowing crystallization (Höhling *et al.* 1978). Collagen serves as a template, and may also initiate and propagate mineralization independent of the matrix vesicles (Mackie 2003). Osteocytes are cells of fully-formed bone. Osteocytes originate from osteoblasts, and are located in small chambers called lacunae, which consist of products secreted by osteoblasts. Cytoplasmic processes of communication between osteocytes take place via small channels called canaliculi. Nutrients and waste products are exchanged through these channels. Osteocytes are also involved in bone remodeling, which is influenced by muscle activity. Osteocytes provide alerts to increase muscle activity by signaling to other osteocytes, and start the whole process of transforming the bone tissue in response to the load. For example, bone becomes compacted and stronger with frequent physical exertion or exercise, and becomes weaker with inactivity or a low level of physical activity.

Osteoclasts are large branched bone cells which are capable of movement. Osteoclasts are multinucleated cells, mostly with up to 50 nuclei. Their origin is still not completely clear. Scientists initially thought that osteoclasts have the same origin as other bone cells, but recent studies have suggested that they originate from monocytes, apparently by merging several of these cells. The main function of osteoclasts is to degrade the bone mass using various collagenases and other enzymes that produce hydrogen ions and cause degradation of calcium crystals. The activity of osteoclasts is tightly regulated by various cytokines and hormones, and also by parathyroid hormone and calcitonin (Young *et al.* 2013).

1.1.1. Two forms of bone that can be found in the human body

Woven bone – this is an immature form with randomly arranged collagen fibers in the osteoid. Woven bone is formed when osteoblasts produce osteoid rapidly, as in fetal development, and in adult bone when pathologically rapid formation of new bone occurs, e.g. in fracture healing. The rapidly formed woven bone is eventually remodeled to form lamellar bone, which is physically stronger and more resilient. Virtually all bones in a healthy adult are lamellar.

Lamellar bone – this is composed of regular parallel bands of collagen arranged in sheets.

Two forms of lamellar bone are known:

Compact bone – this is composed of parallel bony columns which, in long bones, are disposed parallel to the long axis, i.e. in the line of stress exerted on the bone. Each column is formed from concentric bony layers or lamellae arranged around a central channel containing blood vessels, lymphatics and nerves. These neurovascular channels are known as Haversian canals, and together with their concentric lamellae

they form Haversian systems. Neurovascular bundles interconnect between themselves and also with the endosteum and periosteum through Volmann channels, which pierce the columns at right angles to the Haversian canals. Every Haversian system (osteon) develops by osteoclasts tunneling solid bone mass to form a broad channel in which blood vessels and nerves grow. It subsequently becomes internally lined with active osteoblasts, which provide a concentric lamellar bone.

Trabecular (cancellous) bone is a network of interconnecting trabecules orientated in a position to provide maximum strength for minimum mass. Trabeculae have a thin external layer of endosteum containing flat inactive osteoblasts. They are composed of lammelar bone with scanty lacunae containing osteocytes. These spaces exchange metabolites via canaliculi, which communicate with each other and with blood sinusoids in the haematopoietic (red) marrow spaces.

For most bones, we can determine a thick rigid outer shell of compact bone, the cortex, and a central medullary or cancellous zone of thin interconnecting narrow bone trabeculae. The number, thickness and orientation of the trabecular bone depends on the stress to which a particular bone is exposed. For example, there are many thick intersecting trabeculae in the constantly weight-bearing vertebrae, but very few in the centre of the ribs, which are not subjected to constant stress (Young *et al.* 2013).

1.1.2. Types of bones

Long bones – these are the bones of the extremities. The middle part of the bone is called the diaphysis, and the two ends of the bones are called the epiphysis. The external surface of the bone is enveloped in a dense fibrous layer called the periosteum, into which muscles, tendons and ligaments are inserted. The articular

surfaces of the epiphyses of long bones are protected by a layer of specialized hyaline cartilage, called articular cartilage. In the middle of the bone there is a pulp cavity, which in adulthood is filled with yellow bone marrow. Lengthening of the long bones by the process of endochondral ossification occurs at a epiphyseal plate situated at each end of the bone at the junction of the diaphysis and the epiphysis (for example the femur).

Short bone – the structure is no different from that of the long bones, but all the dimensions are approximately the same. For example, vertebrae.

Flat bone - on the outer and inner parts, flat bone has compact bone of different strengths, filled with cancellous bone with large trabeculae. Well into old age, the spaces are filled with red bone marrow (for example, shoulders, ribs and the pelvis) (Young *et al.* 2013).

1.1.3. Bone repair and remodeling

Bone regeneration is a complex of physiological processes of bone induction and conduction, involving several following stages with a numerous cell types and intracellular and extracellular molecular-signalling pathways (Dimitriou *et al.* 2011).

At the bone healing site, a blood clot first forms. During bone fracture integrity of bone tissue is damaged associated with rupture of blood vessels. The blood flowing into the site of injury forms hematoma (Kolar *et al.* 2010). Platelets activate coagulation cascade and mediate fibrin clot formation and provide hemostasis (Figure 1). They also stimulate inflamantation process by interaction with immune cells (May *et al.* 2008) and secretion of numerous growth factors (Karshovska *et al.* 2013). Growth factors bind to the cell surface and stimulate cell proliferation and differentiation. Main growth factors present in bone regeneration include basic

fibroblast growth factor (bFGF) which stimulates mesenchymal stem cell proliferation and maintain their differentiation potential (Ahn *et al.* 2009). Bone morphogenic proteins (BMPs) which play crucial role during early phases of osteogenic differentiation. Proosteogenic BMPs promote expression of early osteogenic markers (e.g. connective tissue growth factor (CTGF), inhibitor of DNA binding (ID) and Core binding factor alpha 1(Cbfa1)/Runt related transcription factor 2 (RunX2) in MSCs and stimulate their proliferation (Mehta *et al.* 2012). Among the most prominent proosteogenic BMPs we include BMP-2 and BMP-7. In addition, insulin-like growth factor – I (IGF-I), an antiapoptotic growth factor, also plays an important role in osteogenic differentiation of MSCs. The combination of rapid growth factor production and hypoxic conditions in the site of injury stimulate angiogenesis, which facilitates better distribution of nutrients, oxygen, pro-healing factors and exchange of waste products. Beside inflamantory and pro-angiogenetic role, the secreted cytokines and chemokines also stimulate activation and migration of progenitor cells. MSCs then differentiate into chondroblasts and progressively replace the fibrous granulation tissue with hyaline cartilage. This bridge, which is still flexible, is known as a provisional callus. The provisional callus then has calcium salts deposited within the cartilage matrix. Meanwhile, activated osteoprogenitor cells in the endosteum and periosteum lay down a meshwork of woven bone within and around the provisional callus. The provisional callus is transformed into a bony callus. Bony union is completed when the fracture site is fully bridged by woven bone. The remodelling of the bony callus to form mature lamellar bone is dependent on functional stresses (Pivonka *et al.* 2008).

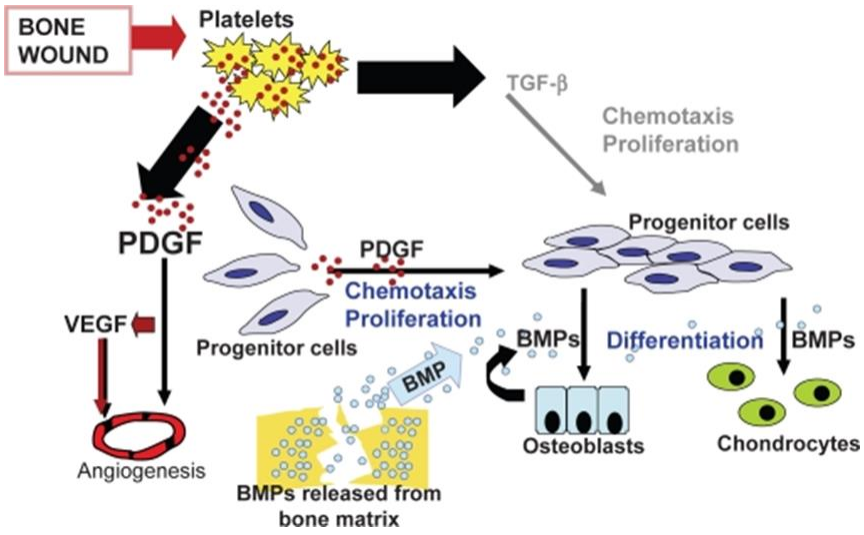

Figure 1: Cell signalling and cell proliferation during wound healing cascade. PDGF, VEGF, and TGF play integral role in the cell migration. BMP releasing from the bone matrix play key role during early phases of osteogenic differentiation into osteoblast and chondrocytes (Hollinger *et al.*, 2008).

In the first year of life, the rate of turnover of the skeleton approaches 100% per year. The rate declines to about 10% per year in late childhood, and then usually continues at approximately this rate, or more slowly, throughout life, up to the age of a hundred years. After skeletal growth has been completed, bone turnover results primarily from remodeling. Remodeling is a coordinated cycle of tissue resorption and formation over extensive regions of bone and over prolonged periods. Physiological remodeling, removal and replacement of bone, at the same location, without affecting the shape or the density of the bone, through a sequence of events, is a process that includes osteoclast activation, bone resorption, osteoblast activation and also the formation of new bone at the resorption site (Figure 2) (Pivonka *et al.* 2008).

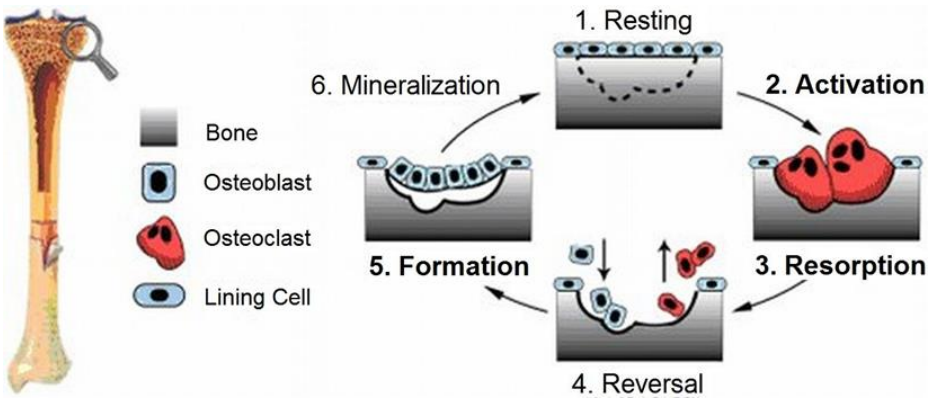

Figure 2: Bone tissue adaption by basic multicellular units executing bone remodelling (Pivonka *et al.*, 2008).

1.1.4. Mechanical properties of bone

The combination of hard inorganic components and resilient organic components results in the excellent mechanical properties of bones. It is fascinating that compact bone specimens have tensile strength in the range of 700 to 1400 kg/cm^2, and compressive strength in the range of 1400 to 2100 kg/cm^2, which is the same magnitude as for aluminum or mild steel, but bone is much lighter. However, bones are characterized not only by significant stiffness. Stiffness, defined by initial modulus of elasticity in pressure. Initial modulus is the slope of the stress-strain curve between strain 2-10%), defines the edurance of material to the pressure loading. In other words, the high value of stiffness (modulus) is related to the high edurance of material to pressure, the low value of stiffness is related to the low edurance of material to pressure. The same value of pressure deforms more the material with low stiffness when compared with high stiffness material.but also by a high degree of elasticity, which is important for the ability of the skeleton to withstand mechanical stresses. Estimates of the modulus of elasticity of bone samples are of the order of 420 to 700 kg/ cm^2. These are much lower than the values for steel. The great

strength of bone is principally along its axis, and is therefor roughly parallel both to the axis of the collagen fiber and to the long axis of the mineral crystals (Young 2013).

1.1.1.1. Methods for measuring the biomechanical properties of bone

From the point of view of its structure, bone is a very complex, anisotropic material. Here we find structures with macro, micro and nano dimensions. Therefore, there are many approaches for investigating and understanding the mechanical properties of bone. The greatest advances over old methods have probably been achieved with the use of ultrasonic measurements. After some disputes, it is now considered that this method is suitable for distinguishing between different types of bone from a histological point of view (Malik *et al.* 2003). Fatigue tests are another approach, which is now often applied using a calculation with the Young's modulus. These methods work well for materials with a smooth surface and an isotropic structure, but they are not fully functional in measuring the properties of materials such as bone. Real bones have complicated shapes, rough surfaces, and are more or less tough. Fracture mechanics has developed a method that can deal with these problems. The method attempts to characterize the tendency of a material to fracture as a material property, independent of the geometry of the specimen. It also attempts to determine how the actual geometry of the specimen, including the presence of flaws, will affect the fracture behavior. An interesting recent development is the concept of the ‘‘R-curve’’ (Oliver and Pharr 1992).

Oliver and Pharr (2004) described nanoindentation, a method that has recently become widely used for determining the Young’s modulus of very small parts of materials. Nanoindentation involves pressing a tiny probe onto the bony surface and

simultaneously measuring the load and the deformation. Finite Element Analysis (FEA) is one of the most widely used engineering analysis techniques in the world today. It originated in the 1970s, when powerful computers began to be widely available. FEA is a computer method for determining the strains in loaded models. FEA programs range from those that allow only two Young's moduli in the whole system, and assume that the bone material is isotropic, to those that allow many Young's moduli, anisotropy, etc. FEA is particularly useful for determining the strains in bones of complex shapes, like skulls and cancellous bone. In the ideal case, we can take a shape, digitize it in some way, turn it into an FEA model, attribute elastic material properties to each element, load the model with any loading, and see the distribution of strains produced in the model. Computer-aided tomography (CT) was a technological advance that enabled FEA to progress greatly in studies of bone. In micro-CT, the specimen is scanned in virtual slices with an x-ray beam, and an algorithm allows the density of various parts of the object to be calculated. The slices are then amalgamated to produce a 3- dimensional (3D) density image of the object. Each part of the object has both its density and its 3D position rendered objectively in numbers, and this data can be turned, almost directly, into an FEA model (Currey 2012). Interferometry (ESPI, or electronic speckle pattern interferometry) is another method that can measure extremely small displacements, but extensive statistical techniques must be used to determine strains (Zaslansky *et al.* 2006).

1.2. Current treatments for bone defects

Under physiological conditions of the remodeling process, bone is able to repair itself until there is a defect of a critical size. Situations where the critical size is exceeded result mostly from trauma, congenital abnormities, infection or tumor resection.

Schmitz and Hollinger (1986) defined critical defects for animals as a defect of a size that will not heal during the lifetime of the animal. For large defects, human interventions are necessary in order to help or stimulate the healing process (Barrere *et al.* 2006).

The introduction of bone banks and the development of standards in bone transplantation raised the false hope that a final solution to the treatment of bone loss had been found. However, the use of allografts is unsatisfactory, due to negative effects such as allergic reactions, rejection reactions, inflammation and other problems. The current standard treatment for damaged tissue is an autograft tissue transplant. The material is usually harvested from the iliac crest, the distal femur or the greater trochanter. The proximal tibia can also be used (Perry 1999).

However, this method has several limitations including patient pain, morbidity at the harvesting site, and limited availability (Hutmacher 2007).

Xenografts acquired from animal bone offer another option. However, the morphology of the bone is different from that of human bone, and there is a risk of cross-species infection (de la Caffiniere *et al.* 1998). At the present time, well-established substitutes are demineralized bone matrix (DBM), composites and calcium phosphates (hydroxy apatite and tri-calcium phosphate). These substances are widely used for their osteoconductive properties, and have been shown to improve the formation of new bone. Although clinical application of these materials has been successful where there are favorable bone health conditions, it is not effective for large and critical bone defects (Schlickewei and Schlickewei 2007).

For regenerating critical bone defects, a promising future lies in improving of our knowledge about bone healing, osteoconductive and osteoinductive materials, and stem cell biology (Hutmacher 2000).

1.3. Bone Tissue Engineering

Better knowledge in material science and technologies, and also in the area of MSCs and bioactive molecules has led to new opportunities in the treatment of large bone defects. Current approaches involve a combination of osteoconductive, osteoinductive and osteogenetic substances, in a biocompatible, bioresorbable, and cost-effective bone graft substitute to enhance the advantages and reduce the disadvantages of the concepts.

The term “tissue engineering” first appeared in the literature in the mid 1980s with reference to surgical manipulation of tissues and organs or, in a broader sense, when prosthetic devices or biomaterials were used. The term “tissue engineering”, as it is used nowadays, was introduced into medicine in 1987. The agreed definition was: “Tissue engineering is the application of the principles and methods of engineering and life sciences toward the fundamental understanding of structure and function relationships in normal and pathologic mammalian tissue and the development of biological substitutes to restore, maintain, or improve function.” The early years of tissue engineering were based on cell and tissue culture approaches (Vacanti 2010; Vacanti and Langer 1999).

Tissue engineering has been considered one of the most promising biomedical technologies of the 21st century, since the time when the BBC showed photos of the “mouse with a human ear”, which originated in the laboratory of Dr. Charles Vacanti from the University of Massachusetts Medical School, published in 1997 (Cao *et al.* 1997). This work catapulted tissue engineering to the attention of the research world and also to attention of the general public.

One of the current strategies is to harvest stem cells from a patient, expand them in a cell culture, and seed them on to a scaffold. Current challenges in tissue engineering are how to optimize the isolation, proliferation and differentiation of cells, and how to develop osteoconductive and osteoinductive scaffolds. When given specific biological stimuli, stem cells can develop into many types of specific mature cells via a process called cell differentiation.The scaffold should then support proliferation and differentiation of stem cells into the specific cells that will generate specific new tissue. The new tissue should grow on a scaffold that will gradually be completely resorbed as the new tissue grows. After implantation, the tissue-engineered construct must be able to survive, restore normal function, e.g. biochemistry, mechanical integrity and structural integrity, and integrate with the surrounding tissues. In addition, the use of autologous cells eliminates the problem of immunorejection that can occur with transplants from donors (Boccaccini 2005).

1.3.1. Bone tissue engineering scaffolds

An ideal scaffold should meet the critical parameters needed for bone regeneration, e. g. appropriate mechanical, structural, chemical and surface properties. It should be biocompatible, biodegradable at a rate adequate for the remodelling of the bone, and also osteoconductive and osteoinductive (Hutmacher 2007; Karageorgiou and Kaplan 2005).

A *biocompatible* scaffold has a positive influence on cellular activity, facilitating molecular and mechanical signalling systems to optimise tissue regeneration, without eliciting any undesirable effects in those cells, and without inducing any undesirable local or systemic responses in the eventual host.

Biodegradable materials are solid polymeric materials which break down due to macromolecular degradation and are dispersed *in vivo* , but it is important to ensure that they remove themselves safely from the body after they are dispersed. The mass loss is accompanied by an increase in acidic byproducts. Massive release of acidic degradation and respiration byproducts can result in inflammatory reactions *in vivo*.

Osteoconductive materials stimulate the growth of bone tissue on the implant surface.

An *osteoinductive* material stimulates osteoprogenitor cells to differentiate into osteoblasts, which then initiate new bone formation.

An osteoinductive and osteoconductive scaffold will serve as a scaffold for existing osteoblasts as well as trigger the formation of new osteoblasts and promote faster integration of the graft (Boccaccini 2005; Hutmacher 2007; Karageorgiou and Kaplan 2005).

1.3.1.1. Materials and fabrication methods for bone tissue scaffolds

Increasing knowledge about polymers has led to new opportunities with materials and also in fabricating suitable scaffolds for tissue engineering.

Several biomaterials, including bioceramics, biopolymers, metals and composites, have been described as suitable materials for bone tissue engineering scaffolds (Bose *et al.* 2012; Dawson and Oreffo 2008; Hutmacher 2000; Karageorgiou and Kaplan 2005). Natural polymers (e.g. collagen, alginate, chitosan, hyaluronic acid, fibrin, silk fibroin) have a great advantage because of their biocompatibility and biodegradability, and because of their basic original function as the structural materials of tissues. However, they have low mechanical strength and high rates of degradation, so they have to be used in composites, or to be chemically modified by

cross-linking (Hutmacher 2007). High producibility, controlled reproducibility and low cost are major advantages of synthetic polymers (e.g. poly(ε-caprolactone) (PCL), poly(lactic-co-glycolic acid) (PLGA), poly(L-lactide-co-ε-caprolactone) (PLCL), polyurethanes) (Bose *et al.* 2012; Hutmacher 2000; Karageorgiou and Kaplan 2005). However, limited biocompatibility and a low rate of biodegradability can be limiting factors for their use.

Brittleness and slow degradation rates are disadvantages associated with ceramic implants, based mainly on HA (Hutmacher 2000).

The disadvantages of any material for osteogenic applications can be overcome by using it in combination with other materials, i.e. by designing a so-called *composite material*. For example, the addition of HA particles into a collagen scaffold improved the mechanical properties of the scaffold (Kim *et al.* 2004; Lickorish *et al.* 2004; Zhao *et al.* 2002). A number of fabrication technologies have been applied to produce 3D polymeric scaffolds with high porosity and a large surface area from biodegradable and bioresorbable materials. Solvent casting, particulate leaching, freeze drying, membrane lamination and melt holding, as well as rapid prototyping technologies, are conventional techniques for fabricating scaffolds fabricated in several structural forms such as hydrogels, porous foams and electrospun nanofibers. The fabrication method and use of polymeric scaffolds for bone tissue engineering has been reviewed by Bose *et al.* (2012) and by Rezwan *et al.* (2006).

The fabrication process influences the properties of the scaffold. For example, Hu *et al.* (2002) observed that a different morphology of the scaffold caused a different amount of water co-solvent content in dioxane. Dioxane contents above 3% (v/v) led to interconnected circular pores, but dioxane contents higher than 7% led to fibrous polymers with poor handling qualities. Increasing the concentration of the polymer

solution led to a smaller pore size and to diminished porosity (Hu *et al.* 2002). O'Brien *et al.* (2004) desribed in their study an influence of freezing rate on pore structure in freezedried collagen scaffolds. Higher polymer molecular weight increased the median pore size and the porosity (Karageorgiou and Kaplan 2005).

An ideal scaffold would not only act as a template for tissue growth and have control resorbability, but should also promote the activity and migration of cells of the tissue for self-regeneration. The scaffold can serve as a delivery system for the controlled release of cell- and gene-stimulating agents. A number of different bioactive substances can be agents of this kind. Bioactive substances could be incorporated into resorbable polymer or hydrogel scaffolds, which would release the substances into the body as the scaffold resorbs. Bioactive glasses and silicon-substituted HA scaffolds could also release silicon and calcium ions in low concentrations. These ions have been found to stimulate seven families of genes in osteoblasts, increasing proliferation and bone extracellular matrix production (Frohbergh *et al.* 2012). Several techniques are used for chemically modifying the surfaces by releasing bioactive molecules such as HA or bioactive glass, for example, plasma-sprayed HA coatings and ion beam sputtering (Yang and Chang 2001; Zyman *et al.* 1994).Heat treatment then needs to be applied to facilitate crystallization of amorphous coated HA to a bioactive crystalline form (Choi *et al.* 2000; Yoshinari *et al.* 1994). However, the very high temperatures that are necessary for crystallization are not favorable for nonmetallic materials, such as polymers and bioactive molecules. Pulsed laser deposition (PLD) can be an alternative technique for HA coating and a more suitable method for non-metallic materials (Prosecka *et al.* 2012).

1.3.1.2. Porosity and pore size

Porosity and pore size, at the macroscopic level and also at the microscopic level, are important morphological properties of a biomaterial scaffold for bone regeneration. They play a critical role in bone formation *in vitro* and *in vivo* (Karageorgiou and Kaplan 2005).

Porosity is defined as the percentage of void space in a solid (Leon 1998), and as a morphological property not dependent on the material. Pores are necessary for bone tissue formation and for integration of the surrounding tissue *in vivo*, because of the migration and proliferation of osteoblasts and mesenchymal cells, and also because of vascularization (Kuboki *et al.* 1998). The most common techniques used for creating porosity in a biomaterial are salt leaching, gas foaming, phase separation, freeze-drying and sintering, depending on the material used to fabricate the scaffold (Kuboki *et al.* 1998).

On the basis of many studies, the minimum pore size required to regenerate mineralized bone is in general considered to be 100 μm, after the study by Hulbert *et al.* (1970). However, subsequent studies have shown better osteogenesis for implants with pores >300 μm (Gotz *et al.* 2004; Kuboki *et al.* 2001; Prosecka *et al.* 2011; Tsuruga *et al.* 1997). Large pores (100–150 and 150–200 μm) showed substantial bone ingrowth. Even pores of smaller size (75–100 μm) resulted in ingrowth of unmineralized osteoma tissue. Smaller pores (10–44 and 44–75 μm) were penetrated only by fibrous tissue (Hulbert *et al.* 1970). These results were correlated with normal Haversian systems that reach an approximate diameter of 100–200 μm (Hulbert *et al.* 1970).

1.3.1.3. Mechanical properties of scaffolds for bone tissue engineering

The mechanical properties of the 3D bone scaffold at the time of implantation should match that of the host tissue as closely as possible (Hollister *et al.* 2005).

The mechanical properties of scaffolds are generally measured by way of their compressive properties. A widely-used method for measuring the mechanical properties of bone scaffolds is via the Young's modulus, also known as the tensile modulus or the elastic modulus, when the Young's modulus is computed by determining the slope of the stress-strain curve along the elastic portion of the deformation (Hou *et al.* 2003; Xiong *et al.* 2002).

1.3.2. Nanofibers in bone tissue engineering

The main reasons why nanofibers are suitable materials for tissue engineering and regenerative medicine are the diameters and the orientation of the fibers, which correlate with the fibers of the extracellular matrix (ECM) (Liao *et al.* 2006; Pham *et al.* 2006). Electrospinning is a recent fiber-forming nanotechnology that enables us to create submicron fibers drawn from polymer solutions and melts by electrical forces. Electrospinning technology can be divided into needle, needleless and core-shell methods (Lukas *et al.* 2009). Electrospun nanofibers are characterized by high porosity and by an abundance of interconnected pores. In addition, nanofibrous scaffolds exhibit a nanotopography with a large surface-to-volume ratio, facilitating cell adhesion and proliferation (Liang *et al.* 2007; Liao *et al.* 2006). Due to this unique property, nanofibrous scaffolds offer numerous contact points for cells. Further advantages of nanofibrous constructs are the versatility of the polymeric materials that are used, and the fact that the surface can be chemically modified. Nanofibers have diameters similar to the diameter of natural extracellular matrix, and they can

be prepared from biocompatible and biodegradable synthetic polymers, e.g. poly (lactic acid) (PLA), PCL, Polyvinyl alcohol (PVA), polyurethanes, or natural polymers, such as chitosan, silk fibroin, collagen, hyaluronic acid and cellulose (Li *et al.* 2005; Liang *et al.* 2007).

Alongside the favourable properties of nanofibers, there are some major limitations to the use of electrospun nanofibers for regenerating critical size defects, due to their insufficient mechanical stiffness and their 2- dimensional (2D) structure. It remains a challenging task to prepare functional 3D nanofiber scaffolds (Rampichova *et al.* 2013).

More promising systems for 3D tissue regeneration involve the use of nanofibers in composite systems, such as polymeric foam/nanofiber composites and hydrogel/nanofiber composites. Albanna *et al.* (2012) used chitosan fibres to improve the mechanical properties of chitosan-based heart valve scaffolds. In this study, PCL nanofibers prepared in our laboratory improved the mechanical properties of a collagen/HA scaffold for bone tissue engineering (Prosecka *et al.* 2014).

Many fabrication methods, combinations of materials as well as functionalization of scaffolds for bone tissue regeneration for improving of their properties were described in recent studies. For their examples please see Table 1.

Table 1: Osteoinductive scaffolds for bone tissue engineering.

Scaffold type	Chemical composition	Modification	Bioactive molecules	Method of preparation	Reference
Hydrogel	Collagen type I		VEGF	Crosslinking by PEG	Koch *et al.* 2006
	Collagen type I		TGF-β	Crosslinking by PEG	Bentz *et al.* 1998
	Blood	PLGA microspheres	IGF-I	Blood clotting	Meinel *et al.* 2003
Foam	Collagen type I	PCL nanofibers	PRP	Freeze-drying	Prosecká *et al.* 2014
	Chitosan/PLA		PDGF	Freeze-drying	Lee *et al.* 2002
	PLA	Alginate fibers	VEGF/BMP-2	Supercritical CO2	Kanczler *et al.* 2010
	Poly(propylene fumarate) (PPF)	Gelatin microparticles	VEGF/BMP-2	Particulate leaching	Patel *et al.* 2008
	PCL	Nanoparticles	BMP-2/BMP-7	3D printing	Huri *et al.* 2013
Nanofibers	PCL	Silk fibroin hydrogel	BMP-2	Electrospinning	Diab *et al.* 2012
	PCL	Fibrin gel	PRP/BMP-7	Electrospinning	Berner *et al.* 2012
	Silk fibroin		BMP-2	Electrospinnig	Li *et al.* 2006
	PLA-PEG		protease K	Emulsion electrospinnig	Li *et al.* 2008
	PLGA	HA particles	BMP-2	Electrospinning	Nie *et al.* 2008
	PLGA		bFGF	Coaxial electrospinnig	Sahoo *et al.* 2010

1.3.2.1. Electrospun nanofibers as a drug delivery system

Nanofibers have been utilized for delivering both water-soluble and water-insoluble substances, and serve as drug delivery systems (Blakeney *et al.* 2011; Liang *et al.* 2007). Due to their enormous surface area, nanofibers enable the adhesion of diverse bioactive agents, such as growth factors, enzymes or nucleic acids (Albanna *et al.* 2012; Schofer *et al.* 2008). The kinetics of the release of the content is determined by the form of the interaction between the fibers and the adhered drug. However, drugs dissolved or dispersed in the materials from which nanofibers are produced are quickly released. Healing processes often require a slower release, over a period of days or even weeks. This is especially important *in vivo*. To overcome this obstacle, bioactive substances have been incorporated in the interior

of the nanofiber (Sill and von Recum 2008). Coaxial electrospinning was introduced as a novel method for drug delivery, resulting in the production of core/shell nanofibers (Jiang *et al.* 2006). Buzgo *et al.* and Míčková *et al.* successfully developed a time-regulated drug delivery system based on coaxially incorporated platelet α - granules for biomedical use (Buzgo *et al.* 2013) and a drug delivery system based on core/shell nanofibers with embedded liposomes (Mickova *et al.* 2012).

A very promising approach for 3D tissues, such as bone, is to prepare composite scaffolds from microspheres and to combine them with various scaffolding systems, including hydrogels, ceramics, titanium implants and polymeric foams (Sahoo *et al.* 2010; Venugopal *et al.* 2008). Microspheres have been used for delivering bioactive molecules, e.g. growth factors and drugs (Kempen *et al.* 2008; Wenk *et al.* 2009).

A promising new approach, described by Knotek *et al.*, was a suitable method for preparing a nano-/micro-mesh via cryogenic grinding (Knotek *et al.* 2012).

The release of substances from nanofibers *in vitro* and *in vivo* has been described in recent studies (Kouhi *et al.* 2013; Martins 2010; Su *et al.* 2012; Zhu *et al.* 2013).

1.3.3. Growth factors

Improved understanding of growth factor action and molecular signalling pathways has opened opportunities for novel therapeutic options. General growth and differentiating factors involved in bone regeneration include BMPs, transforming growth factor-β1 (TGF-β1) and TGF-β2, IGF-1, platelet-derived growth factor (PDGF), basic fibroblast growth factor (bFGF), vascular endothelial growth factor (VEGF) and epidermal growth factor (EGF). Other proteins, such as fibrin, fibronectin and vitronectin support cell adhesion, osteoconduction and matrix formation. In addition, small molecules, such as hydrocortisone, dexamethasone, and β-glycerol

phosphate and synthetic growth factor are involved in osteogenesis (Dohan Ehrenfest *et al.* 2009; Wasterlain *et al.* 2012).

Novel approaches are focused on the application of autologous platelet rich plasma (PRP) and its derivatives, mainly α-granules (Blair and Flaumenhaft 2009). These blood derivatives contain autologous growth factors that are involved in cartilage and bone growth, and that in addition eliminate adverse immunogenic reactions. Autologous PRP has already been used in clinical applications for their stimulating effect on cells and tissue healing, even without cell therapy (Mazor *et al.* 2004).

The positive effect of a combination of MSCs and PRP on bone healing and remodeling have been described in many studies (Chen *et al.* 2012; Kitoh *et al.* 2004). Clearly, TGF-β1 and TGF-β2, as a part of PRP, are general growth and differentiating factors involved in bone regeneration via the mitogenesis of osteoblast precursors, and are also involved in inhibiting osteoclast formation and bone resorption. IGF-1 accelerates bone formation via increasing the number of osteoblasts. In addition, PRP contains three important proteins in blood - fibrin, fibronectin, and vitronectin - which act as cell adhesion molecules for osteoconduction and as a matrix for bone, connective tissue, and epithelial development (Dohan Ehrenfest *et al.* 2009; Wasterlain *et al.* 2012; Wrotniak *et al.* 2007).

Currently, several key factors, such as the positive effect of leucocytes or fibrin and a suitable and reproducible way to prepare PRP, are still under discussion. (Wasterlain *et al.* 2012). In several studies whole PRP has been compared, for example, with PPP (platelet poor plasma), which includes only blood plasma.

Pietrzak *et al.* (1997) found improved wound healing for PPP in comparison with untreated controls *in vivo*, but it was not as effective as PRP.

Injecting growth factors into the site of the defect is one of many approaches. However, these systems are rather difficult to apply in clinical practice, due to rapid diffusion of active substances away from the site of tissue regeneration (Tabata 2000). This problem can be solved by using a suitable biocompatible scaffold, which is able to carry the particular growth factors. The functionalization of biomaterials with growth factors has been well documented in several studies. For example, Swiontowski *et al.* used high doses of osteo-inductive BMP-2 loaded onto degradable collagen sponge matrices for bone regeneration (Swiontkowski *et al.* 2006). However, no system has yet been devised that can deliver the growth factors directly into the defect, protect the bioactivity of the growth factors and control their release in a suitable manner.

1.3.4. Cells in bone tissue engineering

Primary osteoblasts, osteosarcoma cell lines and osteoprogenitor cells have been used for *in vitro* or *in vivo* testing of bone tissue engineered constructs (Mendes *et al.* 2002). Each of them has its pros and cons. For example, the pluripotency of osteoprogenitor cells decreases with passage numbers. However, cell lines that provide more reproducible results may not represent the real situation (Rochet *et al.* 2003).

Stem cell biology has become an important topic in regenerative medicine. Stem cells are undifferentiated cells with the ability to divide in a culture and give rise to different forms of specialized cells. They are found in multicellular organisms. According to their source, stem cells are divided into "adult" and "embryonic" stem

cells. Embryonic stem cells are isolated from the inner cell mass of blastocysts, and adult stem cells are found in various tissues. In adult organisms, stem cells and progenitor cells act as a repair system for the body, replenishing adult tissues (pluripotent cells). In a developing embryo, stem cells can differentiate into all the specialized cells (ectoderm, endoderm and mesoderm), but they also maintain the normal turnover of regenerative organs, such as blood, skin, and intestinal tissues (multipotent cells) (Vernon *et al.* 2012).

Although embryonic stem cells seem to be the gold standard in stem cell research, there is still a large ethical debate about their use (Melville *et al.* 2006). Therefore, Bone-marrow derived MSCs are considered to be the most researched post-natal stem cells. They can be isolated from numerous tissues throughout the body, e.g. bone marrow, adipose tissue, muscle, periosteum, dental tissue, umbilical cord, etc. (Campagnoli *et al.* 2001; Gronthos *et al.* 2002; Seo *et al.* 2004; Schugar *et al.* 2009; Zuk *et al.* 2002).

Under suitable conditions, stem cells clearly have the potential to differentiate cell lineages and thus to play a key role in tissue engineering and regenerative medicine. Stem cells can differentiate into osteogenic lineages when cultured in the presence of dexamethasone, ascorbic acid and *β*-glycerophosphate (Dawson and Oreffo 2008) and can potentially be used for treating large bone defects (Vernon *et al.* 2012). Autologous stem cells as a source of donor cells have numerous advantages for regenerative medicine. These include low donor site morbidity, a diminished or absent immune response, and high proliferative potential (Cancedda 2003; Stevens *et al.* 2008).

It is still an open question which cell type to focus on in order to understand the whole process of bone regeneration, and which cell type is the most suitable for a

tissue engineering approach. A new strategy is focused on co-culture systems. For example, Rochet *et al.* solved the problem of insufficient vascularization of bone tissue-engineered constructs via co-cultures of MSCs with endothelial cells. Co-cultures are initiated in order to stimulate vascularization and bone formation simultaneously (Rochet *et al.* 2002).

De Boer *et al.* have recently addressed another example of co-cultures, the application of transgenic luminescent cell cultures coupled with MSCs (de Boer *et al.* 2006).

1.3.4.1. Static and dynamic cultivation of cells

Control of the hydrodynamic and biochemical environment is essential for the successful *in vitro* engineering of 3D scaffold/tissue constructs for potential clinical use (Hutmacher 2000).

Gradients in tissue quality emerge, including inhomogeneous cellular proliferation and differentiation from outer areas of the scaffolds toward the center with increasing size of the cell-seeded scaffold. *In vivo*, the distance between cells and capillaries, which provide nutrients and oxygen and at the same time account for waste elimination, ranges from 20 to 200 um (Malda *et al.* 2007; Malda *et al.* 2004; Malladi *et al.* 2006; Muschler *et al.* 2004). *In vitro*, sufficient nutrition and oxygenation of cells by diffusion is limited to a distance of 100–200 um, because of poor difusion capacity and solubility in aqueous solutions of oxygen (Carrier *et al.* 2002; McClelland and Coger 2000).

It has been hypothesized that hypoxia is the limiting factor in scaling up 3D cultures *in vitro*. Various cellular mechanisms, including the cell cycle, cell proliferation, apoptosis, and the glucose metabolism are influenced by oxygen

concentration (Wang *et al.* 2007). Recent studies have observed that the process of osteogenic differentiation and new bone tissue development are also highly dependent upon the oxygen level (Wang *et al.* 2007). Bioreactors offer a a promising solution to the diffusional limitations of a static culture, and a way to control the cultivation environment (Abousleiman and Sikavitsas 2006; Martin and Vermette 2005; Schumacher *et al.* 2010). A fluid dynamic microenvironment provided by a bioreactor can mimic the interstitial fluid conditions present in natural bone in a macroporous scaffold architecture. Bioreactors serve larger and better organized 3D cell communities in *in vitro* cultures than can be achieved using standard tissue culture techniques (Freed *et al.* 1998; Goncalves Fda *et al.* 2012; Schumacher *et al.* 2010).

In general, bioreactors are designed to perform at least one of the following functions: provide uniform cell distribution, continuously supply physiological nutrients and gases and regulate the required cell/tissue culture conditions for a long period of time, provide mass transport to the tissue, expose tissue to physical stimuli, provide information about the formation of 3D tissue (Barron *et al.* 2003). Many systems have been developed for the specialized requirements of targeted tissue, including spinner flask bioreactors, rotating wall bioreactors, compression bioreactors, strain bioreactors, hydrostatic pressure bioreactors and flow perfusion bioreactors (Kasper *et al.* 2007). In addition, numerous combinations of various types of bioreactor have been used in order to better mimic the *in vivo* environment *in vitro*. For example, a combination of compression, tensile strain or hydrostatic bioreactors with added perfusion (Carver and Heath 1999; Watanabe *et al.* 2005). Plunkett and O'Brien (2011) described how a combination of a perfusion period for nutrient delivery and waste removal and a stimulation period may deliver enhanced fluid transport with

enhanced stimulation of cells and act as a suitable combined bioreactor for bone cells.

2. The aims of the study

The work presented in this thesis is focused on the following topics:

1. Find the optimal composition for a bone scaffold
2. Functionalize the scaffold with bioactive molecules
3. Test the scaffold *in vitro* and *in vivo*
4. Design a suitable scaffold with potential for clinical use, as an outcome of the experiments

The experimental part of the manuscript describes three experiments, two *in vitro* and one *in vivo*.

3. Experiments

As has been mentioned above, bone is a structure composed of a mineral phase formed by $Ca_{10}(PO_4)_6(OH)_2$ crystals of HA deposited within an organic matrix (≈95% is type I collagen) (Marks and Odgren 2002). Collagen and HA are widely used scaffold materials for bone regeneration, because of their excellent biocompatibility with hard tissues, high osteoconductivity, bioactivity, and noncytotoxicity (Karageorgiou and Kaplan 2005; Sukhodub *et al.* 2004). However, although many reports have been presented, the optimal collagen/HA ratio for bone regeneration, especially for MSCs, remains unclear (Bandyopadhyay-Ghosh 2008; Liu *et al.* 2007; Roveri *et al.* 2003; Serre *et al.* 1993; Wahl and Czernuszka 2006). In addition, the effect of the collagen/HA ratio on the mechanical parameters of a scaffold, and also on cell adhesion and proliferation, is not well established. The main focus of the first experiment *(Experiment I)* presented here was therefore to determine the effect of the collagen/ HA ratio on the scaffold structure, and also on the seeding, adhesion and proliferation of MSCs differentiated into osteoblasts.

Cells, especially autologous cells, and smart (functionalized) scaffolds enriched with bioactive molecules, preferentially serving as a controlled delivery device, represent a new approach in bone tissue engineering (Cancedda 2003).

Improved understanding of growth factor action and molecular signalling pathways has opened opportunities for novel therapeutic options. For most tissue engineering approaches, it is necessary to apply appropriate growth factors concentrations with cells and an optimal scaffold to trigger the sequence of overlapping events required for tissue formation and growth (Prosecka *et al.* 2014).

PRP has excellent properties for tissue engineering and regenerative medicine (Bi *et al.* 2010; Kitoh *et al.* 2004). PRP releases multiple growth factors such as PDGF, TGFβ, FGF, VEGF, IGF-1, and EGF, and is expected to have a tissue regeneration rate higher than that of single growth factors (Bi *et al.* 2010; Everts *et al.* 2006). Platelets also have an important role in the complex local inflammatory response, promote angiogenesis (Simpson *et al.* 2006), and recruit mesenchymal cells (Veillette and McKee 2007).

The key parameters for scaffolds for suitable bone regeneration are their mechanical properties. A combination of 3D matrix and nanofibers can improve the mechanical properties of the scaffold (Albanna *et al.* 2012). The aim of the second experiment *(Experiment II)* was to optimise the previously reported composite collagen/HA foam scaffolds (Prosecka *et al.* 2011) from a biomechanical point of view, and enrich them with proliferation and differentiation factors suitable for clinical applications. A 3D scaffold of type I collagen and HA functionalized with PCL nanofibers (Coll/HA/PCL) to strengthen the mechanical properties of the scaffold and enriched with autologous MSCs in osteogenic media, and a thrombocyte rich solution (TRS) to increase the osteoinduction and osteoconduction of the scaffold was prepared and tested *in vivo* in an experimental rabbit model.

The nanofibers can not only be modified on their surface but also enriched in their core with various drugs that can be released slowly over the course of days or weeks. The aim of the third Experiment *(Experiment III)* was to find a suitable surface modification, which an essential step in constructing artificial cell-seeded systems. HA, which is similar to the apatite of living bone, can be used as a suitable material for improving cell proliferation and differentiation into osteoblasts (Karageorgiou and Kaplan 2005; Kuboki *et al.* 1998). Coating bone implants with HA improves the

osteoinductivity of the scaffolds and promotes ingrowth of the surrounding bone tissue into the implant (Ducheyne *et al.* 1990; Klein *et al.* 1991; Tisdel *et al.* 1994). A number of techniques are used for producing thin HA films. Each of them has its pros and cons. For example, plasma-sprayed HA coatings, where the HA is bound mechanically, have limited chemical bonding, and cracks, pores and other impurities limit their mechanical strength in contact with a substrate and the stability of the layer (Yang and Chang 2001; Zyman *et al.* 1994). Another coating technique is ion beam sputtering, which produces an amorphous coating. Heat treatment is subsequently necessary to produce crystals (Choi *et al.* 2000; Yoshinari *et al.* 1994). The very high temperatures that are necessary for crystallization are not favourable for thermo sensitive materials, such as polymers and bioactive molecules. Pulsed laser deposition (PLD) is used as an alternative HA coating technique (Bao *et al.* 2005; Blind *et al.* 2005). PLD employs an intense laser beam to evaporate the material. Subsequent condensation on a mat can form a very thin layer (only a few atoms in depth).

A comparison of different thicknesses of the HA layer deposited on the surface of nanofibers was studied in Experiment III. In addition, the study confirmed the promising potential of coaxial PCL/PVA nanofibers, e.g. as a drug delivery system (Prosecka *et al.* 2012).

3.1. Experiment I

Optimized conditions for mesenchymal stem cells to differentiate into osteoblasts on a collagen/ hydroxyapatite matrix

Collagen/HA composite scaffolds are known to be suitable for seeding with MSCs differentiated into osteoblasts, and for the *in vitro* production of artificial bones. However, the optimal collagen/HA ratio remains unclear. We demonstrate in our work the influence of the different collagen/HA ratio on cell adhesion, proliferation and differentiation, and the mechanical properties of the scaffold.

3.1.1. Methods I

3.1.1.1. Scaffold preparation

Bovine collagen type I was supplied as an 8 wt % aqueous solution (VUP, Brno, CZ) and was freeze-dried (ALPHA 1-4 LSC, CHRIST, -55º C, 15 Pa, and 24 h) to obtain 100% pure collagen I. HA was used in the form of a nanoparticle powder with an average particle size of 350 nm (Research Institute of Inorganic Chemistry, Usti nad Labem, CZ). N-(3-dimethylamino propyl)-N'-ethylcarbodiimide hydrochloride (EDC) and N-hydroxysuccinimide (NHS) (Sigma Aldrich, Germany), used as cross-linking agents, and Na_2HPO_4.12 H_2O, used as a washing agent, were diluted in water and used as received. Collagen solutions with concentrations of 0.5 (Col0.5/HA50), 1 (Col1.0/HA50), 1.5 (Col1.5/HA50), or 2 (Col0.5/HA50) wt% were prepared from lyophilized collagen in distilled water using an IKA disintegrator at 8000 rpm. The solutions were subsequently centrifuged for 5 min at 2879 x g to remove air bubbles. Defined collagen solutions were then mixed in the disintegrator with a calculated amount of HA powder for 1 min to prepare 30 (Col0.5/HA30), 40 (Col0.5/HA40), 50

(Col0.5/HA50), 60 (Col0.5/HA60), or 70 (Col0.5/HA70) wt% mixtures of HA in the collagen solutions. The mixtures were placed in a glass Petri dish and were allowed to remain until the air bubbles disappeared without centrifugation. The homogenized mixtures were frozen at -35º C in 24-well culture plates for 24 h and were then lyophilized at -55º C and 15 Pa for 24 h. The lyophilized porous collagen-based scaffolds were cross-linked by an ethanol solution containing EDC and NHS. After cross-linking, the samples were washed in a solution of Na_2HPO_4.12 H_2O and finally in distilled water, followed by lyophilization at -55º C and 15 Pa for 24 h. The morphology of the lyophilized cross-linked collagen scaffolds was observed with a Philips Quanta 200 scanning electron microscope (SEM) (Figure I/1). On the sample surface, a conductive layer of 3–4 nm was steamed by a Polaron SC7640 sputter coater before analysis. The pore size of the collagen matrices and the size of the pores were characterized from the images, using the MATLAB image analysis program.

3.1.1.2. Isolation, separation, and cultivation of pig MSCs

Blood marrow aspirates were obtained from the os illium (tuber coxae ala osis illi) of anesthetized miniature pigs (age 6–12 months). The bone marrow blood was aspirated into a 10-mL syringe with 5 mL Dulbecco's phosphate-buffered saline (PBS), 2% fetal bovine serum (FBS, StemCell Technologies), and 25 IU heparin/mL, connected to a bioptic needle (15 G/70 mm). Under sterile conditions, the bone marrow blood (about 20 mL) was deposited over 15 mL of Ficoll-Paque PLUS (StemCell Technologies). After centrifugation at 400 x g for 30 min at room temperature, the dense gradient separated erythrocytes and granulocytes as a pellet in the bottom part of the tube; mononuclear cells were localized in an opalescent layer between the Ficoll and the blood plasma. This layer was removed, washed in

culture medium (see below), and used for propagation under *in vitro* conditions. Cell numbers and viability were analyzed using a Vi-CELL (Series Cell Viability Analyzers), and about 99% viable cells were found. The cells were seeded in tissue culture flasks at a density of 800.000 cells/cm^2 and cultured at 37º C in a humidified atmosphere with 5% CO_2 Minimum Essential Media (MEM) medium with Earle's salts with L-glutamine (PAA), supplemented with 10% FBS, and penicillin/streptomycin (100 I.U./mL and 100 µg/mL, respectively) was used as the culture medium. MSCs seeding on scaffolds 6 mm in diameter and 10 mm in thickness were sterilized using plasma sterilization. Before seeding with MSCs, the scaffolds were de-aerated and incubated in a differentiation medium (MEM with L-glutamine, 20% FBS, 100 I.U./mL penicillin, and 100 µg/mL streptomycin), supplemented with 100 nM dexamethasone, 40 µg/mL ascorbic acid-2-phosphate, and 10 nM glycerol 2-phosphate disodium salt hydrate, at 4–8ºC for 14 days. Cells were seeded on scaffolds at a density of 70 x 10^3/ cm^2 in 96-well plates and centrifuged at 7 x g for 20 min. Scaffolds with seeded MSCs were cultivated in differentiation media supplemented with 10% FBS. The medium was changed every 3 days.

3.1.1.3. Cell adhesion on scaffolds

Staining with the $DiOC_6$ (3,3-diethyloxacarbocyanine iodide) fluorescent probe was used to detect the adhesion of cells on the scaffolds. Samples were fixed with frozen methyl alcohol (-20ºC) for 10 min and rinsed with PBS. Subsequently, $DiOC_6$ (0.1–1 µg/mL in PBS, pH 7.4) was added and incubated with the samples for 45 min at room temperature. The samples were rinsed with PBS (pH 7.4), and proprium iodide (5 µg/mL in PBS, pH 7.4) was added for 10 min; they were then rinsed with PBS (pH 7.4) again and visualized using a confocal microscope (Zeiss LSM 5 DUO) (Figure I/ 2).

3.1.1.4. Cell viability analysis by the MTT test

The MTT test was used for *in vitro* measurements of the metabolic activity of the cells. MTT [3-(4,5- dimethylthiazol-2-yl)-2,5-diphenyl-2H-tetrazolium bromide] is reduced to purple formazan by mitochondrial dehydrogenation in cells, indicating a normal metabolism. 50 µL of MTT (1 mg/mL in PBS, pH 7.4) were added to the medium (150 µL), and the samples were further incubated at 37ºC for 4 h. Formazan crystals were solubilized with 100 µL of 50% N,N-dimethylformamide/20% sodium dodecyl sulfate (SDS)/H_2O, pH 4.7. 200 µL of the suspension were removed, and the optical density of the formazan was measured (sample 570 nm and reference 690 nm). The absorbance of the samples incubated without cells was deducted from the absorbance of the cell-seeded samples (Figure I/ 3).

3.1.1.5. Cell viability analysis by the Live/dead staining

Confocal microscopy and live/dead staining (BCECF-AM/ propidium iodide) were used to determine cell viability. 2,7-Bis(2-carboxyethyl)-5(6)-carboxyfluorescein acetoxymethyl ester (BCECF-AM, diluted 1:100 in medium) was added to scaffolds containing seeded cells and incubated for 45 min at 37ºC and 5% CO_2 for live cell detection. After rinsing with PBS (pH 7.4), propidium iodide (5 µg/mL in PBS, pH 7.4) was added for 10 min, and then the scaffolds were rinsed again with PBS (pH 7.4) and visualized using a Zeiss LSM 5 DUO confocal microscope. For each scaffold, the number of live/dead cells was counted (Ellipse software) and averaged. Viability was calculated as the percentage of live cells from the total cell number in a defined area (Figure I/ 4 a, b, c, d).

3.1.1.6. Detection of osteogenic marker by Imunofluorescent staining

Using indirect immunofluorescent staining, OC and type I collagen were detected as markers of osteogenic differentiation. Samples were fixed with 10% formaldehyde/PBS for 10 min, washed in PBS, and then incubated in 3% FBS in PBS/0.1% Triton at room temperature. The primary antibody against OC (mouse anti-OC, Abcam, USA) or against type I collagen (mouse antiprocollagen type I, Developmental Studies Hybridoma Bank, USA) was diluted 1:20 and added to the samples for 1 h at room temperature. Then, the samples were washed with PBS/0.05% Tween for 3, 10, and 15 min. The secondary antibody (Alexa Fluor 635-conjugated goat anti-mouse IgG, Invitrogen) was diluted 1:300 and added for 45 min at room temperature. After washing, an antifading solution was added [PBS/90% glycerol/2.5% 1,4-diazabicyclo(2,2,2)octane]. OC staining was visualized using a ZEISS LSM 5 DUO confocal microscope (Figure I/ 4 e, f, g, h).

3.1.1.7. Quantitative real-time PCR analysis

Total RNA was extracted using an RNeasy Mini Kit (Qiagen) according to the manufacturer's protocol. This kit is based on a technology that combines the selective binding properties of silica-gel-based membranes with the speed of microspin technology. After the end of the procedure, total RNA was stored at -20ºC. The cDNA from 1µg of total RNA was used as a template. Synthesis of cDNA was performed by a standard procedure described in our previous work (Tvrdik *et al.* 2005). OC and bone sialoprotein (BS) mRNA expression levels were quantified by means of a LightCycler 480 (Roche Diagnostics, Mannheim, Germany) using the double-strand-specific dye SYBR Green I (Roche Diagnostics, Mannheim, Germany) according to the manufacturer's protocol. The following primers were used: BS,

sense 5-CGA CCA AGA GAG TGT CAC-3, antisense 5-GCC CAT TTC TTG TAG AAG C-3 (498 bp); OC, sense 5-TCA ACC CCG ACT GCG ACG AG-3, antisense 5-TTG GAG CAG CTG GGA TGA TGG-3 (204 bp) and beta-actin, sense 5-AGG CCA ACC GCG AGA AGA TGA CC-3, antisense 5-GAA GTC CAG GGC GAC GTA GCA C-3 (332 bp). The quantitative real-time polymerase chain reaction (real- time PCR) conditions were as follows: initial denaturation at 95ºC for 10 min, followed by 45 cycles of denaturation at 95ºC for 15 s, annealing at 54ºC for 10 s, and extension at 72ºC for 20 s. The expression levels of OC and BS mRNA were adjusted using the level of beta-actin or phosphogycerate kinase (PGK) mRNA as housekeeping genes and expressed as the ratio of OC or BS to actin or PGK, respectively. The evaluation of the expression of OC and BS mRNA was performed using quantitative real-time PCR analysis ($p < 0.05$, two-sided t-test) (Figure I/ 5, 6).

3.1.1.8. Mechanical testing of the scaffolds

The Young's moduli of elasticity of the porous bone scaffolds under compression were obtained at room temperature, using a Zwick/Roel traction machine equipped with a 1 kN load cell. The loading velocity was 1 mm/min, in accordance with the studies of Narbat *et al.* (2006) and Olah *et al.* (2006).

The specimens were cylindrical in shape (about 12 mm in height and 12 mm in diameter). Five samples and 10 measurements were performed in each experiment. Mechanical loading was applied until the scaffold was compressed to 75% of its original thickness. The compressive moduli were determined by applying linear regression to part of the stress–strain curves at 2–10% strain (initial modulus E_{init}). The stress was defined as the force divided by the initial area, and the strain was defined as the deformation of the sample (thickness) divided by the initial thickness of

the specimen. Our own software written in Python, an Open Source object-oriented programming language, was used for the evaluation (elfpy2010). This software enables a semiautomatic evaluation of mechanical measurements, namely finding the moduli of elasticity, ultimate stresses, and strains. Pressure or tension loading with various loading variations can be used, e.g. cyclic loading, loading with linear elongation, or loading up to rupture. Text files obtained from the measurement device with force, elongation, and time records can be loaded and processed by the software. The stresses and strains can be determined by defining the initial areas of the measured specimens, as was mentioned above. The software can be left to find the almost-linear parts of the stress–strain curves automatically and, by using the linear approximation of these parts, to determine the moduli of elasticity. The regions used for the linear approximation can also be set by the user. For ressure measurements of the bone scaffolds, a user-defined region was used, determined as the region of strain between 2 and 10%, and the initial modulus was computed (Table I/ 1).

3.1.1.9. Statistical analysis

Quantitative data is presented as mean/standard deviation (SD). For the *in vitro* tests, the average values were determined from at least three independently prepared samples. The results were evaluated statistically using one-way analysis of variance (ANOVA) and the Student–Newman–Keuls method. Statistica base 9.1 (Statsoft, Tulsa, OK) was applied to the results of the mechanical measurements. The normality of the data was tested with the Shapiro–Wilk W test. The correlation between the Young's moduli of elasticity and the amount of collagen and HA, porosity, and pore size was determined by the Spearman Rank Order Correlation test.

3.1.2. Results I

3.1.2.1. SEM of the Col I/ HA composite scaffold

The morphology of the lyophilized cross-linked collagen scaffolds was observed with a Philips Quanta 200 scanning electron microscope (SEM) (Figure I/1).

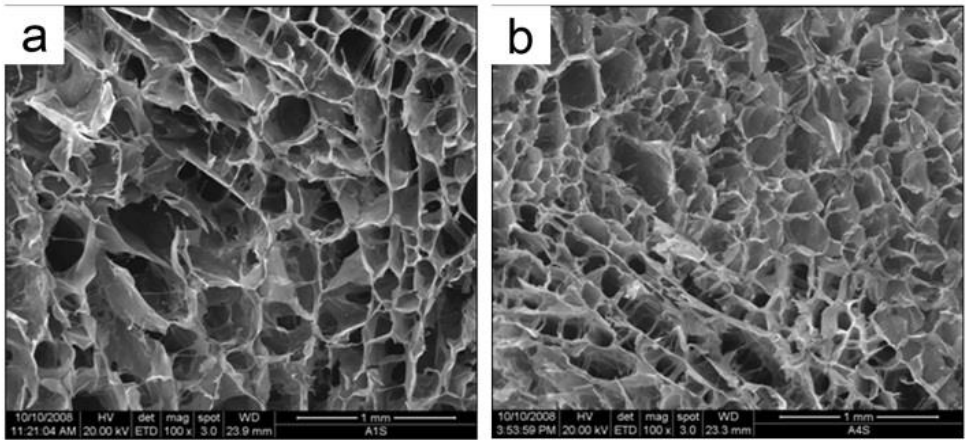

Figure I/ 1: SEM of the Col I/ HA composite scaffold. The presence of Col 0.5/HA 50 in a composite scaffold (a) resulted in a pore size of 405±74, while Col 2.0/HA 50 (b) resulted in an average pore size of 108±28. Quantitative data is presented as mean ± SD. Average values were determined from at least three independently prepared samples.

3.1.2.2. Adhesion of MSCs 1 day after scaffold seeding

MSCs were adhered on all of the samples. The significantly greatest adhesion was observed at sample Col0.5/HA50 in comparison with the other samples (Figure I/ 2).

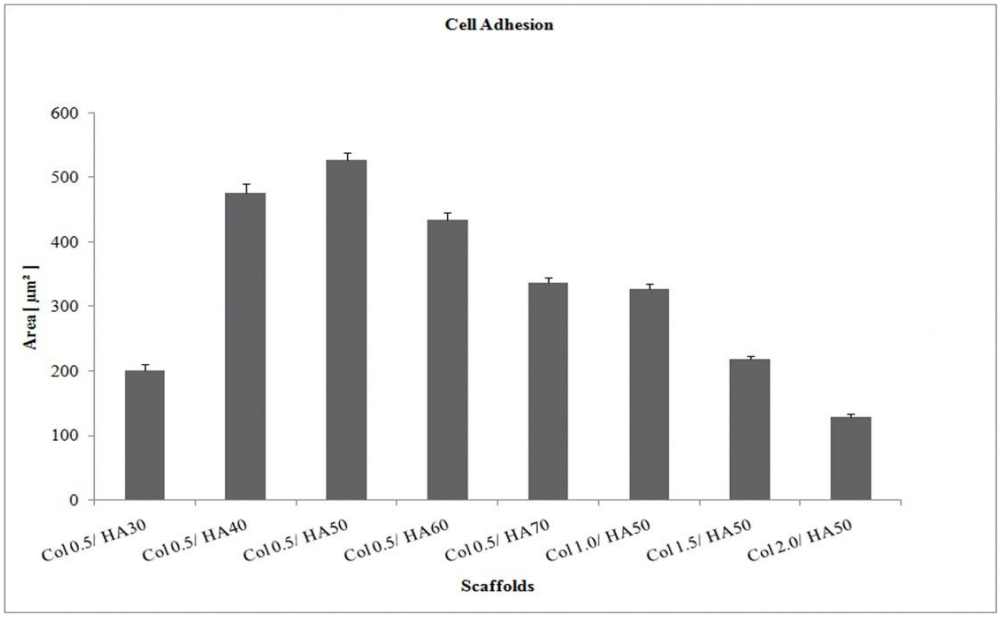

Figure I/ 2: Adhesion of MSC 1 day after scaffold seeding. The MSCs on the scaffolds were stained with a $DiOC_6$ fluorescent dye to vizualize the living cells. The areas covered by adhered cells were measured using a confocal microscope and Ellipsa software. Areas containing 100 cells were measured and averaged for each scaffold. Error bars refer to SD. The results were evaluated statistically using one-way analysis of variance (ANOVA) and the Student–Newman–Keuls method. Significant differences ($p < 0.05$) were observed: Col0.5/HA50 > Col0.5/HA40 > Col0.5/HA60 > Col0.5/HA70> Col1.0/HA50 > Col1.5/HA50> Col0.5/HA30, Col2.0/HA50.

3.1.2.3. Cell proliferation by the MTT test

Despite the lower cell adhesion, the composite scaffold containing 40% HA (Col0.5/HA40), displayed similar cell proliferation 28 days after seeding as did the scaffolds composed of Col0.5/HA50. Similar results were also observed for the composite samples containing 50% HA in the presence of 1.0% collagen (Col1.0/HA50). By contrast, the composite scaffolds containing 70% HA and, in particular, 30% HA (Col0.5/HA70 and Col0.5/HA30) were much less efficient in terms

of cell proliferation. The Col0.5/HA30 scaffolds were eliminated from further testing because of insufficient cell adhesion and proliferation (Figure I/ 3).

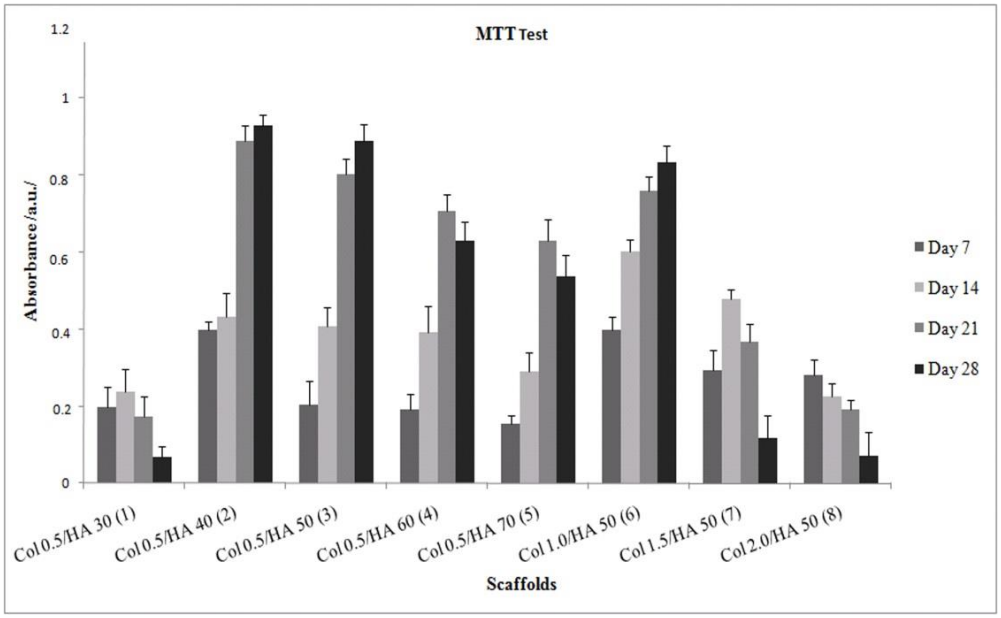

Figure II/ 3: Cell proliferation by the MTT test. Proliferation of differentiated MSCs (MTT test) 7, 14, 21, and 28 days after scaffold seeding. The error bars refer to SD. The results were evaluated statistically using one-way analysis of variance (ANOVA) and the Student–Newman–Keuls method. Significant differences ($p < 0.05$) were observed: *day 7*: 6 > 2 > 7 > 8 > 3 > 1 > 4 > 5; *day 14*: 6 > 7 > 2, 3, 4 > 5 > 1, 8; *day 21*: 2 > 3 > 6, 4 > 5 > 7 > 1; *day 28*: 2 > 3, 6 > 4 > 5 > 1, 7, 8.

3.1.2.4. Cell viability and osteogenic differentiation

Cell viability and osteogenic differentiation were detected by confocal microscopy. The highest viability was again detected on the Col0.5/HA50 scaffolds after 28 days of cultivation and deteriorated with higher concentrations of both collagen and HA. Both OC and type I collagen were present in all samples. The highest concentration of proteins was again detected on the Col0.5/HA50 scaffolds 28 days after seeding, and was reduced with higher concentrations of both collagen and HA (Figure I/ 4).

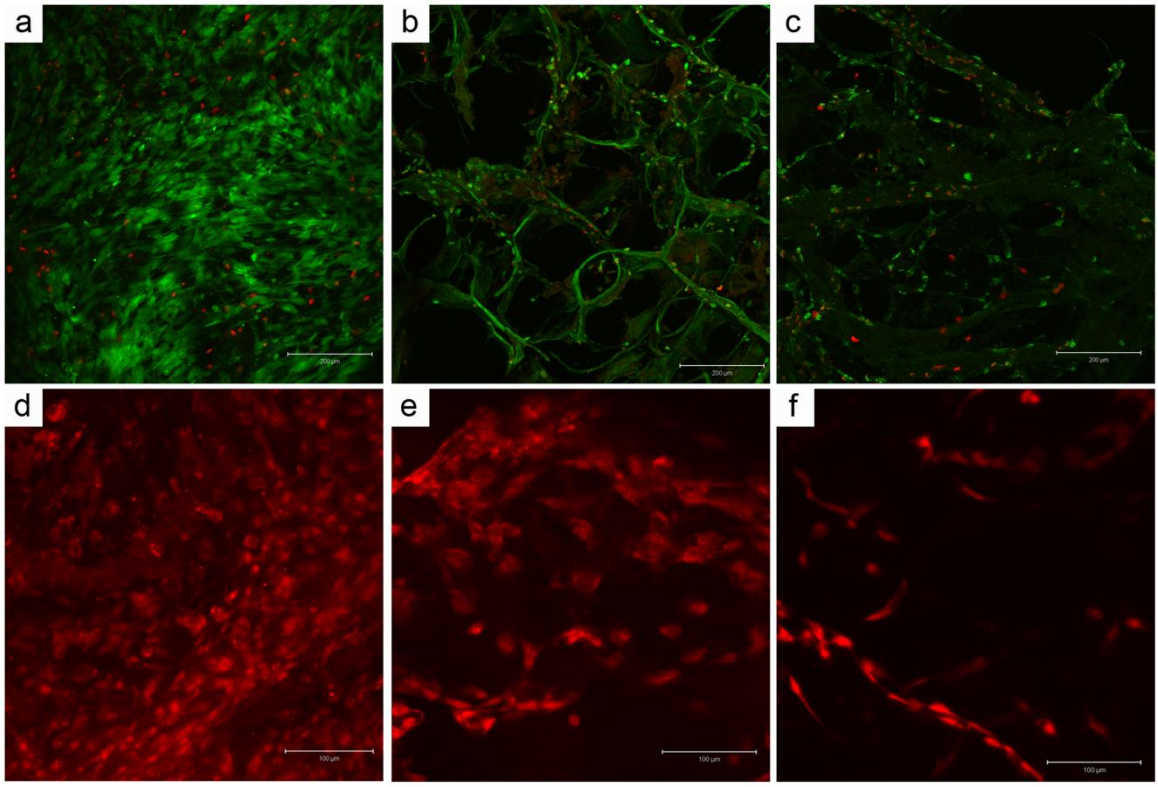

Figure I/ 4: Cell viability and osteogenic differentiation by confocal microscopy. Fluorescence confocal microscopy of differentiated MSCs. Viability of cells by live/dead staining (BCECF-AM/propidium iodide) 28 days after seeding: Col0.5/HA50 scaffold (a), Col0.5/HA70 (b), and Col2.0/HA50 (c). Immunofluorescent detection of OC 28 days after seeding: Col0.5/HA50 scaffold (d), Col0.5/HA70 (e), and Col2.0/HA50 (f).

3.1.2.5. Quantitative Real-time PCR analysis

The concentration of OC and BS were analyzed by quantitative real-time PCR analysis at scaffolds with different amounts of HA and Collagen. The increasing concentration of OC observed over time demonstrated the gradual differentiation of MSCs into osteoblasts. The highest production of OC was observed for the composite scaffolds containing Col0.5/HA40 and Col0.5/HA50 and also Col1.0/HA50. However, the Col0.5/HA60 and Col0.5/HA70 scaffolds were also characterized by a comparable production of OC. The significantly greatest production of BS was observed for the Col0.5/HA50 composite scaffolds 28 days after seeding. The

Col0.5/HA 40 samples were also characterized by a significantly elevated production of BS compared to the Col0.5/HA60 and Col0.5/HA70 samples (Figure I/ 5, 6).

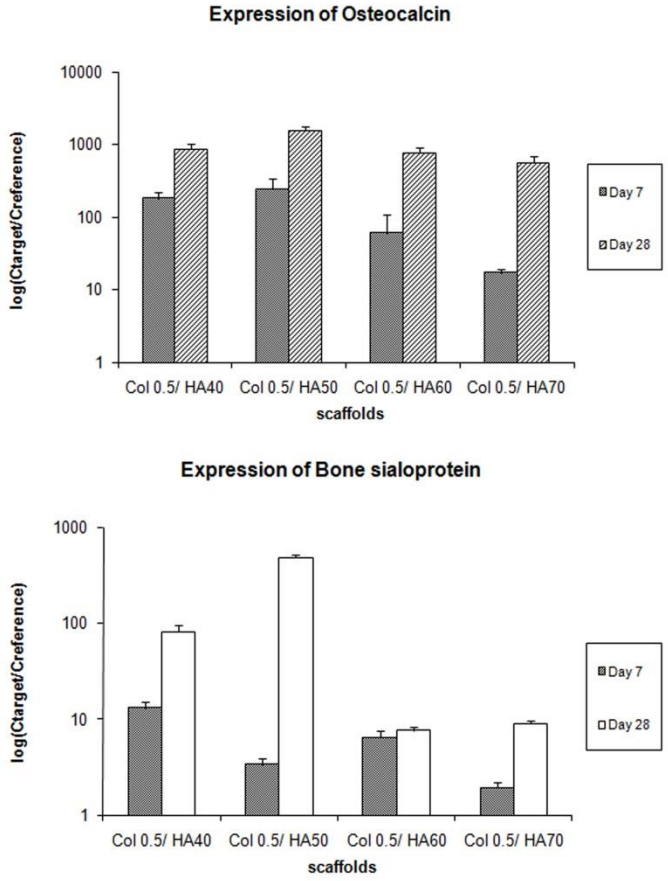

Figure I/ 5: Real-time PCR analysis of scaffolds with different amounts of HA.

The evaluation of OC and BS mRNA expression 7 and 28 days after seeding, performed by quantitative real-time PCR analysis ($p < 0.05$, two-sided t-test). Beta-actin was used as a housekeeping gene control. Due to the very different values, the scale on the Y axis is logarithmic. The error bars refer to SD. Significantly different ($p < 0.05$) values on a given day were identified using one-way analysis of variance (ANOVA) and the Student–Newman–Keuls method: **OC**: *day 7:* Col0.5/HA40> Col0.5/HA60, Col0.5/HA70; Col0.5/HA50> Col0.5/HA60, Col0.5/HA70; *day 28*: Col0.5/HA50 > Col0.5/HA40, Col0.5/HA60, Col0.5/HA70; **BS**: *day 7*: Col0.5/HA40> Col0.5/HA60> Col0.5/HA50, Col0.5/HA70; *day 28*: Col0.5/HA50> Col0.5/HA40> Col0.5/HA60, Col0.5/HA70.

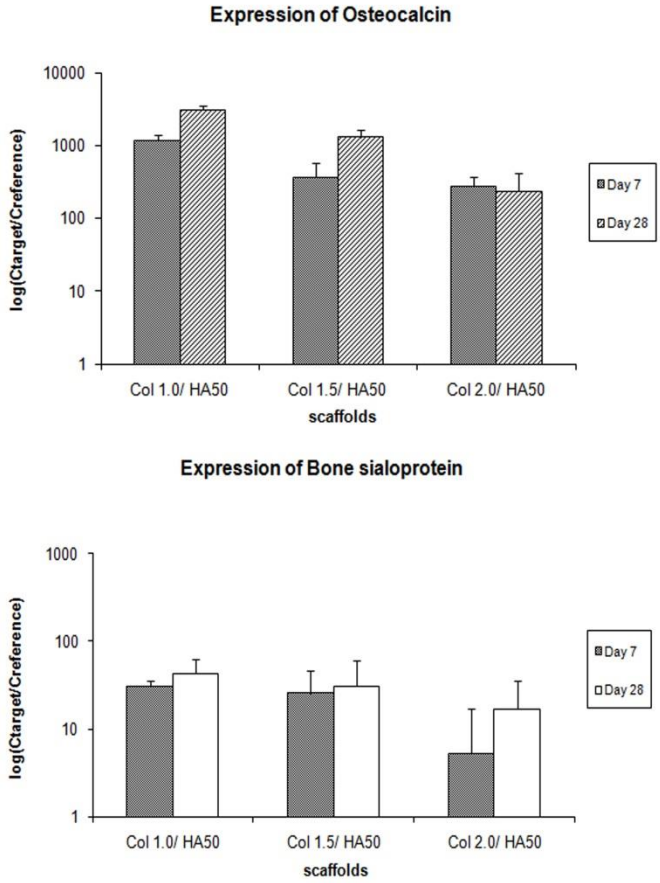

Figure I/ 6: Real-time PCR analysis of scaffolds with different amounts of collagen. The evaluation of OC and BS mRNA expression 7 and 28 days after seeding, performed by quantitative real-time PCR analysis ($p < 0.05$, two-sided t-test). Beta-actin was used as a housekeeping gene control. Due to the very different values, the scale on the Y axis is logarithmic. The error bars refer to SD. Significantly different values ($p < 0.05$) on a given day were identified using one-way analysis of variance (ANOVA) and the Student–Newman–Keuls method: **OC**: *day 7*: Col1.0/HA50> Col1.5/HA50> Col2.0/HA50; *day 28*: Col1.0/HA50> Col1.5/HA50> Col2.0/HA50; **BS**: *day 7*: Col1.0/HA50> Col2.0/HA50; Col1.5/HA50> Col2.0/HA50; *day 28*: Col1.0/HA50> Col1.5/HA50> Col2.0/HA50.

3.1.2.6. Mechanical properties and porosity of the scaffolds

Scaffolds from different collagen/HA mixtures were tested and the initial Young's moduli of elasticity E_{init} in compression were determined at strain 2-10%. Note a strong positive correlation between collagen concentration and Young's modulus (Spearman R = 0.84) and also a strong negative correlation between pore diameter and Young's modulus (Spearman R = -0.84), i.e. enlargement of the pore size led to a decrease in the stiffness of the composite. The mean values and standard deviations were determined from 5 independent experiments (Table I/ 1).

Table I/ 1: Mechanical properties and porosity of the scaffolds.

Scaffold	Percentage of collagen	Percentage of HA	Pore diameter [µm]	Young's moduli of elasticity [kPa]
Col 0.5/HA 30	0.5	30	502±24	1.41±0.76
Col 0.5/HA 40	0.5	40	468±38	3.10±0.63
Col 0.5/HA 50	0.5	50	405±74	4.65±1.57
Col 0.5/HA 60	0.5	60	298±69	5.13±0.23
Col 0.5/HA 70	0.5	70	205±72	6.09±0.11
Col 1.0/HA 50	1.0	50	267±74	62.02±23.62
Col 1.5/HA 50	1.5	50	195±28	168.74±36.94
Col 2.0/HA 50	2.0	50	108±28	289.98±161.89

3.1.3. Discussion I

We have demonstrated in our work the influence of the collagen/HA ratio on cell adhesion, proliferation and differentiation, and the mechanical properties of the scaffold. The mixtures of 40 and 50% HA with 0.5% collagen (Col0.5/HA40 and Col0.5/HA50) were be found the most suitable for cell adhesion, proliferation and

differentiation. The explanation for the results seem to lie in the porosity of the scaffolds. Pores have been reported to play a key role in bone tissue formation. They allow the migration and proliferation of osteoblasts and/or MSCs, and also vascularization (Kuboki *et al.* 1998). The reported minimum pore size is around 100 μm; however, the recommended diameters are larger than 300 μm (Hulbert *et al.* 1970). Dawson and Orefo (2008) prepared composite type I collagen/ HA scaffolds from a 1 wt % solution of type I collagen and 70% HA. Their scaffold was suitable for proliferation and osteal differentiation of human bone MSCs, and was characterized by an average pore size of 135 μm. However, larger pores undisputedly promote better adhesion and proliferation of MSCs (Dawson and Oreffo 2008). The optimal pore diameter in our study was found to be around 400 μm, and was characteristic of the optimal mixture of 40–50% HA with 0.5% collagen (Col0.5/HA40 and Col0.5/HA50). This size evidently enables sufficient cell and nutrition diffusion and, simultaneously, maintains adequate scaffold solidity and firmness. The effect of pore size seems to be crucial, and decreasing the pore diameter below 200 μm resulted in dramatically lower proliferation. The main conclusion of this study is that the optimal collagen/HA mixture of 40–50% HA with 0.5% collagen (Col0.5/HA40 and Col0.5/HA50) was able to induce osteogenic differentiation of MSCs. Naturally, this scaffold could be further modified and improved. Modification of the surface charge would probably improve cell adhesion and the mechanical properties of the scaffolds. However, one of the important findings of this study is our observation that any potential scaffold for seeding with MSCs differentiated into osteoblasts has to be tested over a longer time scale. Clearly, neither cell adhesion nor data obtained 14 days after seeding can be taken as sufficiently reliable. Results 28 days after seeding are needed.

3.1.4. Conclusion I

Our study confirmed that a higher collagen content increased scaffold stiffness, but that the greater stiffness was not sufficient for bone tissue formation. Bone tissue formation is a complex process, evidently also dependent on scaffold porosity. In addition, we found that the scaffold pore diameter was dependent on the concentration of collagen and HA, and that it could play a key role in cell seeding. The suitable pore size for optimal cell proliferation was evaluated to be around 400 μm. In conclusion, the optimal composite scaffold for new bone formation and cell proliferation was found to be formed from 50 wt % HA in 0.5 wt % collagen type I solution.

3.2. Experiment II

Collagen/hydroxyapatite scaffold enriched with polycaprolactone nanofibers, thrombocyte-rich solution and mesenchymal stem cells promotes regeneration in large bone defect *in vivo*

A 3D scaffold Col0.5/HA50 (Coll/HA) prepared in our previous work *(Experiment I)* was enriched with polycaprolactone nanofibres (Coll/HA/PCL), autologous MSCs in osteogenic media, and thrombocyte-rich solution (TRS) in this study as an optimal implant for bone regeneration *in vivo* in white rabbits. Nanofibres were used to optimize the viscoelastic properties of the Coll/HA scaffold for bone regeneration. MSCs and TRS in the composite scaffold were used to promote new bone tissue formation. Three types of Coll/HA/PCL scaffold were prepared: an MSCs-enriched scaffold, a TRS-enriched scaffold, and a scaffold enriched with both MSCs and TRS. These scaffolds were implanted into femoral condyle defects 6 mm in diameter and 10 mm in depth. Untreated defects were used as a control. Macroscopic and histological analyses of the regenerated tissue from all groups were performed 12 weeks after implantation.

3.2.1. Methods II

3.2.1.1. Scaffold composite preparation

Our previous study describes the preparation of a Coll/HA scaffold without PCL nanofibres (Prosecka *et al.*, 2010). Briefly, bovine collagen type I as an 8 wt% aqueous solution (VUP, Brno, Czech Republic), HA as a 350 nm nanoparticle powder (Research Institute of Inorganic Chemistry, Usti nad Labem, Czech Republic), N-(3-dimethylamino propyl)-N'-ethylcarbodiimide hydrochloride, and N-hydroxysuccinimide

(Sigma Aldrich, Germany) were used as received. A collagen solution (0.5 wt% concentration) was mixed with a calculated amount of HA powder to prepare a 50 wt% mixture of HA powder in a collagen solution. In this study, 0.065 g PCL nanofibres (prepared as described below) were added to the Coll/HA mixture (10 x 10 cm of PCL nanofibres were cut into approximately 2mm pieces and mixed into the Coll/HA solution) (Coll/HA/PCL). The homogenized mixture was frozen on 12-hole culture plates and lyophilized (-55°C, 15 Pa, 24 h; CHRIST ALPHA 1-4 LSC).

The lyophilized porous collagen-based scaffolds were cross-linked with an ethanol solution containing N-(3-dimethylamino propyl)-N′-ethylcarbodiimide hydrochloride and N-hydroxysuccinimide in a molar ratio of 2:1. The samples were then washed in a 0.1 M solution of $Na_2HPO_4 \cdot 12\ H_2O$ and subsequently in distilled water and freeze-dried at -55°C and 15 Pa for 24 h.

The morphology of these scaffolds was observed using a scanning electron microscope (Philips Quanta 200) (Figure II/ 3). The pore size of the Coll/HA and Coll/HA/PCL matrices were characterized using the MATLAB image analysis program. Quantitative data are presented as mean ± SD. Average values were determined from at least 3 independently prepared samples.

3.2.1.2. Mechanical testing of the scaffolds

The initial moduli of elasticity of the Coll/HA and Coll/HA/PCL porous bone scaffolds under compression were obtained at room temperature using a traction machine (Zwick Roell, Ulm, Germany) equipped with a 1-kN load cell as was already mentioned in previous section *3.1.1.8*. The loading velocity was 1 mm/min, in accordance with the studies of Narbat *et al.* (2006) and Olah *et al.* (2006). Statistica base 9.1 (StatSoft, Inc., Tulsa, OK, USA) was used for the statistical analysis of the

initial moduli of elasticity. Normality was tested with the Shapiro-Wilk W test. The difference in the initial moduli between the Coll/HA and Coll/HA/PCL scaffolds was tested with the Mann-Whitney *U* test. The initial moduli are presented as mean value ± standard error (Table II/ 2).

3.2.1.3. Fabrication of PCL nanofibres

The fabrication of PCL nanofibres has been described in our previous study (Jakubova *et al.* 2011). Briefly, we used an electrospinning method (Sachlos *et al.* 2006) or prepared PCL nanofibres from PCL with a molecular weight of 40 000 (Wako Chemicals GmbH, Neuss, Germany). Electrospinning was performed using 10% PCL dissolved in chloroform:ethanol (9:1). A high-voltage source generating voltages of up to 50 kV was applied to the polymer solution. Electrospun nanofibres were deposited on the grounded collecting electrode. The nanofibres were stored in a desiccator until use.

3.2.1.4. Isolation of rabbit autologous MSCs

Blood marrow aspirates were obteined from the os illium (*tuber coxae ala osis illi*) of anesthetised rabbits (age 3 months) into a 10-mL syringe with 1 mL PBS and 25 IU heparin/mL (Zentiva, Czech Republic) connected to a bioptic needle (16 gauge) as was already mentioned in previous section *3.1.1.2*.

3.2.1.5. Preparation of TRS

Preparation of TRS took place through the Hematology Service of the General Teaching Hospital, Prague, Czech Republic. PRP (volume, 400 mL; thrombocyte concentration, 225 x 10^9) was centrifuged (2250 x g, 15 min), and the supernatant was discarded. The resulting thrombocytes were washed in washing buffer (pH 6.5,

113 mM NaCl, 4.3 mM K_2HPO_4, 4.3 mM Na_2HPO_4, 24.4 mM NaH_2PO_4, and 5.5 mM glucose), as described by Baenziger *et al.* (1971). Thrombocyte washing was repeated 3 or 4 times. Contaminating leukocytes and erythrocytes were removed through further centrifugation (120 x g, 7 min). The thrombocytes were then resuspended in 40 mL washing buffer and centrifuged again at 120 x g for 7 min to recover those that were sedimented in the first spin. The thrombocytes were pelleted via centrifugation (2000 x g, 15 min), washed once, and finally resuspended in buffer (109 mM NaCl, 4.3 mM K_2HPO_4, 16 mM Na_2HPO_4, 8.3 mM NaH_2PO_4, and 5.5 mM glucose, pH 7.5).

A TRS concentration of 1.35 x 10^6/µL was used for each sample. Thrombocytes and TRS were manipulated in a sterile tissue culture hood in a clean room. TRS was stored in centrifuge tubes in a clean room until use. The temperature in the room was set at 22°C.

3.2.1.6. Preparation of scaffold types

MSCs-enriched scaffolds

Scaffolds with a diameter of 10 mm and a height of 20 mm were sterilized using plasma sterilization. Two weeks before seeding with MSCs, the scaffolds were de-aerated and incubated in differentiation medium (MEM with L-glutamine, 10% FBS, 100 IU/mL penicillin, and 100 µg/mL streptomycin) supplemented with 100 nM dexamethasone, 40 µg/mL ascorbic acid-2-phosphate, and 10 nM glycerol 2-phosphate disodium salt hydrate at 4–8°C for 14 days. One day before surgery, the autologous cells in the culture medium were trypsinated, and in a second passage were seeded on the scaffolds at a density of 2 x 10^6/cm^2 on a 24-well plate. The

differentiation medium was added. The plate was centrifuged at 7x g for 20 min and cultured at 37°C in a humidified atmosphere with 5% CO2.

TRS-enriched scaffolds

Scaffolds on the 24-well plate were immersed in TRS (1.35 x 10^6 thrombocytes/µL) for 2 h for adhesion. After incubation, the functionalized scaffolds were rinsed twice in PBS (pH 7.4). The differentiation medium was added and cultured at 37°C in a humidified atmosphere with 5% CO_2.

MSCs- and TRS-enriched scaffolds

Scaffolds on the 24-well plate were immersed in TRS (1.35 x 10^6 thrombocytes/µL) for 2 h to enable adhesion. After incubation, the functionalized scaffolds were rinsed twice in PBS (pH 7.4). Then, the autologous cells were seeded on the scaffolds at a density of 2 x $10^6/cm^2$ and differentiation medium was added. The plate was centrifuged at 7 x g for 20 min and cultured at 37°C in a humidified atmosphere with 5% CO_2.

3.2.1.7. Surgical procedure and scaffold implantation

Thirty 3-month-old male New Zealand white rabbits weighing 3.0 ± 0.5 kg were obtained from a conventional breeder (BioTest, Czech Republic) and housed in standard cages without bedding. The rabbits were fed *ad libitum* using a standard granular mixture for rabbits (TM-MaK 1, Bergman, Czech Republic). The maintenance and handling of the experimental animals followed European Union Council Directive 86/609 EEC and the *Ethical Principles and Guidelines for Scientific Experiments on Animals*. The study was approved by the expert committee of the Institute of Physiology at the Academy of Sciences (Prague, Czech Republic) and conformed to Czech Animal Protection Law No. 246/92.

The surgical procedure was conducted under general anaesthesia using ketamine (35 mg/kg^{-1}) and xylazine (3 mg/kg^{-1}) and subsequent inhalation of O_2 + 1.5–2.0% halothane during surgery. A critical size defect (Katthagen 1986) was made in the femoral condyles using a 3.2-mm drill gradually expanded to obtain a 6-mm defect that was 10 ± 0.5 mm in depth (Figure II/1). The defects in 7 rabbits were filled with MSCs-enriched scaffolds, 8 rabbits received TRS-enriched scaffolds, and MSCs- and TRS-enriched scaffolds were placed in 8 rabbits. The defects were left empty in 7 rabbits (control group). Before implantation, the scaffolds were sized to fit the defect exactly. Wound healing was uncomplicated in all cases throughout the postoperative period. Antibiotics (10 mg/kg/day i.m. cefalexin monohydrate ad us. vet.) and analgesic (0.1 mg·kg^{-1}·day^{-1} s.c. of butorphanol tartrate ad us. vet.) were administered during the first 5 days. The rabbits were not limited in their movement after surgery. The rabbits were euthanized 12 weeks later, and their femoral condyles were examined. All of the harvested samples were fixed in 4% phosphate-buffered formaldehyde.

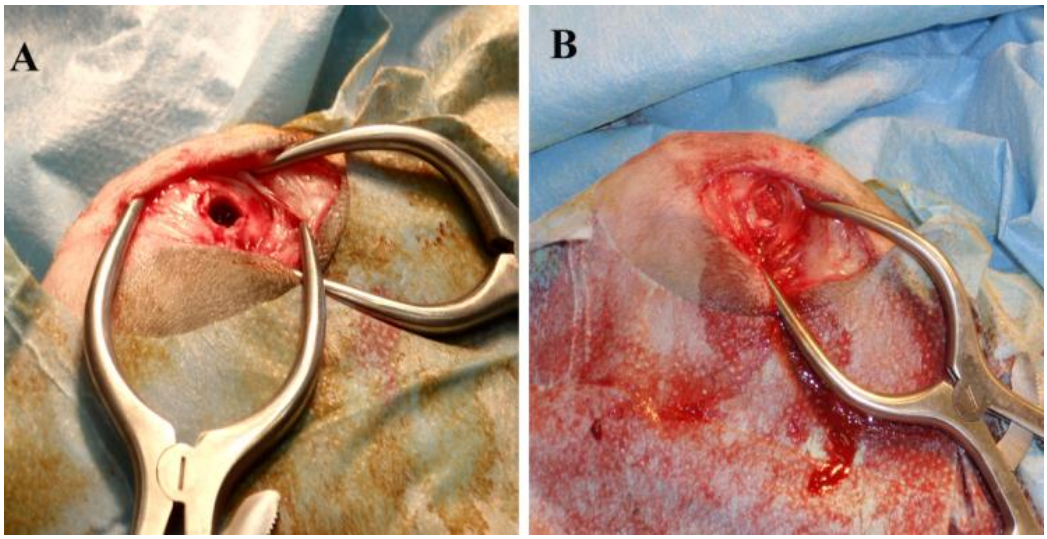

Figure II/ 1: Surgical procedure. Critical size defects were made in femoral condyles using a 3.2-mm drill gradually expanded to obtain defects 6 mm in diameter and 10 ± 0.5 mm in depth.

3.2.1.8. Histological processing

All of the fixed samples were demineralised in 12.5% ethylenediaminetetraacetic acid solution (Komplexon III, Penta, Prague, Czech Republic) for 3 months and embedded in paraffin.

Qualitative analyses

Five serial histological sections 5 μm in thickness (between-section distance, 50 μm) were processed from each paraffin-embedded tissue block. In a randomly selected tissue block, another series of 20 consecutive sections was cut to examine the variability among the serial sections. The sections were stained with hematoxylin-eosin, blue Mallory trichrome, and green trichrome (Kocova 1970).

Bone quantification

Four serial histological sections 5 μm in thickness (between-section distance, 50 μm) were processed from each paraffin-embedded tissue block. In a randomly selected

tissue block, another series of 20 consecutive sections was cut to examine the variability among the serial sections. The sections were stained with blue Mallory trichrome and green trichrome.

Four micrographs per tissue block (i.e. 1 micrograph per section) were taken using a 2× objective. The image field was broad enough to capture the regenerating bone defect, which was centred in the micrographs. Using Ellipse software (Košice, Slovak Republic), 3 concentric circles of increasing diameter (2, 4, and 6 cm) were projected onto each micrograph. The outer circle delineated the borders of the original 6-cm defect (area *A*) drilled within the femoral condyle. The 3 compartments defined by these circles were 2 annuli (*A1* was the area between the outer and the inner concentric circles; *A2* was the area between the inner and the central concentric circles) and the area of the central circle (*A3*). The geometric characteristics of these areas are summarised in Table II/ 1, and their positions are illustrated in Figure II/ 2A. The outer compartment close to the borders of the original bone defect was represented by the area of *A1*, the inner compartment by the area of *A2*, and the central compartment of the original bone defect by the area of *A3.*

Next, a randomly positioned uniform grid of equidistant points was placed on the micrographs in an overlay (Figure II/ 2B), so the number of points striking each compartment was proportional to its area (see Table II/ 1). In each of the 4 micrographs per tissue sample, we counted the number of points striking the bone tissue within the total area of bone defect *A*, and also within the individual compartments (*A1*, *A2*, and *A3*). The area of bone was calculated by multiplying the number of counted points by the area corresponding to each point (Mouton et al. 2002). The volumes of the corresponding three-dimensional compartments were calculated by multiplying the areas by the number and the thickness of the sections

(see Table II/ 1). We calculated the volume fraction of each compartment within the total examined volume (see Table II/ 1). The bone volume was expressed as the volume fraction of bone tissue within the whole defect and within the outer, inner, and central compartments. If the bone tissue had regenerated equally within all 3 compartments (i.e. in the same manner within the whole volume of the defect), the volume of bone tissue found within the individual compartments was proportional to the volume of these compartments, and we predicted that all 3 compartments would harbour the same concentration of bone tissue.

To test which of the compartments was preferentially occupied by bone tissue, we divided the total number of points striking the bone tissue by the volume fraction of each compartment within the examined volume of the defect. In this way, we calculated the expected number of points (P_{exp}) striking the bone tissue within each volume-occupying compartment, provided that the bone tissue had regenerated equally within all 3 compartments. The ratio between the observed number of points striking the bone tissue (P_{obs}) and P_{exp} was the relative deposition index (RDI = P_{obs}/P_{exp}), which was used to compare the outer, inner, and central compartments. For uniform bone regeneration, RDI was equal to 1, but for preferential bone growth, the index was >1. This principle for quantifying the preferential distribution of immunogold nanoparticles using electron microscopy has been described and thoroughly evaluated by (Mayhew *et al*. 2002; Mayhew *et al.* 2009). However, the use of RDI is not limited to electron microscopy, because between-compartment comparisons and mathematical apparatus are scale independent.

We then calculated the partial chi-squared values for each pair using the following equation: $(P_{obs} - P_{exp})^2/P_{exp}$. The total chi-squared values were compared with the chi-squared distribution to test the null hypothesis stating that the distribution pattern

among the compartments was random. Our study had 2 degrees of freedom (Table II/ 3). Estimates of bone volume were based on 4 tissue sections per tissue block sampled from the approximate middle of the bone defect. However, the bone content might have differed among the histological sections. We therefore assessed the bone area in a series of 20 equidistant sections in a randomly selected tissue sample. The variation in the bone area quantified in the serial sections was estimated using the error coefficient calculated with the quadratic approximation formula of Matheron, which was modified for use in a stereological context (Gundersen and Jensen 1987). The resulting value was <0.1, which quantified the sampling error in our study (Figure II/ 2C).

The data was processed with Statistica Base 9.1 (StatSoft, Inc., Tulsa, OK, USA). The tests on the randomness of the bone distribution among compartments was based on a chi-squared distribution. The Man-Whitney U test was used to test the equality of population medians among the groups under study. All results were considered statistically significant if p was <0.05.

Table II/ 1. Outer, inner, and central compartments of bone defects under examination.

	Compartment		
Parameter	**Outer**	**Inner**	**Central**
Circle diameter (mm)	6	4	2
Area per section (mm^2)	15.71	9.42	3.14
Area label	*A1*	*A2*	*A3*
Volume in 4 sections (mm^3)	3.142	1.884	0.628
Volume fraction	0.552	0.331	0.114

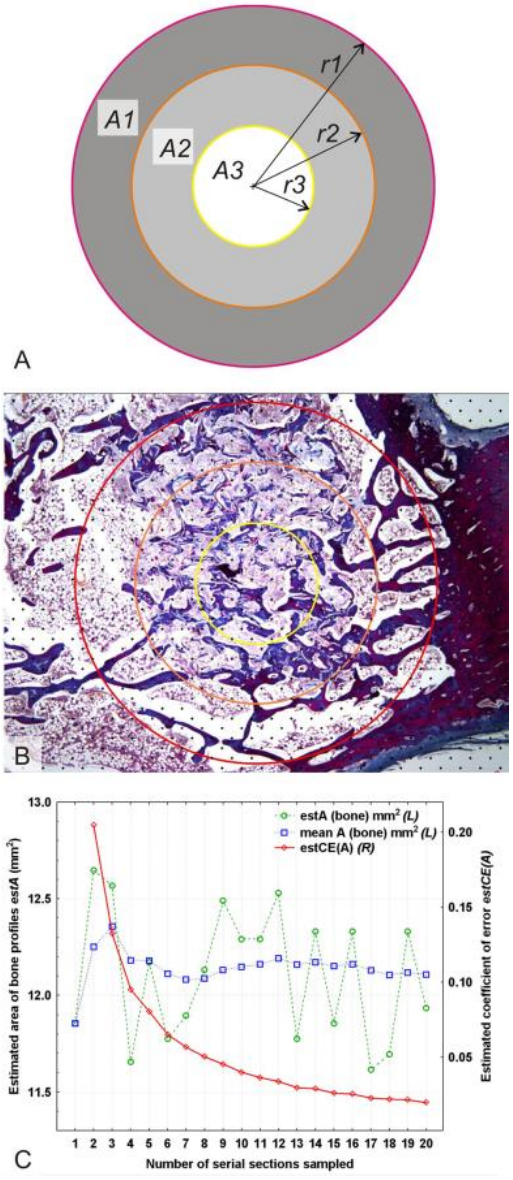

Figure II/ 2: Histological assessment of bone quantity and distribution. (A) The total area of bone defect *A* on the histological sections was divided with 3 concentric circles (radius *r1* = 3 cm, *r2* = 2 cm, and *r3* = 1 cm) into 3 arbitrary compartments. The outer compartment (dark grey) was designated *A1*, the inner compartment (light grey) was *A2*, and the central compartment (white) was *A3*. (B) A stereological point grid was superimposed on the histological micrographs, and the points striking the bone tissue within the total area of the bone defect were counted. (C) The area of bone (*estA*) estimated with a stereological point grid varied within the series of adjacent histological sections (green dashed line, left y-axis), thus affecting the moving average (blue dotted line, left y-axis). The coefficient of error (*estCE*), which was estimated according to the method of (Gundersen and Jensen 1987), decreased as the number of serial sections included in the study increased (red line, right y-axis), thus illustrating the effect of histological sampling on the resulting data. This graph demonstrates that taking 4 sections for quantification reduced the sampling error to an acceptable value of <0.1.

3.2.2. Results II

3.2.2.1. Morphological characterization of scaffolds

The morphology of these scaffolds was observed using a scanning electron microscope (Philips Quanta 200) (Figure II/ 3).

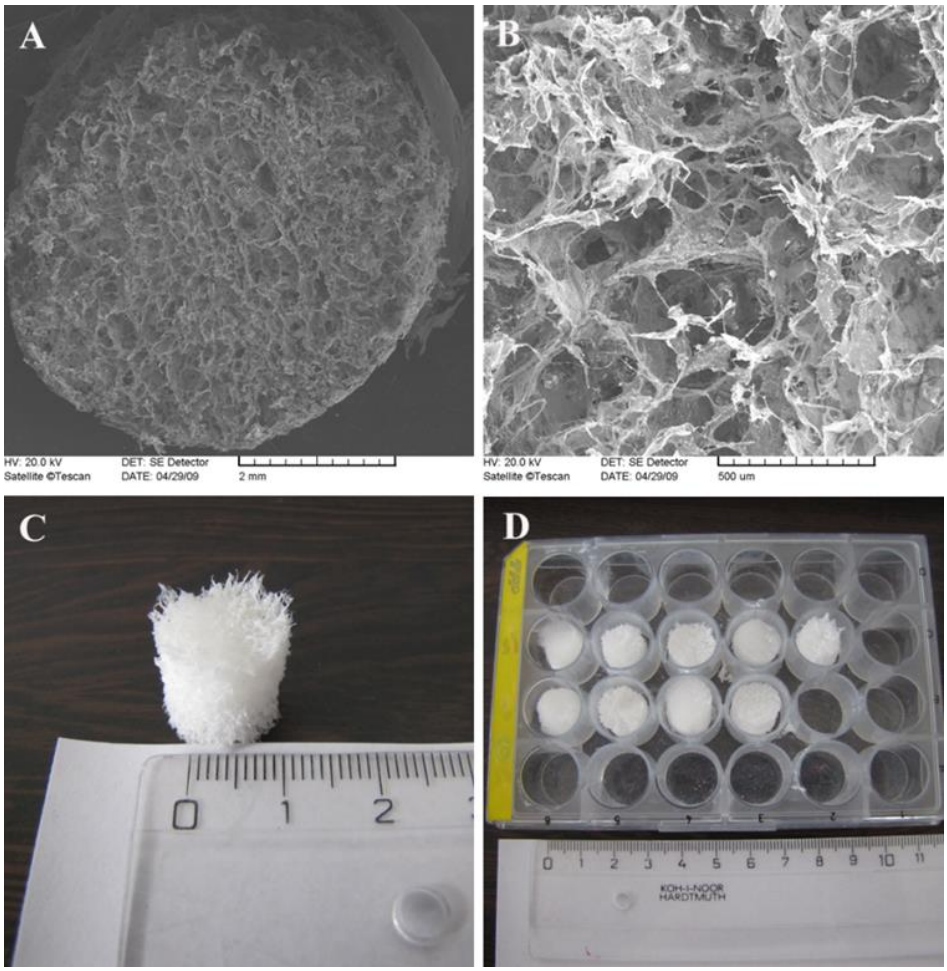

Figure II/ 3: Morphology of a collagen and HA (Coll/HA) scaffold enriched with polycaprolactone nanofibres (Coll/HA/PCL). The scaffold morphology was analysed using scanning electron microscopy (A, B) and macroscopic evaluation (C, D).

3.2.2.2. Characterization and mechanical testing of scaffolds

The pore size of the scaffolds was observed using scanning electron microscopy and the MATLAB image analysis program. The initial moduli of elasticity under compression for the Coll/HA/PCL scaffolds were higher than the moduli of the Coll/HA scaffolds (Table II/ 2).

Mechanical testing of scaffolds: Our results clearly proved that the presence of PCL nanofibre at a low concentration was sufficient to stiffen the collagen scaffold. The initial modulus of elasticity under compression was higher for the Coll/HA/PCL scaffolds namely 8.5 ± 3.3 kPa than for the collagen/HA scaffolds (3.5 ± 0.4 kPa). The goal of our *in vivo* study and histology analysis was to determine whether such scaffold strengthening is optimal for bone regeneration (Table II/ 2).

Table II/ 2: Characterization and mechanical testing of a collagen and HA (Coll/HA) scaffold enriched with polycaprolactone nanofibres (Coll/HA/PCL).

Scaffold	Percentage of collagen	Percentage of HA	Pore diameter (µm)	Amount of PCL nanofibers (g)	Young's modulus of elasticity (kPa)
Coll/HA	0.5	50	402 ± 52	0	3.5 ± 0.4
Coll/HA/PCL	0.5	50	397 ± 24	0.065	8.5 ± 3.3

3.2.2.4. Macroscopic evaluation

A macroscopic evaluation of samples from all groups was made after the joint capsule in the articular cavity had been removed to obtain a small amount of synovial fluid. The joint capsule and the articular surface showed no signs of inflammation in any of the groups (Figure II/ 4).

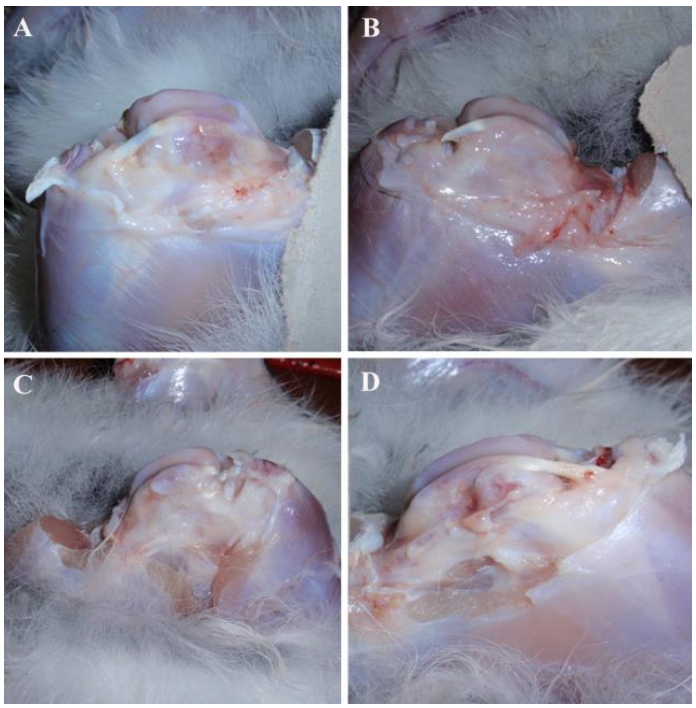

Figure II/ 4: Macroscopic evaluation. The defects in rabbits in the groups treated with MSCs-enriched (A), TRS-enriched (B), and MSCs- and TRS-enriched (C) scaffolds were completely healed. The same result was observed in the control group (D), but the localization of the defect revealed deformation of the condyles.

3.2.2.3. Histological evaluation

Qualitative analyses

Qualitative histological analysis revealed the formation of new bone trabecules in the enriched scaffold groups but not in the control group, which had no scaffolds (Figure II/ 5). The differences among the scaffold types were further quantified.

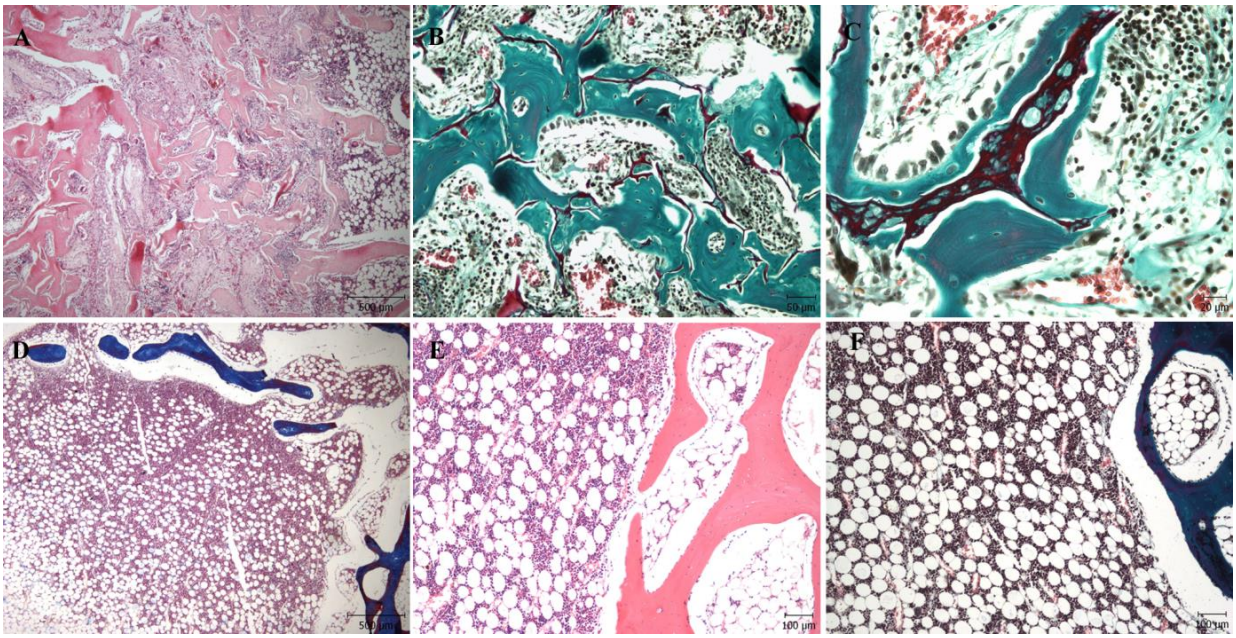

Figure II/ 5: Histology of the healing bone defects with implanted MSCs- and TRS-enriched scaffolds (A-C) compared with the defects in the control group (D-F). (A) Newly formed bone trabecules were found growing from the periphery of the healing bone defect toward its centre. Eosinophilic remnants of bone scaffolds were partially incorporated into the bone trabecules. The space among the trabecules was filled with granulation connective tissue and adipose tissue. (B, C) Newly formed bone (stained green) contained partially resorbed scaffold trabecules (stained reddish). In some parts of the bone, the lamellae formed concentric layers with embedded osteocytes. Most of the surface of the bone was covered with osteoblasts. (D) Bone trabecules were found predominantly at the periphery of the healing defects. (E, F) Central parts of the healing defects were often occupied by bone marrow and adipose tissue without any signs of bone formation. Hematoxylin-eosin (A, E), green trichrome (B, C, F), and Mallory blue trichrome (D) staining.

Bone quantification

With the exception of the samples with scaffolds enriched with both TRS and MSCs, the distribution of the bone tissue was not random, and the null hypothesis of no difference in bone deposition among the compartments was rejected ($p < 0.001$; see Table II/ 3). The use of scaffolds enriched with MSCs, scaffolds enriched with TRS,

or no scaffolds resulted in preferential bone deposition in the outer compartment of the experimental defect (RDI > 1). Only samples containing bone scaffolds enriched with both MSCs and TRS showed uniform bone deposition in all 3 compartments.

The intersections represent the numbers of points of a stereological grid striking the bone tissue. The relative deposition index (RDI) was calculated as the ratio between observed intersections (P_{obs}) and expected intersections (P_{exp}), according to the volume fraction of each compartment within the bone defect. Partial chi-squared values were summed to the total chi-squared value, which was tested against the chi-squared distribution for degrees of freedom = (3-1) rows*(2-1) columns = 2. In the TRS-enriched scaffold, MSCs and TRS-enriched scaffold, in MSC-enriched scaffold samples and in samples without scaffolds, total the chi-squared value was $p < 0.001$. With the exception of the distribution in the MSC- and TRS-enriched scaffold samples, the distribution of bone tissue was nonrandom, and bone was deposited preferentially in the outer compartment (RDI > 1). The proportion of the partial chi-squared value is given in the last column for the compartments in groups with significantly preferential bone deposition (Table II/ 3).

Table II/ 3: Distribution of bone tissue within individual volume compartments in the groups under study.

TRS-enriched scaffold compartment	P_{obs}	P_{exp}	RDI = P_{obs}/P_{exp}	Partial chi-squared values	Proportion of partial chi-squared to total chi-squared values
Outer	1558	1447.78	1.08	8.39	33.32
Middle	823	868.67	0.95	2.40	
Central	225	289.56	0.78	14.39	
				25.18	
Column totals	2606	2606	1	**p < 0.001**	
MSCs- and TRS-enriched scaffold compartment					
Outer	2128	2093.33	1.02	0.57	
Middle	1212	1256.00	0.96	1.54	
Central	428	418.67	1.02	0.21	
Column totals	3768	3768	1	2.32	
MSCs-enriched scaffold compartment					
Outer	1491	1197.22	1.25	72.09	43.65
Middle	521	718.33	0.73	54.21	
Central	143	239.44	0.60	38.85	
				165.14	
Column totals	2155	2155	1	**p < 0.001**	
No scaffold compartment					
Outer	444	338.89	1.31	32.60	44.20
Middle	129	203.33	0.63	27.17	
Central	37	67.78	0.55	13.98	
Column totals	610	610	1	**73.75 p < 0.001**	

The highest bone volume fraction within the healing defect was found in the samples with scaffolds enriched with both MSCs and TRS. The bone volume fraction was comparable between the samples with TRS-enriched scaffolds and MSCs-enriched scaffolds, and the samples without scaffolds contained the lowest bone volume fraction (Figure II/ 6A). A comparison of individual compartments revealed that the bone volume fraction was highest in the samples with scaffolds enriched with both MSCs and TRS. The variability of the bone volume fraction increased from the outer compartment toward the centre of the healing defects (Figure II/ 6 B, C, and D).

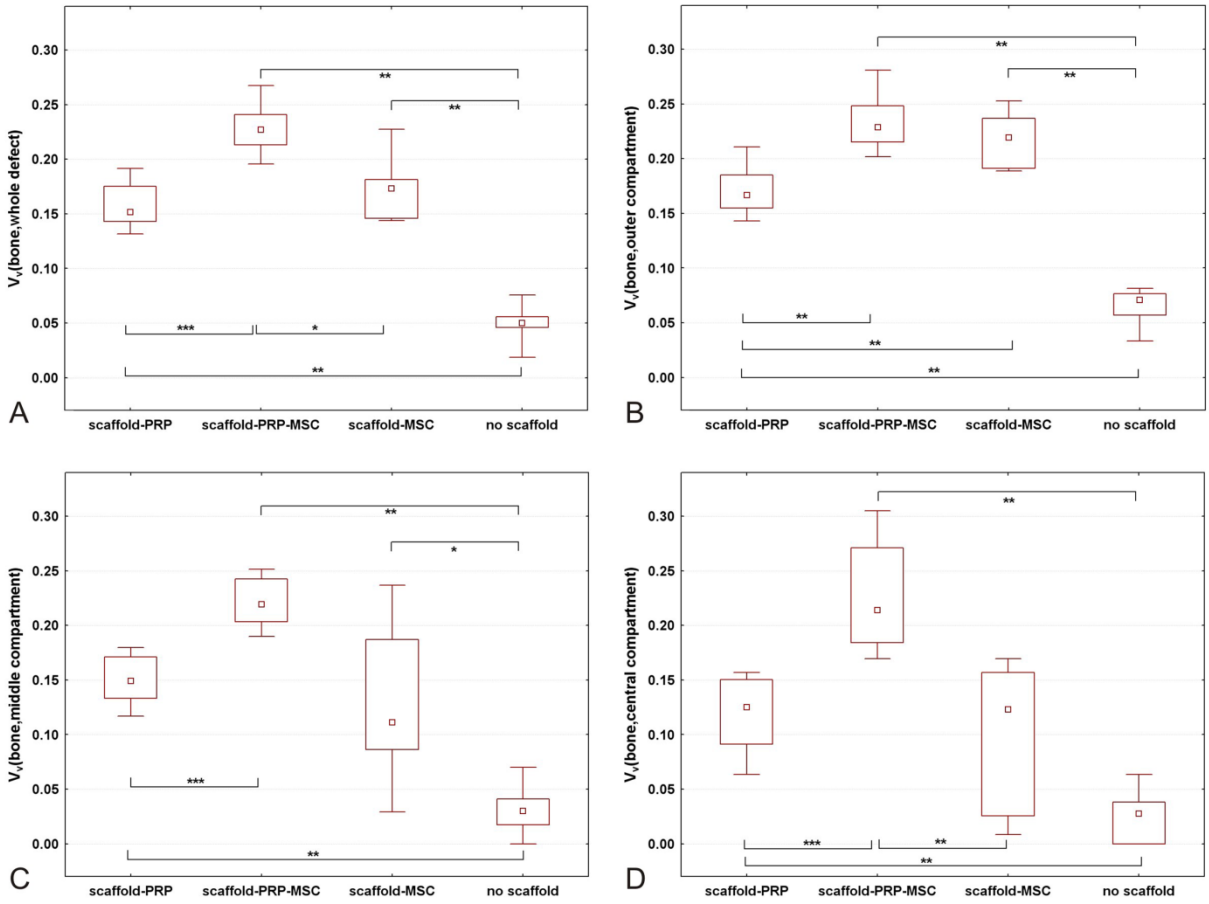

Figure II/ 6: Between-group comparison of bone volume. Bone quantity was expressed as volume fraction (V_v) of the bone tissue within the whole reference volume of the defect (A) or within the outer (B), inner (C), and central (D) compartments. Data is presented as medians. The boxes span the limits of the first and third quartiles, and the whiskers show the non-outlier range for each group. The differences were considered statistically significant as follows: *p < 0.05, **p < 0.01, and ***p < 0.001 (Mann-Whitney *U* test, only significant results are presented here).

Whereas Figure II/ 7 demonstrates examples of good and poor bone regeneration at low magnification in the whole defect (see Figure II/ 7 A, B) and also in the outer, inner, and central compartments (see Figure II/ 7 C-F).

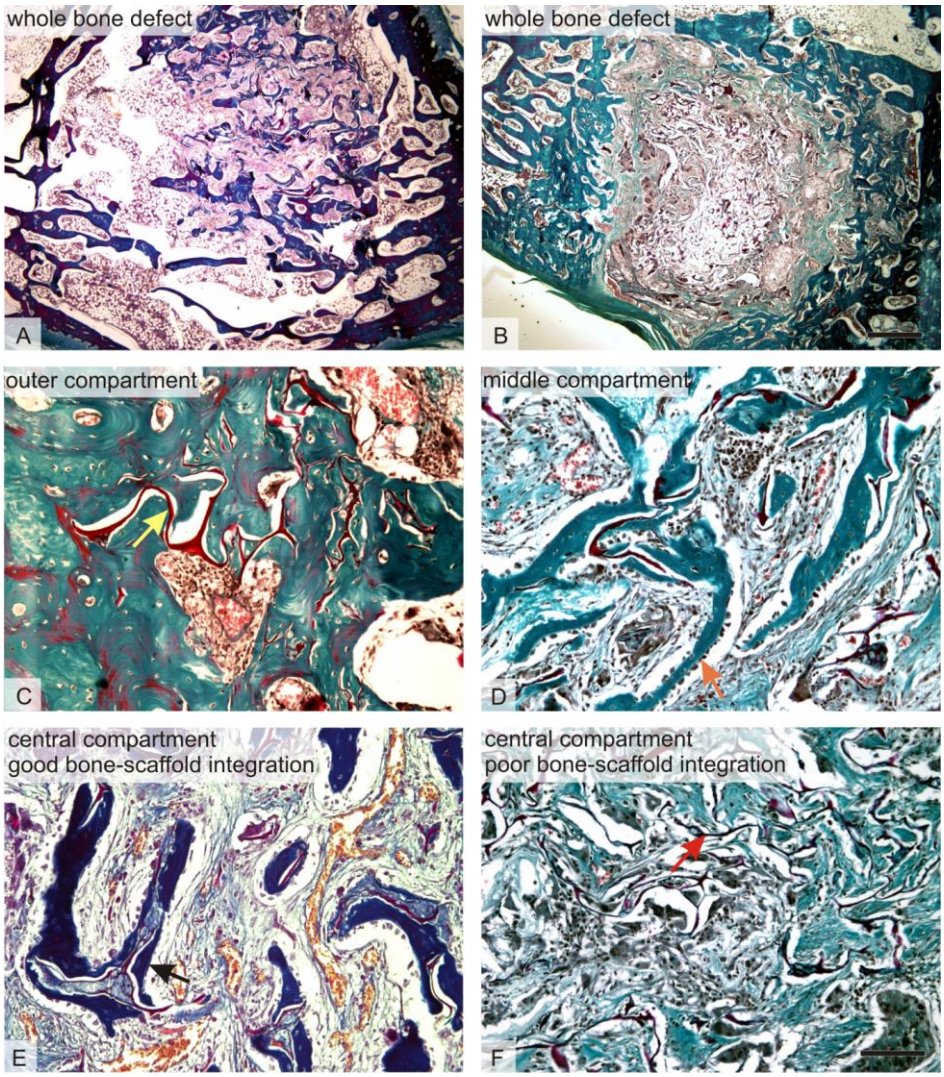

Figure II/ 7: Histology of healing bone defects. (A) In most samples with scaffolds enriched with both TRS and MSCs, bone formation was visible within the whole volume of the healing defect. (B) In some bone defects with MSCs-enriched scaffolds, the centre of the bone defect lacked newly formed bone trabecules. (C) In most samples of the outer compartment, advanced bone formation was found with all scaffold types. Remnants of the scaffolds (yellow arrow) were well integrated with thick bone trabecules. (D,E) The inner (D) and central (E) compartments of samples treated with scaffolds enriched with both TRS and MSCs contained growing bone trabecules covered with osteoblasts (orange [D] and black [E] arrows). (F) Several samples with MSCs-enriched scaffolds lacked bone within the central compartment, and the scaffold remnants (red arrow) were surrounded by connective tissue. Green trichrome (B-D, F) and Mallory stain (A, E). Scale bars: 1 mm (A, B), 100 µm (C-F).

3.2.3. Discussion II

Nanofibers optimized the viscoelastic properties of the Coll/HA scaffold for bone regeneration. The correlation between scaffold stiffness and cell behavior is a key factor in the fabrication of scaffolds for tissue engineering (Hutmacher 2000; Karageorgiou and Kaplan 2005). Scaffold stiffness influences the migration and differentiation of MSCs (Reilly and Engler 2010). Our study is in accordance with several studies which have reported that fibers can improve scaffold mechanical properties (Albanna *et al.* 2012; Chen *et al.* 2013). Clearly, the moduli of elasticity under compressive testing increased significantly when PCL nanofibers were added to the Coll/HA scaffold.

Moreover, recent studies have shown that there is promising potential for drug delivery from nanofibers embedded in a composite foam or gel. In an analogous study focusing on chondral regeneration, we showed that the addition of PVA nanofibers with adsorbed growth factors simultaneously improved the biomechanical properties and cell proliferation on scaffolds in cartilage regeneration (Filova *et al.* 2013).

Our data showed clearly that bone healing throughout the defects was promoted when our novel Coll/HA/ PCL composite scaffold enriched with TRS and seeded with MSCs was applied. This result is in accordance with several previous clinical and animal studies, which have proved that a combination of PRP and autogenous bone grafting can improve osteogenesis and enhance bone formation (Kitoh *et al.* 2004; Martins *et al.* 2010).

However, PRP has several shortcomings. The first concerns standardization of the preparation process, i.e. whether to apply a simple and cheap two-step centrifugation method or to use plasmaphaeresis. While the definition of the parameters for the

centrifugation method seems to be empirical, for plasmaphaeresis we can clarify the content of the product, although the procedure is much more expensive and is uncomfortable for patients. (Prosecká *et al.*, 2014). Another much discussed topic concerns the PRP content, i. e. the presence of leucocytes and fibrin. Whereas leucocytes influence cell proliferation, differentiation, immunity and infection, fibrin changes the biomechanical properties (Dohan Ehrenfest *et al.* 2009). Promotion of bone regeneration in rabbits, even with the use of human TRS was shown in our study. This outcome clearly suggests a minimal immunological negative response, and favors TRS for further preclinical and clinical studies. The application of TRS is also more reproducible than the use of autologous PRP from whole blood. Also, several studies have discussed and compare the effect of synthetic growth factors and PRP. Calori *et al.* (2008) compared the efficacy of recombinant BMP-7 and PRP as bone promoting agents. They support the view that the application of recombinant BMP-7 as a bone-stimulating agent is superior to the application of PRP in terms of clinical and radiological efficiency in the treatment of persistent long bone non-unions.

Many problems remain to be solved, e.g. an effective PRP concentration, donor-based changes, the presence or absence leucocytes or other activators, and differences in scaffold structure. These parameters, and also the time-dependent release of growth factors, may influence bone formation. The relationship between platelet concentration and growth factor liberation seems to provide a key to bone regeneration, but its mechanism is still unclear (Dohan Ehrenfest *et al.* 2009). The effect of various PRP concentrations on tissue healing was reviewed by Wasterlain *et al.* (2012). They described a positive effect of a low PRP number (2 million

platelets/μL) on the promotion of anastomotic wound healing, whereas a higher amount (5 million platelets/μL) inhibited healing (Wasterlain *et al.* 2012).

In our study, we used a TRS concentration of 1.35 x 10^6 thrombocytes/μL, in accordance with the definition of PRP as a minimum of 1 x 10^6 platelets/μL suspended in plasma (Dohan Ehrenfest 2009; Kitoh *et al.* 2004; Wasterlain *et al.* 2012) and 2-h incubation with our composite Coll/HA/PCL scaffold. This TRS concentration promotes bone regeneration and is one of the main outputs of this study (Prosecka *et al.* 2014).

Moreover, calcium ions contained in biomaterials based on bone cement likely work as thrombocyte activators.This is an important consideration in the use of PRP in bone regeneration (Chen *et al.* 2012; Kasten *et al.* 2008).

3.2.4. Conclusion II

The highest volume and the most uniform distribution of newly-formed bone while scaffold biodegradation was gradually taking place was found in defects treated with scaffolds enriched with both MSCs and TRS. There were lower values in defects treated with scaffolds enriched by either component alone. The modulus of elasticity in compressive testing was significantly higher in the Coll/HA/PCL scaffold than in the scaffold without nanofibres. The composite collagen/HA scaffold functionalized with PCL nanofibres and enriched with MSCs and TRS offers a novel, promising treatment for bone defects which could meet the rules for human use.

3.3. Experiment III

Thin-layer hydroxyapatite deposition on a nanofiber surface stimulates Mesenchymal stem cell proliferation and their differentiation into osteoblasts

The aim of the study was to introduce a modern system which will serve as a source of bioactive molecules suitable for regenerating bone defects. The system is based on MSCs and functionalized nanofibers. The nanofibers can be modified on their surface and also enriched in their core with various drugs that could be released slowly over the course of days or weeks.

Pulsed laser deposition was shown to be a suitable method for HA coating of coaxial poly-ε-caprolactone/polyvinylalcohol (PCL/PVA) nanofibers. Thin layers 200, 400, or 800 nm in thickness were deposited onto the nanofiber surface. HA deposition clearly modified the nanofiber surface and significantly influenced the surface properties.

3.3.1. Methods III

3.3.1.1. Coaxial electrospinning of PCL/PVA nanofibers

A 14% (w/v) PCL solution was prepared as the shell solution by dissolving 7 g PCL in 50mL chloroform/ethanol (8 : 2) and Journal of Biomedicine and Biotechnology 3 stirring at room temperature. The core solution consisted of 5% PVA (v/v). The coaxial spinneret apparatus consisted of two needles placed together coaxially (Lukáš *et al.* 2009). Two syringe pumps were used to deliver the core solution and the shell solution. A high-voltage power supply was used to generate voltages of up

to 60 kV, and a span bond was used as the receiving plate to collect the electrospun nanofibers. The distance between the tip of the syringe needle and the collecting plate was 12 cm. All electrospinning processes were performed at room temperature with 56% humidity. In the release study, the core solution consisted of FITC-dextran (2 mg/mL, 10,000 MW) dissolved in 1%, 3%, or 5% (v/v) PVA. The process was performed on the apparatus described above at room temperature with 52% humidity.

3.3.1.2. HA coatings of nanofibers

The prepared nanofibers were coated by HA layers of various thicknesses. HA [$Ca_{10}(PO_4)_6(OH)_2$] films were formed by a KrF epimer laser (COMPexPro 205 F) with 248 nm wavelength, frequency 10 Hz, and energy 600 mJ. The energy density of the laser beam was 2 Jcm^{-2}. The deposition proceeded in an H_2O + Ar atmosphere at a pressure of 40 Pa. The substrate was fixed at a distance of 5 cm from the target HA material (cake of pressed powder). The substrate was at room temperature. HA films of 200 (PCL/PVA200HA), 400 (PCL/PVA400HA), and 800 nm thickness (PCL/PVA800HA) were grown. Pure PCL/PVA core-shell nanofibers were used as a control (PCL/ PVA).

3.3.1.3. Characterization of the scaffolds

The prepared nanofibrous scaffolds were characterized by scanning electron microscopy. Air-dried samples of electrospun HA-coated nanofibers were mounted on aluminum stubs and sputter-coated with a layer of gold approximately 60 nm in thickness using a Polaron sputter coater (SC510, Polaron, now QuorumTechnologies Ltd.) The samples were examined in an Aquasem (Tescan) scanning electron microscope in the secondary electron mode at 15 kV (Figure III/ 1 a, b, c, d).

3.3.1.4. Mechanical characterization of the scaffolds

The Young's moduli of elasticity, the ultimate stresses and the ultimate strains of the scaffolds were obtained at room temperature using a Zwick/Roell traction machine equipped with a 1 kN load cell. Due to difficulty in producing a layer of PCL/PVA nanofibers of uniform thickness, only the samples with the same thickness of the basic layer of PCL/PVA nanofibers of pure samples and also with the layer of HA were used for mechanical testing. The samples without a layer of HA were therefore marked as type I (n = 4), and the samples with the HA layer were marked as type II (n = 7). The samples themselves were thin strips of the nanofibers. The initial length of all samples was 10 mm. All samples were 10 mm in width. The individual samples were about 60 μm in thickness. The samples were prepared in accordance with Narbath *et al.* (2006) and Olah *et al.* (2006).The template of paper 20 x 50 mm (height x width) with a centered rectangular hole 10 x 40 mm was cut, and lines marking sample strips 10 mm in width were drawn on its top and bottom stripes. Then it was glued to the sheet of composite, and two other strips of paper 5 x 50 mm were glued to the back faces of the top and bottom stripes. The individual scaffolds were then cut, resulting in four 20 x 10 mm strips consisting of a 10 x 10 mm sample between two 5 x 10 mm strips of paper. A tensile test with a loading velocity of 10 mm/min was applied to the samples. The load was applied until the scaffold ruptured. The Young's moduli of elasticity were determined using linear regression of the stress-strain curves at a strain of approximately 1–6% (linear region depending on the shape of the curve). The ultimate stress and the ultimate strain were determined at the start of the rupture. The stress was defined as the force divided by the initial area, and the strain was defined as the elongation of the specimen divided by its

initial length. Our own software written in Python programming language was used for the evaluation (Figure III/ 2).

3.3.1.5. Isolation and cultivation of MSCs

Blood marrow aspirates were obtained from the os ilium (tuber coxae Ala ossis iili) of anesthetized miniature pigs (age 6–12 months) as was already mentioned in previous section *3.1.1.2.*

3.3.1.6. Seeding MSCs on the scaffolds

The scaffolds were cut into a round shape with a diameter of 6mm and were sterilized using ethylene oxide. Cells were seeded on the scaffolds at a density of 70 × 10^3/cm^2 in a 96-well plate. Scaffolds with seeded MSCs were cultivated in differentiation media: MEM supplemented with 10% FBS, penicillin/streptomycin (100 IU/ mL and 100 µg/mL, resp.), 100nM dexamethasone, 40 µg/ mL ascorbic acid-2-phosphate and 10nM glycerol 2-phosphate disodium salt hydrate. The medium was changed every 3 days.

3.3.1.7. Cell viability analysis by the MTT test

50 µL of [3-(4,5-dimethylthiazol-2-yl)-2,5-diphenyltetrazolium bromide] (MTT), and 1mg/mL in PBS (pH 7.4) were added to 150 µL of sample medium and incubated for 4 hours at 37°C as was already mentioned in previous section *3.1.1.4*. The results were examined by spectrophotometry in an ELISA reader at 570 nm (reference wavelength 690 nm) (Figure III/ 3).

3.3.1.8. Cell viability analysis by the Live/dead staining

Live/dead staining (BCECF-AM/propidium iodide) and visualization using confocal microscopy were performed to determine cell viability as was already mentioned in previous section *3.1.1.5*. Zeiss LSM 5 DUO confocal microscope (wavelengths: BCECF-AM λ_{ex} = 488 nm and λ_{em} = 505– 535 nm; propidium iodide λ_{ex} = 543 nm and λ_{em} = 630– 700 nm) (Figure III/ 1 e, f, g, h).

3.3.1.9. Cell proliferation analysis by the PicoGreen

The PicoGreen assay was carried out using the Invitrogen PicoGreen assay kit (Invitrogen Ltd., Paisley, UK). The proliferation of MSCs on the scaffolds was tested on days 1, 7, and 14. The material for an analysis of the DNA content, 250 µL of cell lysis solution (0.2% v/v Triton X-100, 10mM Tris (pH 7.0), 1mM EDTA), was added to each well containing a scaffold sample. To prepare the cell lysate, the samples were processed through a total of three freeze/thaw cycles. A scaffold sample was first frozen at −70°C and then thawed at room temperature. Between each freeze/thaw cycle, the scaffolds were roughly vortexed. The prepared samples were stored at −70°C until analysis. To quantify the cell number on the scaffolds, a cell-based standard curve was prepared using samples with known cell numbers (range 100–10^6 cells). The DNA content was determined by mixing 100 µL of PicoGreen reagent and 100 µL of the DNA sample. The samples were loaded in triplicate, and the florescence intensity was measured on a multiplate fluorescence reader (Synergy HT, λ_{ex} = 480–500 nm, λ_{em} = 520– 540 nm). The measured data was used to derive the absorbance values measured by the MTT assay to the cell counts on the scaffolds (Figure III/ 3).

3.3.1.10. Quantitative real-time PCR Analysis

Total RNA was extracted using an RNeasy Mini Kit according to the manufacturer's protocol. Total RNA was stored at –20°C. The cDNA from 1 µg of total RNA was used as a template. cDNA synthesis was performed by a standard procedure described in our previous work (Tvrdik *et al.* 2005). BS and OC mRNA expression levels were quantified by means of a LightCycler 480 (Roche Diagnostics, Mannheim, Germany) using the double-strand specific dye SYBR Green I according to the manufacturer's protocol. The following primers were used: BS, sense 5-CGA CCA AGA GAG TGT CAC-3, antisense 5-GCC CAT TTC TTG TAG AAG C-3 (498 bp); OC, sense 5-TCA ACC CCG ACT GCG ACG AG-3, antisense 5-TTG GAG CAG CTG GGA TGA TGG-3 (204 bp) and beta-actin, sense 5-AGG CCA ACC GCG AGA AGA TGA CC-3, antisense 5-GAA GTC CAG GGC GAC GTA GCA C-3 (332 bp) as was already mentioned in previous section *3.1.1.7.* (Figure III/ 4).

3.3.1.11. Measurement of the FITC-Dextran release profile

In order to study the release profile of FITC-dextran, core-shell nanofiber meshes with 1% PVA, 3% PVA, or 5% PVA were cut into round patches and incubated with 1mL of TBS buffer at room temperature. At specific intervals, the TBS buffer was withdrawn and replaced with a fresh buffer. The time interval was determined keeping in mind the balance between the release of a detectable amount of FITC-dextran and maintenance of the sink condition. Drug release was quantified using fluorescence spectroscopy. Briefly, 200 µL of samples and blank samples were measured on a multiplet fluorescence reader (Synergy HT, λ_{ex} = 480–500 nm, λ_{em} = 520–540 nm) and background subtraction was performed. The cumulative release profile of FITC-dextran was obtained, and the half time of release was determined as

the time at which the initial fluorescence intensity I_0 decreased to $I = I_0 \times e^{-1}$ (Figure III/ 5).

3.3.1.12. Statistical analysis

Quantitative data are presented as mean SD. For the *in vitro* tests, average values were determined from at least three independently prepared samples. The results were evaluated statistically using one-way analysis of variance (ANOVA) and the Student-Newman-Keuls Method and the Shapiro-Wilk W test was used to determine the normality of the Young's moduli of elasticity, the ultimate strains and the ultimate stresses. The t-test was used to determine the differences between values. The Student t-test was used to evaluate the statistical significance of the results of quantitative real-time PCR analysis. Differences with P values <0.05 were considered significant.

3.3.2. Results III

3.3.2.1. Visualization of scaffolds

Scanning electron microscopy revealed the fibrous morphology of the PCL/PVA nanofibers (Figure III/ 1a). Pulsed laser deposition of an HA layer 200 nm in thickness did not affect the fibrous morphology or the porosity of the nanofibers (Figure III/ 1b). However, the fibrous character of the samples with an HA layer 400 nm in thickness (Figure III/ 1c) was less well preserved, and the porosity of the scaffold decreased. The fibrous morphology disappeared completely in samples with an HA coating 800 nm in thickness (Figure III/ 1d).

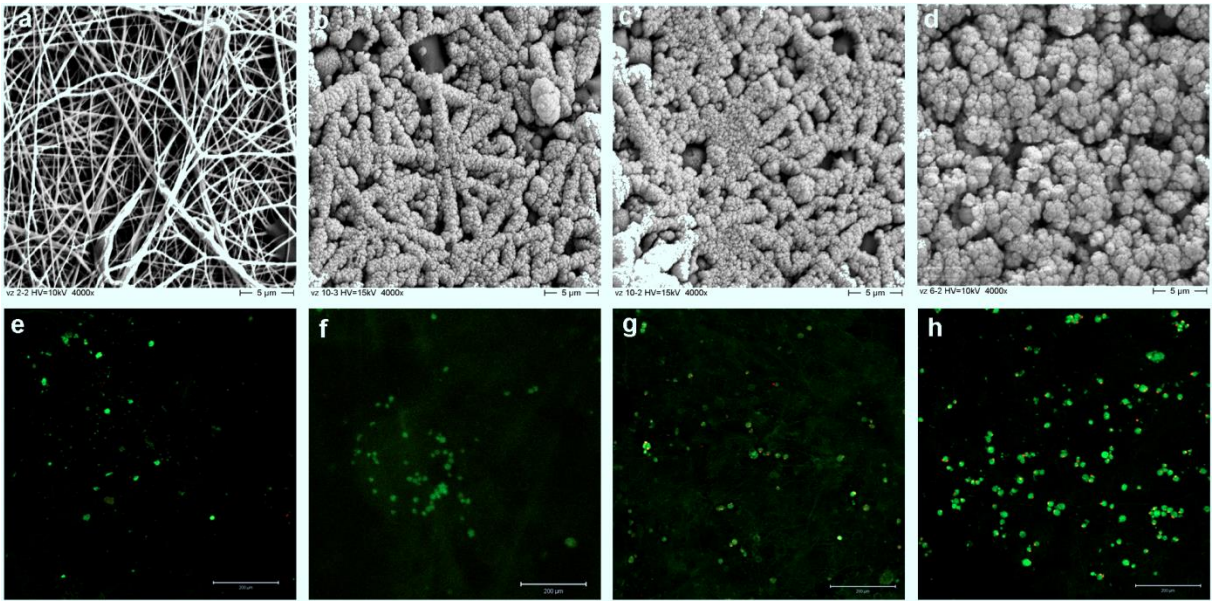

Figure III/ 1: Visualization of scaffolds by SEM and confocal microscopy. The prepared scaffolds were visualized using SEM (a, b, c, d). On day 7, MSCs were stained using BCECF-AM and propidium iodide for live/dead staining and the samples were visualized by confocal microscopy (e, f, g, h); PCL/PVA (a, e), PCL/PVA200HA (b, f), PCL/PVA400HA (c, g) and PCL/PVA800HA (d, h).

3.3.2.2. Mechanical characterization of the scaffolds

There is a significant difference in the moduli of elasticity between these groups (determined by the T-test; p = 0.04) (Figure III/ 2a) and also in the ultimate strain (p<0.001) (Figure III/ 2b), but not in the ultimate stress (p = 0.26) (Figure III/ 2c). We found significant differences in Young's moduli of elasticity between samples without an HA layer and those with an HA layer (*P* = 0.04). The Young's modulus of elasticity in the case of pure PCL/PVA nanofibers was 1.76 ± 0.50 Mpa, while the modulus for the samples with an HA layer was 5.40 ± 3.09 MPa; the difference was significant (see Figure III/ 2a). Significant differences between these two groups were also found in the case of ultimate strains (*P* < 0.001). Here, the value obtained for pure PCL/PVA scaffolds was 0.23 ± 0.03, while for scaffolds with an HA layer the value

was 0.09 ± 0.04, (see Figure III/ 2b). No significant differences were found when analyzing the ultimate stresses (P = 0.26), although the value for the group with an HA layer, 0.36 ± 0.27 MPa, was higher than the value for the pure PCL/PVA scaffolds, 0.19 ± 0.07 MPa (see Figure III/ 2c).

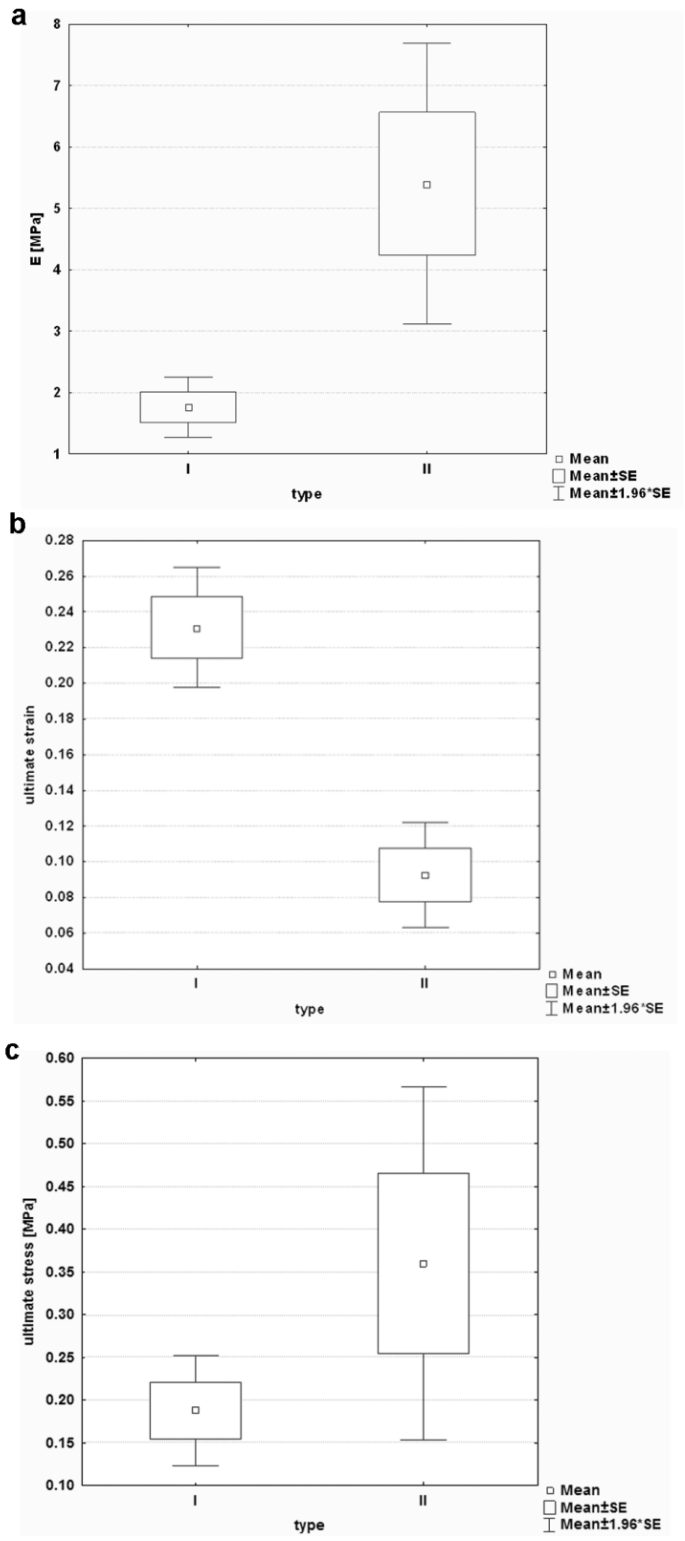

Figure III/ 2: The moduli of elasticity, the ultimate strain and ultimate stress of the group of the pure PCL/PVA composite (type I) and the group of the PCL/PVA composite covered by an HA layer (type II). Mean indicates the mean value, SE is the standard error.

3.3.2.3. Cell metabolic activity and viability

The metabolic activity of viable MSCs was detected by MTT assay on day 1, 7, and 14 (Figure III/ 3).

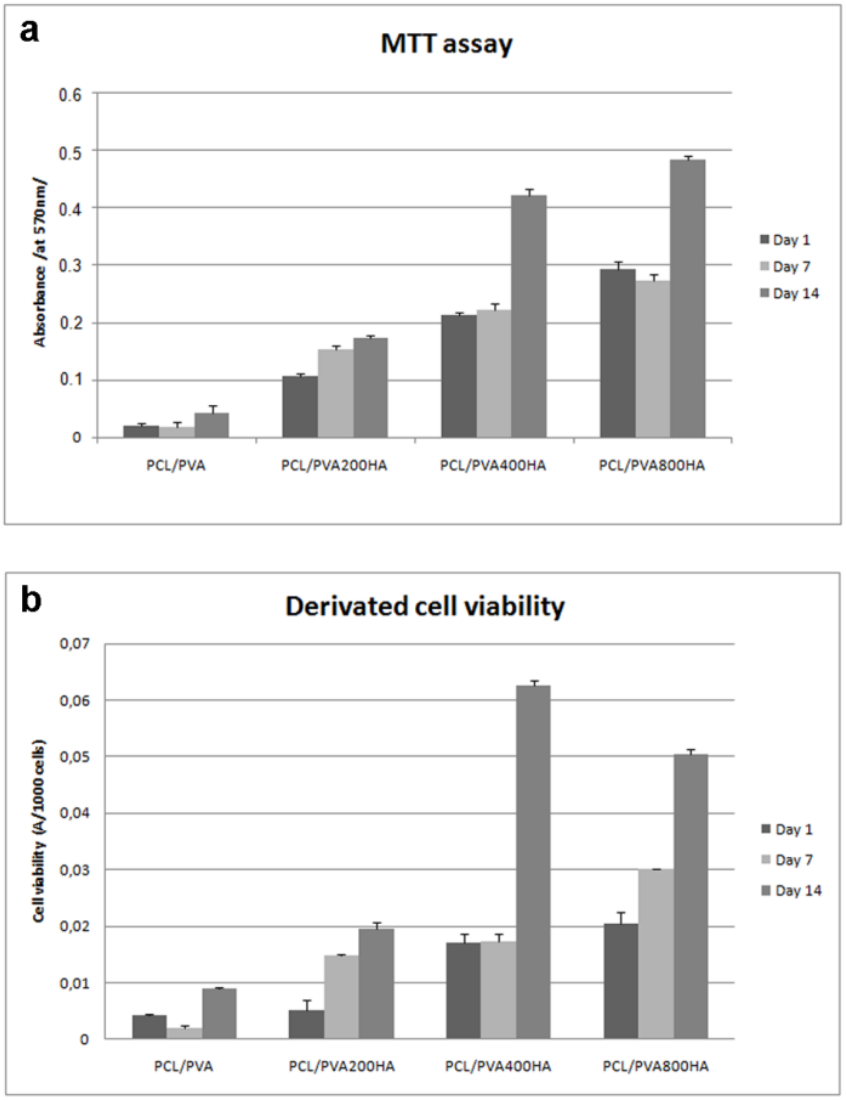

Figure III/ 3: Cell metabolic activity and viability. Results of the MTT assay for PCL/PVA, PCL/PVA200HA, PCL/PVA400HA, PCL/PVA800HA samples (a). Cell viability calculated as derivation of absorbance values from the MTT assay to the cell counts determined by Pico Green assay (b). (Mean ± SD). Statistical significant differences between scaffolds were observed by MTT test on day 14: PCL/PVA800HA> PCL/PVA, PCL/PVA200HA; PCL/PVA400HA> PCL/PVA, PCL/PVA200HA.The significant differences between scaffolds

were also found on day 14 after MTT/Pico Green results derivation: PCL/PVA400HA> PCL/PVA, PCL/PVA200HA, PCL/PVA800HA; PCL/PVA800HA> PCL/PVA, PCL/PVA200HA.

3.3.2.4. Expression of bone tissue markers

Osteogenic differentiation of MSCs was detected by real-time PCR analysis of OC and BS expression on day 7 and 14. Interestingly, the samples with an HA coating 800 nm in thickness were characterized by a significantly higher expression of BS and OC genes than the pure PCL/PVA samples (Figure III/ 4).

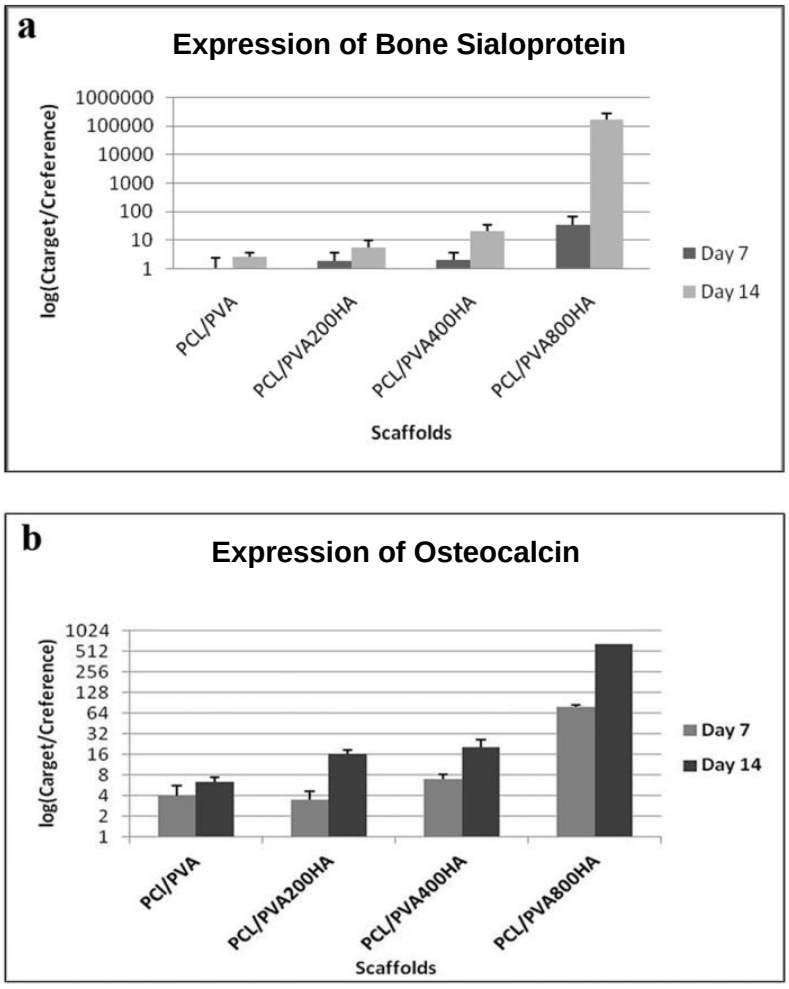

Figure III/ 4: Expression of bone tissue markers. The expression levels of BS and OC mRNAs, osteogenic markers, were detected on day 7 and 14 for all samples. (Mean ± SD).

3.3.2.5. Time-dependent release profile of coaxial PCL/PVA nanofibers

The release of FITC-dextran from samples with a different content of PVA core was analyzed using fluorescence spectroscopy. Samples were analyzed for 240 h, supernatants were collected at intervals of 24 h. The half-time of release from coaxial nanofibers was strongly dependent on the presence of a hydrophilic core polymer (Figure III/ 5).

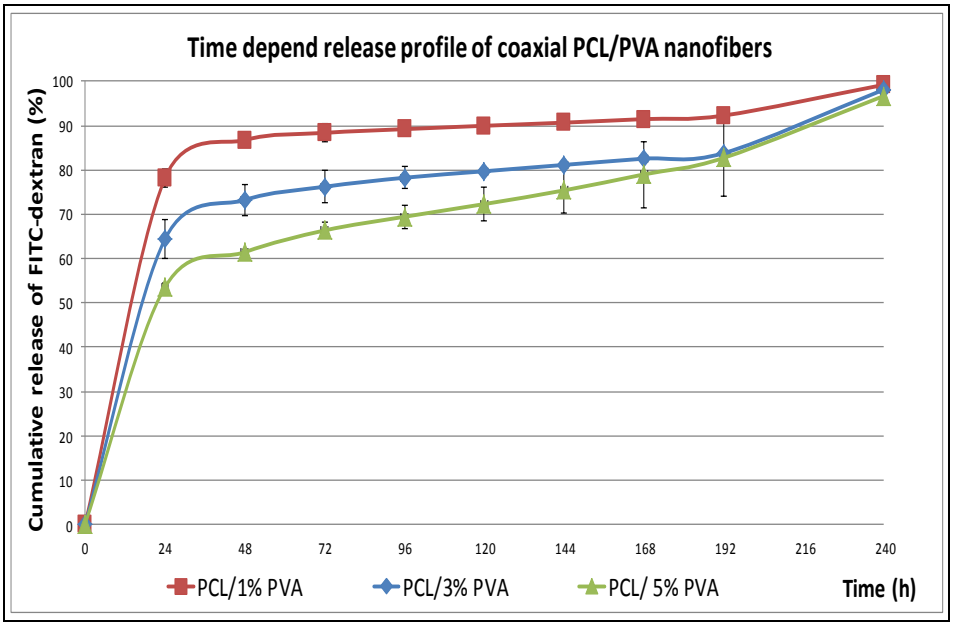

Figure III/ 5: Time-dependent release profile of coaxial PCL/PVA nanofibers. Core/shell nanofibers containing FITC-dextran dissolved in 1% PVA showed the highest burst release (79% of FITC-dextran released in 24 h). The half time of release was calculated as τr = 18 h. The release of FITC/dextran from fibers with 3% PVA showed a slower release; however, an intense burst release was observed (65% of FITC-dextran released in 24 h). The half-time of release was prolonged to 24 h. Interestingly, samples with 5% PVA as the core polymer showed the most sustained release profile. The burst release was reduced to 52% of FITC-dextran release in 24 h, and the half-time of release was shifted to 54 h. The results show

clearly that different concentrations of the water-soluble core significantly affect the release profiles of incorporated substances. (Mean ± SD).

3.3.3. Discussion III

Coaxial core-shell nanofibers were prepared from PCL as a shell material and PVA as a core material. PCL has good biocompatibility and enables the successful cultivation of MSCs (Jakubova *et al.* 2011) and osteogenic cells (Rampichova *et al.* 2013). However, PVA is a water-soluble material and has been employed as a suitable substance for the delivery of bioactive compounds from the nanofiber core (Buzgo *et al.* 2013). To improve the surface parameters for MSCs seeding, coaxial nanofibers were further functionalized by pulsed laser deposition of HA. Thin layers 200, 400, or 800 nm in thickness were deposited onto the nanofiber surface. HA deposition clearly modified the nanofiber surface and significantly influenced the surface properties. Scanning electron microscopy revealed the fibrous morphology of PCL nanofibers (Figure III/ 1a). Pulsed laser deposition of an HA layer 200 nm in thickness did not affect the fibrous morphology or the porosity of the nanofibers (Figure III/ 1b). However, the fibrous character of samples with an HA layer 400 nm in thickness (Figure III/ 1c) was less well preserved, and the porosity of the scaffold decreased. The fibrous morphology disappeared completely in samples with an HA coating 800 nm in thickness (Figure III/ 1d).

The proliferation and the differentiation of MSCs on HA coated scaffolds are separate processes. Our HA-coated nanofiber scaffolds clearly displayed a positive effect on the differentiation of MSCs into osteogenic cells, but not on cell proliferation.

On the basis of these results, the HA layer 800 nm in thickness has been demonstrated to be optimal for osteogenic differentiation of cells and for bone tissue engineering applications.

3.3.4. Conclusion III

The more positive effect of HA coated nanofiber scaffolds on cell proliferation observed in our study could be improved. Core/shell nanofibers offer a promising new approach as a system for delivering bioactive molecules directly into a tissue defect site. Proliferation and stimulating factors can be encapsulated into the core of the nanofibers. The encapsulation of bioactive agents inside the nanofibers can increase their ability to stimulate proliferation and thus further improve the positive effect of nanofiber scaffolds on MSCs proliferation and differentiation. HA coated coaxial PCL/PVA nanofibers seems to be a promising novel drug delivery system suitable for bone tissue engineering.

In addition, the biomechanical properties were improved after HA deposition on PCL/PVA nanofibers, as the value of the Young's modulus of elasticity increased significantly after HA deposition (Prosecka *et al.* 2012).

4. Conclusion

The causes of large bone defects include tumours, infectious diseases and traumas. There is a medical need for bone regeneration as a way to treat these defects. It is well known nowadays that the successful treatment of bone loss requires a combination of an osteoinductive signal, an osteoconductive matrix, and cell response to the osteogenic potential (Bose *et al.* 2012; Cancedda 2003).

Therefore, there is a major clinical need to promote the development of strategies to replace diseased bone tissue with a graft capable of integrating with the surrounding healthy tissue (Kitoh *et al.* 2004).

Many materials have been reported to fulfil these requirements, including natural/synthetic polymers, metals and ceramics (Cancedda 2003; Liu *et al.* 2007). Many of them, e.g. HA and collagen, are known as osteoinductive and osteoconductive materials and they enhance osteogenic differentiation when seeded with MSCs (Heino *et al.* 2004; Kraus and Kirker-Head 2006; Mao *et al.* 2005; Marks and Odgren 2002).

The current standard in tissue engineering is to combine cells, especially autologous cells, and osteoconductive scaffolds, which can be functionalized with growth factors, preferentially serving as a controlled delivery device (Bose *et al.* 2012).

On the basis of a study of current literature, we prepared a promising new smart scaffold with potential for clinical use. We found an optimal ratio of biocompatible, biodegradable, osteoconductive and also osteoinductive materials for a 3D scaffold with optimal pores for cell ingrowth and vascularization (Prosecka *et al*. 2014). During our *in vitro* and *in vivo* studies, we found that a 0.5% Type I collagen and 50% of HA

(1:1 wt%) 3D scaffold with pore size around 400 um is the most suitable for cell proliferation, viability and differentiation of MSCs differentiated into osteoblasts, while the mechanical properties were still good (Prosecka *et al*. 2011). However, we also wanted to improve the mechanical properties of the scaffold, and make it more suitable for *in vivo* testing. We found that PCL nanofibers mixed into the 3D Coll/HA scaffold significantly improved the mechanical properties of the scaffold. We also wanted to know the effect of PRP on accelerating bone healing. We found in the *in vivo* study, that Coll/HA scaffolds enriched with MSCs or with TRS, or with both MSCs and TRS, promoted much better formation of new bone tissue throughout the defect than when the defect was left to heal without treatment. However, the scaffold enriched with both MSCs and TRS supported the best formation of new bone tissue and also the most uniform distribution of newly-formed bone (Prosecka *et al*. 2014).

We went on to investigate a fabrication process, and we prepared a scaffold from materials that meet the European Medicines Agency requirements and can be developed for human applications.

We also found pulsed laser deposition, a suitable method for modifying the surface of high temperature sensitive materials, and a suitable thickness (800 nm) of the HA layer for MSCs differentiation (Prosecka *et al*. 2012).

However, one of the most discussed issues in the area of tissue engineering is the ability to generate appropriate numbers of cells when too many cells can be just as detrimental as too few, and the capacity for those cells to differentiate from, and maintain, the correct phenothype and perform specific biological functions. Other issues are invasivity and site morbidity due to cell harvesting, *in vitro* cultivation, sterility, high costs, the use of fetal bovine serum, time duration, etc. (Filova *et al.* 2013).

It is nowadays increasingly accepted that there is a “wound healing cascade” thanks to which the self-healing capacity of patients can be supported by artificial acceleration of the proliferation and differentiation of the recruited cells by applying growth factors and cytokines (Andreadis and Geer 2006; Varkey 2004; Vasita and Katti 2006).

However, a complication caused by a burst release of high doses of growth factors has led to extensive ongoing studies to develop a drug delivery system that can provide efficacy of growth factors at lower doses, or release them gradually, or retard their release. Controlled delivery of growth factors can be achieved by using a scaffold which prevents proteolysis and loss of bioactivity, and thus enables a prolonged therapeutic effect (Babensee *et al.* 2000).

Controlled release could lead to a more physiological healing cascade and be of significant importance for the tissue regeneration outcomes. For example, TGF-β plays a critical role in bone fracture healing through the production of ECM during the late phases, while SDF-1 acts in the early phases. In order to achieve improved healing effects, it is therefore beneficial to produce a system enabling fast release of SDF-1 and delayed release of TGF-beta. The delivery system should provide time- and dose-controlled release of the bioactive growth factor, should offer a scaffold that enhances cell recruitment and attachment, and should promote cell migration and angiogenesis. Natural growth factors from platelets deliver numerous growth factors in a balanced physiological ratio, and have been shown to successfully regenerate bone defects in clinical practice (Kitoh *et al.* 2004; Saluja *et al.* 2011; Simman *et al.* 2008). However, there are some disadvantages, e.g. short retention and delivery time of platelets, which do not correspond with the requirements for slowly-healing

fractures (Saluja *et al.* 2011). A combination of platelets with advanced drug delivery systems could solve this problem (Puppi *et al.* 2014).

5. Future perspectives

Controlled release of proliferation and growth factors *in situ* is a promising bionanotechnological approach to tissue regeneration. Nanofibers with controlled release of proliferation and differentiation factors are undoubtedly a suitable tool for tissue engineering. The incorporation of nanofibers functionalized with bioactive agents, such as PRP derivatives or growth factors, into 3D composite scaffolds has a positive effect not only on the biomechanical properties of the scaffold, but also on enhancing bone or osteochondral regeneration, mainly by recruiting stem cells from the subchondral bone and subsequently differentiating them. In addition, the development of functionalized scaffolds mimicking and fitting to the bone part of the defect is an important task for the future that has an impact on successful healing.

6. Summary

A promising new smart scaffold with potential for clinical use was prepared during our experiments. The biocompatible, biodegradable, osteoconductive and also osteoinductive 3D scaffold contains 0.5% type I collagen and 50% of hydroxyapatite with pore size around 400 um suitable for cell ingrowth and vascularization. Subsequently added poly-ε-caprolactone nanofibers improved the mechanical properties of the scaffold. The scaffold was enriched with mesenchymal stem cells and thrombocyte rich solution. The functionalized scaffold promoted new bone tissue formation throughout the defects, with uniform distribution of the newly-formed bone *in vivo* in a rabbit model, while the scaffold gradually degraded and was replaced by newly-formed bone tissue. In addition, we have found a fabrication process and materials which meet the European medicines agency requirements and can be developed for human applications. Hydroxyapatite-coated coaxial poly-ε-caprolactone/polyvinylalcohol nanofibers have been developed as a promising novel drug-delivery system suitable for bone tissue engineering.

7. Abstrakt

Výsledkem *in vitro* a *in vivo* studií je nový, biokompatibilní, biodegradabilní, osteokonduktivní a osteoinduktivní 3D scaffold s vysokým potenciálem pro klinické použití. Scaffold složený z 0.5% kolagenu typu I s 50 % hydroxyapatitu s velikostí pórů v průměru 400 μm, je vhodný pro buněčnou migraci, proliferaci, diferenciaci a vaskularizaci. Následně přidaná poly-ε-kaprolaktonová nanovlákna zlepšila mechanické vlastnosti scaffoldu. Scaffold byl dále obohacen mesenchymálními kmenovými buňkami a trombocytárním koncentrátem jako přírodním zdrojem růstových faktorů. Tento funkcionalizovaný scaffold byl postupně nahrazen novou kostní tkání po implantaci *in vivo*, a to v celém objemu defektu, v kondylu femuru králíka za jeho postupné biodegradace. Pro výrobu tohoto scaffoldu byly navíc použity materiály a výrobní postupy splňující podmínky Evropské lékové agentury pro humánní použití. V průběhu experimentů byl též vyvinut slibný systém pro dodávání bioaktivních látek pro regeneraci kostní tkáně založený na koaxiálních nanovláknech z poly-ε-kaprolaktonu a polyvinylalkoholu.

8. References

1. ABDAL-HAY, A., L. D. TIJING AND J. K. LIM *Characterization of the surface biocompatibility of an electrospun nylon 6/CaP nanofiber scaffold using osteoblasts.* Chemical Engineering Journal, Jan 15 2013, 215, 57-64.
2. ABOUSLEIMAN, R. I. AND V. I. SIKAVITSAS *Bioreactors for tissues of the musculoskeletal system*. Adv Exp Med Biol, 2006, 585, 243-259.
3. AHN, H. J., W. J. LEE, K. KWACK AND Y. D. KWON *FGF2 stimulates the proliferation of human MSCs through the transient activation of JNK signaling*. FEBS Lett, Sep 3 2009, 583(17), 2922-2926.
4. ALBANNA, M. Z., BOU-AKL, T. H., WALTERS, H. L., 3RD, MATTHEW, H. W. *Improving the mechanical properties of chitosan-based heart valve scaffolds using chitosan fibers*. J Mech Behav Biomed Mater, Jan 2012, 5(1), 171-180.
5. ANDREADIS, S. T. A. G., D. J. *Biomimetic approaches to protein and gene delivery for tissue regeneration*. Trends Biotechnol, Jul 2006, 24(7), 331-337.
6. BABENSEE, J. E., MCINTIRE, L. V., MIKOS, A. G. *Growth factor delivery for tissue engineering*. Pharm Res, May 2000, 17(5), 497-504.
7. BAENZIGER, N. L., G. N. BRODIE AND P. W. MAJERUS *A thrombin-sensitive protein of human platelet membranes*. Proc Natl Acad Sci U S A, Jan 1971, 68(1), 240-243.
8. BANDYOPADHYAY-GHOSH, S. *Bone as a collagen-hydroxyapatite composite and its repair*. Trends Biomater Artif Org, 2008, 22, 112–120.
9. BAO, Q. H., C. Z. CHEN, D. G. WANG, Q. M. JI, *et al. Pulsed laser deposition and its current research status in preparing hydroxyapatite thin films*. Applied Surface Science, Dec 2005, 252(5), 1538-1544.
10. BARRERE, F., C. A. VAN BLITTERSWIJK AND K. DE GROOT *Bone regeneration: molecular and cellular interactions with calcium phosphate ceramics*. Int J Nanomedicine, 2006, 1(3), 317-332.
11. BARRON, V., E. LYONS, C. STENSON-COX, P. E. MCHUGH, *et al. Bioreactors for cardiovascular cell and tissue growth: a review*. Ann Biomed Eng, Oct 2003, 31(9), 1017-1030.
12. BENTZ, H., SCHROEDER, J.A., ESTRIDGE, T.D. *Improved local delivery of TGF-β2 by binding to injectable fibrillar collagen via difunctional polyethylene glycol.* Journal of Biomedical Materials Research. 1998(39):539-48.
13. BERNER, A., BOERCKEL, J.D., SAIFZADEH, S., STECK, R., *et al*. *Biomimetic tubular nanofiber mesh and platelet rich plasma-mediated delivery of BMP-7 for large bone defect regeneration.* Cell and tissue research. 2012(347):603-12.
14. BI, L., CHENG, W., FAN, H., PEI, G. *Reconstruction of goat tibial defects using an injectable tricalcium phosphate/chitosan in combination with autologous platelet-rich plasma*. Biomaterials, Apr 2010, 31(12), 3201-3211.
15. BLAIR, P. AND R. FLAUMENHAFT *Platelet alpha-granules: basic biology and clinical correlates*. Blood Rev, Jul 2009, 23(4), 177-189.
16. BLAKENEY, B. A., A. TAMBRALLI, J. M. ANDERSON, A. ANDUKURI, *et al. Cell infiltration and growth in a low density, uncompressed three-dimensional electrospun nanofibrous scaffold*. Biomaterials, Feb 2011, 32(6), 1583-1590.
17. BLIND, O., L. H. KLEIN, B. DAILEY AND L. JORDAN. *Characterization of hydroxyapatite films obtained by pulsed-laser deposition on Ti and Ti-6AL-4v substrates*. Dent Mater, Nov 2005, 21(11), 1017-1024.

18. BOCCACCINI, A. R. *3 - Ceramics*. In L.L. HENCH AND J.R. JONES. *Biomaterials, Artificial Organs and Tissue Engineering.* Woodhead Publishing, 2005, http://dx.doi.org/10.1533/9781845690861.1.26, p. 26-36.
19. BOSE, S., ROY, M. AND BANDYOPADHYAY, A. *Recent advances in bone tissue engineering scaffolds*. Trends Biotechnol, Oct 2012, 30(10), 546-554.
20. BUZGO, M., JAKUBOVA, R., MICKOVA, A., RAMPICHOVA, M., *et al. Time-regulated drug delivery system based on coaxially incorporated platelet alpha-granules for biomedical use*. Nanomedicine (Lond), Jul 2013, 8(7), 1137-1154.
21. CALORI, G. M., L. TAGLIABUE, L. GALA, M. D'IMPORZANO, *et al. Application of rhBMP-7 and platelet-rich plasma in the treatment of long bone non-unions: a prospective randomised clinical study on 120 patients*. Injury, Dec 2008, 39(12), 1391-1402.
22. CAMPAGNOLI, C., I. A. ROBERTS, S. KUMAR, P. R. BENNETT, *et al. Identification of mesenchymal stem/progenitor cells in human first-trimester fetal blood, liver, and bone marrow*. Blood, Oct 15 2001, 98(8), 2396-2402.
23. CANCEDDA, R., DOZIN, B., GIANNONI, P., QUARTO, R. *Tissue engineering and cell therapy of cartilage and bone*. Matrix Biol, Mar 2003, 22(1), 81-91.
24. CAO, Y., J. P. VACANTI, K. T. PAIGE, J. UPTON, *et al. Transplantation of chondrocytes utilizing a polymer-cell construct to produce tissue-engineered cartilage in the shape of a human ear*. Plast Reconstr Surg, Aug 1997, 100(2), 297-302; discussion 303-294.
25. CARRIER, R. L., M. RUPNICK, R. LANGER, F. J. SCHOEN, *et al. Perfusion improves tissue architecture of engineered cardiac muscle*. Tissue Eng, Apr 2002, 8(2), 175-188.
26. CARVER, S. E. AND C. A. HEATH *Semi-continuous perfusion system for delivering intermittent physiological pressure to regenerating cartilage*. Tissue Eng, Feb 1999, 5(1), 1-11.
27. CURREY, J. D. *The structure and mechanics of bone*. Journal of Materials Science, Jan 2012, 47(1), 41-54.
28. DAWSON, J. I. AND R. O. OREFFO *Bridging the regeneration gap: stem cells, biomaterials and clinical translation in bone tissue engineering*. Arch Biochem Biophys, May 15 2008, 473(2), 124-131.
29. DE BOER, J., C. VAN BLITTERSWIJK AND C. LOWIK *Bioluminescent imaging: emerging technology for non-invasive imaging of bone tissue engineering*. Biomaterials, Mar 2006, 27(9), 1851-1858.
30. DE LA CAFFINIERE, J. Y., E. VIEHWEGER AND A. WORCEL *Long-term radiologic evolution of coral implanted in cancellous bone of the lower limb. Madreporic coral versus coral hydroxyapatite*. Rev Chir Orthop Reparatrice Appar Mot, Oct 1998, 84(6), 501-507.
31. DIAB, T., PRITCHARD, E.M., UHRIG, B.A., BOERCKEL, J.D., *et al*. *A silk hydrogel-based delivery system of bone morphogenetic protein for the treatment of large bone defects.* Journal of the mechanical behavior of biomedical materials. 2012(11):123-31.
32. DIMITRIOU, R., E. JONES, D. MCGONAGLE AND P. V. GIANNOUDIS *Bone regeneration: current concepts and future directions*. BMC Med, 2011, 9, 66.
33. DOHAN EHRENFEST, D. M., RASMUSSON, L., ALBREKTSSON, T. *Classification of platelet concentrates: from pure platelet-rich plasma (P-PRP) to leucocyte- and platelet-rich fibrin (L-PRF)*. Trends Biotechnol, Mar 2009, 27(3), 158-167.

34. DUCHEYNE, P., J. BEIGHT, J. CUCKLER, B. EVANS, *et al. Effect of calcium phosphate coating characteristics on early post-operative bone tissue ingrowth*. Biomaterials, Oct 1990, 11(8), 531-540.
35. EVERTS, P. A., C. BROWN MAHONEY, J. J. HOFFMANN, J. P. SCHONBERGER, *et al. Platelet-rich plasma preparation using three devices: implications for platelet activation and platelet growth factor release*. Growth Factors, Sep 2006, 24(3), 165-171.
36. FERREIRA, A. M., GENTILE, P., CHIONO, V., CIARDELLI, G. *Collagen for bone tissue regeneration*. Acta Biomater, Sep 2012, 8(9), 3191-3200.
37. FILOVA, E., RAMPICHOVA, M., LITVINEC, A., DRZIK, M., *et al. A cell-free nanofiber composite scaffold regenerated osteochondral defects in miniature pigs*. Int J Pharm, Apr 15 2013, 447(1-2), 139-149.
38. FREED, L. E., A. P. HOLLANDER, I. MARTIN, J. R. BARRY, *et al. Chondrogenesis in a cell-polymer-bioreactor system*. Exp Cell Res, Apr 10 1998, 240(1), 58-65.
39. FROHBERGH, M. E., A. KATSMAN, G. P. BOTTA, P. LAZAROVICI, *et al. Electrospun hydroxyapatite-containing chitosan nanofibers crosslinked with genipin for bone tissue engineering*. Biomaterials, Dec 2012, 33(36), 9167-9178.
40. GONCALVES FDA, C., A. H. PAZ, P. S. LORA, E. P. PASSOS, *et al. Dynamic culture improves MSC adhesion on freeze-dried bone as a scaffold for bone engineering*. World J Stem Cells, Feb 26 2012, 4(2), 9-16.
41. GOTZ, H. E., M. MULLER, A. EMMEL, U. HOLZWARTH, *et al. Effect of surface finish on the osseointegration of laser-treated titanium alloy implants*. Biomaterials, Aug 2004, 25(18), 4057-4064.
42. GRONTHOS, S., J. BRAHIM, W. LI, L. W. FISHER, *et al. Stem cell properties of human dental pulp stem cells*. J Dent Res, Aug 2002, 81(8), 531-535.
43. GUNDERSEN, H. J. AND E. B. JENSEN *The efficiency of systematic sampling in stereology and its prediction*. J Microsc, Sep 1987, 147(3), 229-263.
44. HEINO, T. J., HENTUNEN, T. A., VAANANEN, H. K. *Conditioned medium from osteocytes stimulates the proliferation of bone marrow MSCs and their differentiation into osteoblasts*. Exp Cell Res, Apr 1 2004, 294(2), 458-468.
45. HÖHLING, H. J., R. H. BARCKHAUS AND E. R. KREFTING *Hard tissue formation in collagen-rich systems: calcium phosphate nucleation and organic matrix*. Trends in Biochemical Sciences, 1978, DOI 10.1016/j.cej.2012.10.046.
46. HOLLISTER, S. J., C. Y. LIN, E. SAITO, C. Y. LIN, *et al. Engineering craniofacial scaffolds*. Orthod Craniofac Res, Aug 2005, 8(3), 162-173.
47. HOU, Q., D. W. GRIJPMA AND J. FEIJEN *Porous polymeric structures for tissue engineering prepared by a coagulation, compression moulding and salt leaching technique*. Biomaterials, May 2003, 24(11), 1937-1947.
48. HU Y, G. D., WINN SR, HOLLINGER JO. *Fabrication of poly(alpha-hydroxy acid) foam scaffolds using multiple solvent systems*. J BiomedMater Res, 2002, 59(3), 563–572.
49. HULBERT, S. F., YOUNG, F. A., MATHEWS, R. S., KLAWITTER, J. J., *et al. Potential of ceramic materials as permanently implantable skeletal prostheses*. J Biomed Mater Res, Sep 1970, 4(3), 433-456.

50. HURI, P.Y., HURI, G., YASAR, U., UCAR, Y., *et al*. *A biomimetic growth factor delivery strategy for enhanced regeneration of iliac crest defects.* Biomed Mater. 2013(8):45-9.
51. HUTMACHER, D. W. *Scaffolds in tissue engineering bone and cartilage*. Biomaterials, Dec 2000, 21(24), 2529-2543.
52. HUTMACHER, D. W., SCHANTZ, J. T., LAM, C. X., TAN, K. C., *et al. State of the art and future directions of scaffold-based bone engineering from a biomaterials perspective*. J Tissue Eng Regen Med, Jul-Aug 2007, 1(4), 245-260.
53. CHEN, J. C., KO, C. L., SHIH, C. J., TIEN, Y. C., CHEN, W. C. *Calcium phosphate bone cement with 10 wt% platelet-rich plasma in vitro and in vivo*. J Dent, Feb 2012, 40(2), 114-122.
54. CHEN, X., X. FU, J. G. SHI AND H. WANG *Regulation of the osteogenesis of pre-osteoblasts by spatial arrangement of electrospun nanofibers in two- and three-dimensional environments*. Nanomedicine, Nov 2013, 9(8), 1283-1292.
55. CHOI, J. M., H. E. KIM AND I. S. LEE *Ion-beam-assisted deposition (IBAD) of hydroxyapatite coating layer on Ti-based metal substrate*. Biomaterials, Mar 2000, 21(5), 469-473.
56. CHOI, J. M., KIM, H. E., LEE, I. S. *Ion-beam-assisted deposition (IBAD) of hydroxyapatite coating layer on Ti-based metal substrate*. Biomaterials, Mar 2000, 21(5), 469-473.
57. JAKUBOVA, R., MICKOVA, A., BUZGO, M., RAMPICHOVA, M., *et al. Immobilization of thrombocytes on PCL nanofibres enhances chondrocyte proliferation in vitro*. Cell Prolif, Apr 2011, 44(2), 183-191.
58. JIANG, H., Y. HU, P. ZHAO, Y. LI, *et al. Modulation of protein release from biodegradable core-shell structured fibers prepared by coaxial electrospinning*. J Biomed Mater Res B Appl Biomater, Oct 2006, 79(1), 50-57.
59. KANCZLER, J.M., GINTY, P.J., WHITE, L., CLARKE, N.M.P., *et al. The effect of the delivery of vascular endothelial growth factor and bone morphogenic protein-2 to osteoprogenitor cell populations on bone formation.* Biomaterials. 2010(31):1242-50.
60. KARAGEORGIOU, V. AND D. KAPLAN *Porosity of 3D biomaterial scaffolds and osteogenesis*. Biomaterials, Sep 2005, 26(27), 5474-5491.
61. KARSHOVSKA, E., C. WEBER AND P. VON HUNDELSHAUSEN *Platelet chemokines in health and disease*. Thromb Haemost, Nov 2013, 110(5), 894-902.
62. KASPER, G., N. DANKERT, J. TUISCHER, M. HOEFT, *et al. MSCs regulate angiogenesis according to their mechanical environment*. Stem Cells, Apr 2007, 25(4), 903-910.
63. KASTEN, P., J. VOGEL, I. BEYEN, S. WEISS, *et al. Effect of platelet-rich plasma on the in vitro proliferation and osteogenic differentiation of human MSCs on distinct calcium phosphate scaffolds: the specific surface area makes a difference*. J Biomater Appl, Sep 2008, 23(2), 169-188.
64. KATTHAGEN, B. D. *Bone Regeneration with Bone Substitutes. An Animal Study,*. Springer-Verlag, New York, USA, 1986.
65. KEMPEN, D. H., L. LU, T. E. HEFFERAN, L. B. CREEMERS, *et al. Retention of in vitro and in vivo BMP-2 bioactivities in sustained delivery vehicles for bone tissue engineering*. Biomaterials, Aug 2008, 29(22), 3245-3252.

66. KIM, H. W., J. C. KNOWLES AND H. E. KIM *Hydroxyapatite/poly(epsilon-caprolactone) composite coatings on hydroxyapatite porous bone scaffold for drug delivery*. Biomaterials, Mar-Apr 2004, 25(7-8), 1279-1287.
67. KITOH, H., KITAKOJI, T., TSUCHIYA, H., MITSUYAMA, H., NAKAMURA, H., KATOH, M., ISHIGURO, N. *Transplantation of marrow-derived MSCs and platelet-rich plasma during distraction osteogenesis--a preliminary result of three cases*. Bone, Oct 2004, 35(4), 892-898.
68. KLEIN, C. P., P. PATKA, H. B. VAN DER LUBBE, J. G. WOLKE, *et al. Plasma-sprayed coatings of tetracalciumphosphate, hydroxyl-apatite, and alpha-TCP on titanium alloy: an interface study*. J Biomed Mater Res, Jan 1991, 25(1), 53-65.
69. KNOTEK, P., M. POUZAR, M. BUZGO, B. KRIZKOVA, *et al. Cryogenic grinding of electrospun poly-epsilon-caprolactone mesh submerged in liquid media*. Mater Sci Eng C Mater Biol Appl, Aug 1 2012, 32(6), 1366-1374.
70. KOCOVA, J. *Overall staining of connective tissue and the muscular layer of vessels*. Folia Morphol (Praha), 1970, 18(3), 293-295.
71. KOCH, S., YAO, C., GRIEB, G., PRÉVEL, P., *et al. Enhancing angiogenesis in collagen matrices by covalent incorporation of VEGF.* J Mater Sci: Mater Med. 2006(17):735-41.
72. KOLAR, P., K. SCHMIDT-BLEEK, H. SCHELL, T. GABER, *et al. The early fracture hematoma and its potential role in fracture healing*. Tissue Eng Part B Rev, Aug 2010, 16(4), 427-434.
73. KOUHI, M., M. MORSHED, J. VARSHOSAZ AND M. H. FATHI *Poly (epsilon-caprolactone) incorporated bioactive glass nanoparticles and simvastatin nanocomposite nanofibers: Preparation, characterization and in vitro drug release for bone regeneration applications*. Chemical Engineering Journal, Jul 2013, 228, 1057-1065.
74. KRAUS, K. H. AND C. KIRKER-HEAD *MSCs and bone regeneration*. Vet Surg, Apr 2006, 35(3), 232-242.
75. KUBOKI, Y., Q. JIN AND H. TAKITA *Geometry of carriers controlling phenotypic expression in BMP-induced osteogenesis and chondrogenesis*. J Bone Joint Surg Am, 2001, 83-A Suppl 1(Pt 2), S105-115.
76. KUBOKI, Y., TAKITA, H., KOBAYASHI, D., TSURUGA, E., *et al. BMP-induced osteogenesis on the surface of hydroxyapatite with geometrically feasible and nonfeasible structures: topology of osteogenesis*. J Biomed Mater Res, Feb 1998, 39(2), 190-199.
77. LEE, J.Y., NAM, S.H., IM, S.Y., PARK, Y.J., *et al. Enhanced bone formation by controlled growth factor delivery from chitosan-based biomaterials.* Journal of Controlled Release. 2002(78):187-97.
78. LEON, C. *New perspectives in mercury porosimetry*. Advances in Colloid and Interface Science, Jul 1998, (76):341-372.
79. LI, M., M. J. MONDRINOS, M. R. GANDHI, F. K. KO, *et al. Electrospun protein fibers as matrices for tissue engineering*. Biomaterials. 2005,26(30): 5999-6008.
80. LI, C., VEPARI, C., JIN, H.-J., KIM, H.J., KAPLAN, D.L. *Electrospun silk-BMP-2 scaffolds for bone tissue engineering.* Biomaterials. 2006(27):3115-24.
81. LI, X., ZHANG, H., LI, H., TANG, G., ZHAO, Y., YUAN, X. *Self-accelerated biodegradation of electrospun poly(ethylene glycol)–poly(l-lactide) membranes by loading proteinase K.* Polymer Degradation and Stability. 2008;93:618-26.

82. LIANG, D., HSIAO, B. S., CHU, B. *Functional electrospun nanofibrous scaffolds for biomedical applications*. Adv Drug Deliv Rev, Dec 10 2007, 59(14), 1392-1412.
83. LIAO, S., LI, B., MA, Z., WEI, H., CHAN, C., RAMAKRISHNA, S. *Biomimetic electrospun nanofibers for tissue regeneration*. Biomed Mater, Sep 2006, 1(3), 45-53.
84. LICKORISH, D., J. A. RAMSHAW, J. A. WERKMEISTER, V. GLATTAUER, *et al. Collagen-hydroxyapatite composite prepared by biomimetic process*. J Biomed Mater Res A, Jan 1 2004, 68(1), 19-27.
85. LIU, C., XIA, Z., CZERNUSZKA, J.T. *Design and development of threedimensional scaffolds for tissue engineering*. Chem Eng Res Des, 2007(85), 1051–1064.
86. LUKAS, D., SARKAR, A., MARTINOVA, L., VODSEDALKOVA, K., *et al. Physical principles of electrospinning (electrospinning as a nano-scale technology of the twenty-first century)*. Textile Progress, 2009(41), 59–140.
87. MACKIE, E. J. *Osteoblasts: novel roles in orchestration of skeletal architecture*. Int J Biochem Cell Biol, Sep 2003, 35(9), 1301-1305.
88. MALDA, J., T. J. KLEIN AND Z. UPTON *The roles of hypoxia in the in vitro engineering of tissues*. Tissue Eng, Sep 2007, 13(9), 2153-2162.
89. MALDA, J., J. ROUWKEMA, D. E. MARTENS, E. P. LE COMTE, *et al. Oxygen gradients in tissue-engineered PEGT/PBT cartilaginous constructs: measurement and modeling*. Biotechnol Bioeng, Apr 5 2004, 86(1), 9-18.
90. MALIK, C. L., S. M. STOVER, R. B. MARTIN AND J. C. GIBELING *Equine cortical bone exhibits rising R-curve fracture mechanics*. J Biomech, Feb 2003, 36(2), 191-198.
91. MALLADI, P., Y. XU, M. CHIOU, A. J. GIACCIA, *et al. Effect of reduced oxygen tension on chondrogenesis and osteogenesis in adipose-derived mesenchymal cells*. Am J Physiol Cell Physiol, Apr 2006, 290(4), C1139-1146.
92. MAO, X., CHU, C. L., MAO, Z., WANG, J. J. *The development and identification of constructing tissue engineered bone by seeding osteoblasts from differentiated rat marrow stromal stem cells onto three-dimensional porous nano-hydroxylapatite bone matrix in vitro*. Tissue Cell, Oct 2005, 37(5), 349-357.
93. MARKS, S. C., ODGREN, P.R. *Chapter 1: Structure and Development of the Skeleton, Principles of Bone Biology, 2nd ed.* New York: Academic Press, 2002, 3-15.
94. MARTIN, Y. AND P. VERMETTE *Bioreactors for tissue mass culture: design, characterization, and recent advances*. Biomaterials, Dec 2005, 26(35), 7481-7503.
95. MARTINS, A., DUARTE, A. R., FARIA, S., MARQUES, A. P., REIS, R. L., NEVES, N. M. *Osteogenic induction of hBMSCs by electrospun scaffolds with dexamethasone release functionality*. Biomaterials, Aug 2010, 31(22), 5875-5885.
96. MAY, A. E., P. SEIZER AND M. GAWAZ *Platelets: inflammatory firebugs of vascular walls*. Arterioscler Thromb Vasc Biol, Mar 2008, 28(3), s5-10.
97. MAYHEW, T. M., LUCOCQ, J. M., GRIFFITHS, G. *Relative labelling index: a novel stereological approach to test for non-random immunogold labelling of organelles and membranes on transmission electron microscopy thin sections*. J Microsc, Feb 2002, 205(Pt 2), 153-164.

98. MAYHEW, T. M., MUHLFELD, C., VANHECKE, D., OCHS, M. *A review of recent methods for efficiently quantifying immunogold and other nanoparticles using TEM sections through cells, tissues and organs*. Ann Anat, Apr 2009, 191(2), 153-170.
99. MAZOR, Z., M. PELEG, A. K. GARG AND J. LUBOSHITZ *Platelet-rich plasma for bone graft enhancement in sinus floor augmentation with simultaneous implant placement: patient series study*. Implant Dent, Mar 2004, 13(1), 65-72.
100. MCCLELLAND, R. E. AND R. N. COGER *Use of micropathways to improve oxygen transport in a hepatic system*. J Biomech Eng, Jun 2000, 122(3), 268-273.
101. MEHTA, M., K. SCHMIDT-BLEEK, G. N. DUDA AND D. J. MOONEY *Biomaterial delivery of morphogens to mimic the natural healing cascade in bone*. Adv Drug Deliv Rev, Sep 2012, 64(12), 1257-1276.
102. MEINEL, L., ZOIDIS, E., ZAPF, J., HASSA, P., *et al. Localized insulin-like growth factor I delivery to enhance new bone formation.* Bone. 2003(33):660-72.
103. MELVILLE, A. J., J. HARRISON, K. A. GROSS, J. S. FORSYTHE, *et al. Mouse embryonic stem cell colonisation of carbonated apatite surfaces*. Biomaterials, Feb 2006, 27(4), 615-622.
104. MENDES, S. C., J. M. TIBBE, M. VEENHOF, K. BAKKER, *et al. Bone tissue-engineered implants using human bone marrow stromal cells: effect of culture conditions and donor age*. Tissue Eng, Dec 2002, 8(6), 911-920.
105. MICKOVA, A., M. BUZGO, O. BENADA, M. RAMPICHOVA, *et al. Core/shell nanofibers with embedded liposomes as a drug delivery system*. Biomacromolecules, Apr 9 2012, 13(4), 952-962.
106. MOUTON, P. R. *Principles and Practices of Unbiased Stereology. An Introduction for Bioscientists*. Johns Hopkins University Press, Baltimore, MD, USA, 2002.
107. MUSCHLER, G. F., C. NAKAMOTO AND L. G. GRIFFITH *Engineering principles of clinical cell-based tissue engineering*. J Bone Joint Surg Am, Jul 2004, 86-a(7), 1541-1558.
108. NARBAT, M. K., ORANG, F., HASHTJIN, M.S., GOUDARZI, A. *Fabrication of porous hydroxyapatite-gelatin composite scaffolds for bone tissue engineering*. Iran Biomed, 2006, 10, 215-223.
109. NIE, H., SOH, B.W., FU, Y.C., WANG, CH. *Three-dimensional fibrous PLGA/HAp composite scaffold for BMP-2 delivery.* Biotechnol Bioeng. 2008(99):223-34.
110. O'BRIEN, F. J., B. A. HARLEY, I. V. YANNAS AND L. GIBSON *Influence of freezing rate on pore structure in freeze-dried collagen-GAG scaffolds*. Biomaterials, Mar 2004, 25(6), 1077-1086.
111. OLAH, L., FILIPCZAK, K., JAEGERMANN, Z., CZIGANY, *et al*. *Synthesis, structural and mechanical properties of porous polymeric scaffolds for bone tissue regeneration based on neat poly(e-caprolactone) and its composites with calcium carbonate*. Polym Adv Technol, 2006, 17, 889-897.
112. OLIVER, W. C. AND G. M. PHARR *An improved technique for determining hardness and elastic-modulus using load and displacement sensing inentation experiments*. Journal of Materials Research, Jun 1992, 7(6), 1564-1583.
113. OLIVER, W. C. AND G. M. PHARR *Measurement of hardness and elastic modulus by instrumented indentation: Advances in understanding and*

refinements to methodology. Journal of Materials Research, Jan 2004, 19(1), 3-20.
114. PATEL, Z.S., YOUNG, S., TABATA, Y., JANSEN, J.A., *et al. Dual delivery of an angiogenic and an osteogenic growth factor for bone regeneration in a critical size defect model.* Bone. 2008(43):931-40.
115. PEARCE, A. I., RICHARDS, R. G., MILZ, S., SCHNEIDER, E.,PEARCE, S. G. *Animal models for implant biomaterial research in bone: A review*. European Cells & Materials, Jan-Jun 2007, 13, 1-10.
116. PERRY, C. R. *Bone repair techniques, bone graft, and bone graft substitutes*. Clin Orthop Relat Res, Mar 1999, (360), 71-86.
117. PHAM, Q. P., U. SHARMA AND A. G. MIKOS *Electrospinning of polymeric nanofibers for tissue engineering applications: a review*. Tissue Eng, May 2006, 12(5), 1197-1211.
118. PIETRZAK, W. S., D. R. SARVER, S. D. BIANCHINI AND K. D'ALESSIO. *Effect of simulated intraoperative heating and shaping on mechanical properties of a bioabsorbable fracture plate material*. J Biomed Mater Res, Spring 1997, 38(1), 17-24.
119. PIVONKA, P., J. ZIMAK, D. W. SMITH, B. S. GARDINER, *et al. Model structure and control of bone remodeling: a theoretical study*. Bone, Aug 2008, 43(2), 249-263.
120. PLUNKETT, N. AND F. J. O'BRIEN *Bioreactors in tissue engineering*. Technol Health Care, 2011, 19(1), 55-69.
121. PROSECKA, E., BUZGO, M., RAMPICHOVA, M., KOCOUREK, T., *et al. Thin-layer hydroxyapatite deposition on a nanofiber surface stimulates mesenchymal stem cell proliferation and their differentiation into osteoblasts*. J Biomed Biotechnol, 2012, 2012, 428503.
122. PROSECKA, E., RAMPICHOVA, M., LITVINEC, A., TONAR, Z., *et al. Collagen/hydroxyapatite scaffold enriched with polycaprolactone nanofibers, thrombocyte-rich solution and MSCs promotes regeneration in large bone defect in vivo*. J Biomed Mater Res A, May 16 2014, 10.1002/jbm.a.35216.
123. PROSECKA, E., RAMPICHOVA, M., VOJTOVA, L., TVRDIK, D., *et al. Optimized conditions for MSCs to differentiate into osteoblasts on a collagen/hydroxyapatite matrix*. J Biomed Mater Res A, Nov 2011, 99(2), 307-315.
124. PUPPI, D., ZHANG, X., YANG, L., CHIELLINI, F., SUN, X., CHIELLINI, E. *Nano/microfibrous polymeric constructs loaded with bioactive agents and designed for tissue engineering applications: A review*. J Biomed Mater Res B Appl Biomater, Oct 2014, 102(7), 1562-1579.
125. RAMPICHOVA, M., CHVOJKA, J., BUZGO, M., PROSECKA, *et al.* E., *Elastic three-dimensional poly (epsilon-caprolactone) nanofibre scaffold enhances migration, proliferation and osteogenic differentiation of MSCs*. Cell Prolif, Feb 2013, 46(1), 23-37.
126. REILLY, G. C. AND A. J. ENGLER *Intrinsic extracellular matrix properties regulate stem cell differentiation*. J Biomech, Jan 5 2010, 43(1), 55-62.
127. REZWAN, K., Q. Z. CHEN, J. J. BLAKER AND A. R. BOCCACCINI *Biodegradable and bioactive porous polymer/inorganic composite scaffolds for bone tissue engineering*. Biomaterials, Jun 2006, 27(18), 3413-3431.
128. ROCHET, N., A. LOUBAT, J. P. LAUGIER, P. HOFMAN, *et al. Modification of gene expression induced in human osteogenic and osteosarcoma cells by*

culture on a biphasic calcium phosphate bone substitute. Bone, Jun 2003, 32(6), 602-610.
129. ROCHET, N. M., N. TIEULIE, L. OLLIER, A. LOUBAT, *et al. Influence of human osteoblasts on hematopoietic stem cells: Analysis in coculture on a synthetic biphasic calcium phosphate ceramic*. Journal of Bone and Mineral Research, Sep 2002, 17, S434-S435.
130. ROVERI, N., G. FALINI, M. C. SIDOTI, A. TAMPIERI, *et al. Biologically inspired growth of hydroxyapatite nanocrystals inside self-assembled collagen fibers*. Materials Science & Engineering C-Biomimetic and Supramolecular Systems, Mar 2003, 23(3), 441-446.
131. SAHOO, S., L. T. ANG, J. C. GOH AND S. L. TOH *Growth factor delivery through electrospun nanofibers in scaffolds for tissue engineering applications*. J Biomed Mater Res A, Jun 15 2010, 93(4), 1539-1550.
132. SACHLOS, E., D. GOTORA AND J. T. CZERNUSZKA *Collagen scaffolds reinforced with biomimetic composite nano-sized carbonate-substituted hydroxyapatite crystals and shaped by rapid prototyping to contain internal microchannels*. Tissue Eng, Sep 2006, 12(9), 2479-2487.
133. SALUJA, H., DEHANE, V. AND MAHINDRA, U. *Platelet-Rich fibrin: A second generation platelet concentrate and a new friend of oral and maxillofacial surgeons*. Ann Maxillofac Surg, Jan 2011, 1(1), 53-57.
134. SEO, B. M., M. MIURA, S. GRONTHOS, P. M. BARTOLD, *et al. Investigation of multipotent postnatal stem cells from human periodontal ligament*. Lancet, Jul 10-16 2004, 364(9429), 149-155.
135. SERRE, C. M., M. PAPILLARD, P. CHAVASSIEUX AND G. BOIVIN *In vitro induction of a calcifying matrix by biomaterials constituted of collagen and/or hydroxyapatite: an ultrastructural comparison of three types of biomaterials*. Biomaterials, 1993, 14(2), 97-106.
136. SCHLICKEWEI, W. AND C. SCHLICKEWEI *The use of bone substitutes in the treatment of bone defects - the clinical view and history*. Macromolecular Symposia, 2007, 253, 10-23.
137. SCHMITZ, J. P. AND J. O. HOLLINGER *The critical size defect as an experimental model for craniomandibulofacial nonunions*. Clin Orthop Relat Res, Apr 1986, (205), 299-308.
138. SCHOFER, M. D., S. FUCHS-WINKELMANN, C. GRABEDUNKEL, C. WACK, *et al. Influence of poly(L-lactic acid) nanofibers and BMP-2-containing poly(L-lactic acid) nanofibers on growth and osteogenic differentiation of human MSCs*. ScientificWorldJournal, 2008, 8, 1269-1279.
139. SCHUGAR, R. C., S. M. CHIRIELEISON, K. E. WESCOE, B. T. SCHMIDT, *et al. High harvest yield, high expansion, and phenotype stability of CD146 mesenchymal stromal cells from whole primitive human umbilical cord tissue*. J Biomed Biotechnol, 2009, 2009, 11 pages.
140. SCHUMACHER, M., UHL, F., DETSCH, R., DEISINGER, U., ZIEGLER, G. *Static and dynamic cultivation of bone marrow stromal cells on biphasic calcium phosphate scaffolds derived from an indirect rapid prototyping technique*. J Mater Sci Mater Med, Nov 2010, 21(11), 3039-3048.
141. SILL, T. J. AND H. A. VON RECUM *Electrospinning: applications in drug delivery and tissue engineering*. Biomaterials, May 2008, 29(13), 1989-2006.
142. SIMMAN, R., HOFFMANN, A., BOHINC, R. J., PETERSON, W. C., RUSS, A. J. *Role of platelet-rich plasma in acceleration of bone fracture healing*. Ann Plast Surg, Sep 2008, 61(3), 337-344.

143. SIMPSON, A. H., L. MILLS AND B. NOBLE *The role of growth factors and related agents in accelerating fracture healing*. J Bone Joint Surg Br, Jun 2006, 88(6), 701-705.
144. STEVENS, B., YANG, Y., MOHANDAS, A., STUCKER, B., NGUYEN, K. T. *A review of materials, fabrication methods, and strategies used to enhance bone regeneration in engineered bone tissues*. J Biomed Mater Res B Appl Biomater, May 2008, 85(2), 573-582.
145. SU, Y., Q. SU, W. LIU, M. LIM, *et al. Controlled release of bone morphogenetic protein 2 and dexamethasone loaded in core-shell PLLACL-collagen fibers for use in bone tissue engineering*. Acta Biomater, Feb 2012, 8(2), 763-771.
146. SUKHODUB, L. F., C. MOSEKE, L. B. SUKHODUB, B. SULKIO-CLEFF, *et al. Collagen-hydroxyapatite-water interactions investigated by XRD, piezogravimetry, infrared and Raman spectroscopy*. Journal of Molecular Structure, Oct 2004, 704(1-3), 53-58.
147. SWIONTKOWSKI, M. F., H. T. ARO, S. DONELL, J. L. ESTERHAI, *et al. Recombinant human bone morphogenetic protein-2 in open tibial fractures. A subgroup analysis of data combined from two prospective randomized studies*. J Bone Joint Surg Am, Jun 2006, 88(6), 1258-1265.
148. TABATA, I. I. *The importance of drug delivery systems in tissue engineering*. Pharm Sci Technolo Today, Mar 2000, 3(3), 80-89.
149. TISDEL, C. L., V. M. GOLDBERG, J. A. PARR, J. S. BENSUSAN, *et al. The influence of a hydroxyapatite and tricalcium-phosphate coating on bone growth into titanium fiber-metal implants*. J Bone Joint Surg Am, Feb 1994, 76(2), 159-171.
150. TSURUGA, E., H. TAKITA, H. ITOH, Y. WAKISAKA, *et al. Pore size of porous hydroxyapatite as the cell-substratum controls BMP-induced osteogenesis*. J Biochem, Feb 1997, 121(2), 317-324.
151. TU, J., H. WANG, H. LI, K. DAI, *et al. The in vivo bone formation by MSCs in zein scaffolds*. Biomaterials, Sep 2009, 30(26), 4369-4376.
152. TVRDIK, D., POVYSIL, C., SVATOSOVA, J., DUNDR, P. *Molecular diagnosis of synovial sarcoma: RT-PCR detection of SYT-SSX1/2 fusion transcripts in paraffin-embedded tissue*. Med Sci Monit, Mar 2005, 11(3), Mt1-7.
153. VACANTI, J. *Tissue engineering and regenerative medicine: from first principles to state of the art*. J Pediatr Surg, Feb 2010, 45(2), 291-294.
154. VACANTI, J. P. AND R. LANGER *Tissue engineering: the design and fabrication of living replacement devices for surgical reconstruction and transplantation*. Lancet, Jul 1999, 354 Suppl 1, Si32-34.
155. VARKEY, M., GITTENS, S. A., ULUDAG, H. *Growth factor delivery for bone tissue repair: an update*. Expert Opin Drug Deliv, Nov 2004, 1(1), 19-36.
156. VASITA, R. A. K., D. S. *Growth factor-delivery systems for tissue engineering: a materials perspective*. Expert Rev Med Devices, Jan 2006, 3(1), 29-47.
157. VEILLETTE, C. J. AND M. D. MCKEE *Growth factors--BMPs, DBMs, and buffy coat products: are there any proven differences amongst them?* Injury, Mar 2007, 38 Suppl 1, S38-48.
158. VENUGOPAL, J., M. P. PRABHAKARAN, S. LOW, A. T. CHOON, *et al. Nanotechnology for nanomedicine and delivery of drugs*. Curr Pharm Des, 2008, 14(22), 2184-2200.
159. VERNON, L., KAPLAN, L., HUANG CHUN-YUH, CH. *Bone Regeneration, Stem cell based bone tissue engineering*. InTechOpen, New York, 2012.

160. WAHL, D. A. AND J. T. CZERNUSZKA *Collagen-hydroxyapatite composites for hard tissue repair*. Eur Cell Mater, 2006, 11, 43-56.
161. WANG, Y., WAN, C., DENG, L., LIU, X., *et al. The hypoxia-inducible factor alpha pathway couples angiogenesis to osteogenesis during skeletal development*. J Clin Invest, Jun 2007, 117(6), 1616-1626.
162. WASTERLAIN, A. S., BRAUN, H.J., DRAGOO, J.L. *Contents and formulations of platelet-rich plasma* Oper Tech Orthop, 2012, 22, 33-34.
163. WATANABE, S., S. INAGAKI, I. KINOUCHI, H. TAKAI, *et al. Hydrostatic pressure/perfusion culture system designed and validated for engineering tissue*. J Biosci Bioeng, Jul 2005, 100(1), 105-111.
164. WENK, E., A. J. MEINEL, S. WILDY, H. P. MERKLE, *et al. Microporous silk fibroin scaffolds embedding PLGA microparticles for controlled growth factor delivery in tissue engineering*. Biomaterials, May 2009, 30(13), 2571-2581.
165. WROTNIAK, M., T. BIELECKI AND T. S. GAZDZIK *Current opinion about using the platelet-rich gel in orthopaedics and trauma surgery*. Ortop Traumatol Rehabil, May-Jun 2007, 9(3), 227-238.
166. XIONG, Z., Y. N. YAN, S. G. WANG, R. J. ZHANG, *et al. Fabrication of porous scaffolds for bone tissue engineering via low-temperature deposition*. Scripta Materialia, Jun 2002, 46(11), 771-776.
167. YANG, Y. C., CHANG, E. *Influence of residual stress on bonding strength and fracture of plasma-sprayed hydroxyapatite coatings on Ti-6Al-4V substrate*. Biomaterials, Jul 2001, 22(13), 1827-1836.
168. YOSHINARI, M., OHTSUKA, Y., DERAND, T. *Thin hydroxyapatite coating produced by the ion beam dynamic mixing method*. Biomaterials, Jun 1994, 15(7), 529-535.
169. YOUNG, B., WOODFORD, PHILLIP, O'DOWD, GERALDINE *Wheater's functional histology: a text and colour atlas*. Edtion ed., 2013. ISBN 978-0443068508
170. ZASLANSKY, P., A. A. FRIESEM AND S. WEINER *Structure and mechanical properties of the soft zone separating bulk dentin and enamel in crowns of human teeth: insight into tooth function*. J Struct Biol, Feb 2006, 153(2), 188-199.
171. ZHANG, Z., HU, J., MA, P. X. *Nanofiber-based delivery of bioactive agents and stem cells to bone sites*. Adv Drug Deliv Rev, Sep 2012, 64(12), 1129-1141.
172. ZHAO, F., Y. YIN, W. W. LU, J. C. LEONG, *et al. Preparation and histological evaluation of biomimetic three-dimensional hydroxyapatite/chitosan-gelatin network composite scaffolds*. Biomaterials, Aug 2002, 23(15), 3227-3234.
173. ZHU, H., D. YU, Y. ZHOU, C. WANG, *et al. Biological activity of a nanofibrous barrier membrane containing bone morphogenetic protein formed by core-shell electrospinning as a sustained delivery vehicle*. J Biomed Mater Res B Appl Biomater, May 2013, 101(4), 541-552.
174. ZUK, P. A., M. ZHU, P. ASHJIAN, D. A. DE UGARTE, *et al. Human adipose tissue is a source of multipotent stem cells*. Mol Biol Cell, Dec 2002, 13(12), 4279-4295.
175. ZYMAN, Z., WENG, J., LIU, X., LI, X., ZHANG, X. *Phase and structural changes in hydroxyapatite coatings under heat treatment*. Biomaterials, Jan 1994, 15(2), 151-155.

Reprints of papers published by the author

1. *Prosecká E, Rampichová M, Vojtová L, Tvrdík D, Melčáková Š, Juhasová J, Plencner M, Jakubová R, Jančář J, Nečas A, Kochová P, Klepáčekek J, Tonar Z, Amler E.* Optimized conditions for MSCs to differentiate into osteoblasts on a collagen/hydroxyapatite matrix. *Journal of Biomedical Materials Research-Part A* 2011:99A:307–315. IF 2,88

2. *Prosecká E,* Buzgo M,* Rampichová M, Kocourek T, Kochová P, Vysloužilová L, Tvrdík D, Jelínek M, Lukáš D, Amler E.* Thin-layer hydroxyapatite deposition on a nanofiber surface stimulates mesenchymal stem cell proliferation and their differentiation into osteoblasts. *Journal of Biomedicine and Biotechnology*, Volume 2012 (2012), Article ID 428503, 10 pages. IF 2,84

3. *Prosecká E, Rampichová M, Litvinec A, Tonar Z, Králíčková M,Vojtová L, Kochová P, Plencner M, Buzgo M, Míčková A, Jančář J, Amler E.* Collagen/hydroxyapatite scaffold enriched with polycaprolactone nanofibres, thrombocyte-rich solution and MSCs accelerates regeneration in large bone defect *in vivo*. *Journal of Biomedical Materials Research- Part A*, 2014 May 16. doi: 10.1002/jbm.a.35216. IF 2,88

Articles not directly related to the topic of this thesis

1. *Jakubova R, Mickova A, Buzgo M, Rampichova M, Prosecka E, Tvrdik D, Amler E.* Immobilization of thrombocytes on PCL nanofibers enhances chondrocytes proliferation in vitro. *Cell proliferation*., 2011; 44: 183-191. IF 2.521
2. *Rampichová M, Košťáková E, Filová E, Prosecká E, Plencner M, Ocheretná L, Lytvynets A, Lukáš D, Amler E.* Non-woven PGA/PVA fibrous mesh as an appropriate scaffold for chondrocyte proliferation. *Physiological Research*. 2010;59(5):773-81. IF 1.646
3. *Rampichová M, Filová E, Varga F, Lytvynets A, Prosecká E., Koláčná L, Motlík J, Nečas A,Vajner L, Uhlík J, Amler E:* Fibrin/Hyaluronic Acid Composite Hydrogels as Appropriate Scaffolds for In Vivo Artificial Cartilage Implantation. *ASAIO J.,* 2010, November/December;56(6):563-568. IF 1,221
4. *Rampichová M, Chvojka J, Buzgo M, Prosecká E, Mikeš P, Vysloužilová L, Tvrdík D, Kochová P, Gregor T, Lukáš D, Amler E.* Elastic three-dimensional poly (ε-caprolactone) nanofibre scaffold enhances migration, proliferation and osteogenic differentiation of MSCs. *Cell Proliferation*, 2013 Feb;46(1):23-37.IF 2.521
5. *Buzgo M, Jakubova R, Mickova A, Rampichova M, Prosecka E, Kochova P, Lukas D, Amler E.* Time-regulated drug delivery system based on coaxially incorporated platelet α-granules for biomedical use. *Nanomedicine* (Lond), 2013 Jul;8(7):1137-54. IF 5.055
6. *Amler E, Buzgo M, Filová E, Jakubová R, Koláčná L, Kotyk A, Míčková A, Plencner M, Prosecká E, Rampichová M, Varga F, Zavřelová T.* Lékařské textilie – 1. díl.; Centrum pro podporu konkurenceschopnosti v

biomedicínských technologiích; Amler E (ed) Ústav experimentální medicíny AV ČR, v.v.i., Praha, 2008

7. *Gregor T, Kochová P, Eberlová L, Nedorost L, Prosecká E, Liška V, Mírka H, Kachlík D, Pirner I, Zimmermann P, Králíčková A, Králíčková M, Tonar Z.* Correlating Micro-CT Imaging with Quantitative Histology. – In: Goswami T. (Ed): Injury and Skeletal Biomechanics. (2012) *InTech*, Rijeka, pp. 173-196. ISBN 978-953-51-0690-6.
8. *Kochová P, Gregor T, Prosecká E, Eberlová L, Tonar Z.* Multiscale heterogeneity of bone microporosities and tissue scaffolds. *Key Engineering Materials*, 2014, 592-593:350-353. ISSN 1662-9795.
9. *Filová E, Rampichová M, Litvinec A, Držík M, Míčková A, Buzgo M, Košťáková E, Martinová L, Usvald D, Prosecká E, Uhlík J, Motlík J, Vajner L, Amler E.* A cell-free nanofiber composite scaffold regenerated osteochondral defects in miniature pigs. *International Journal of Pharmaceutics*, 2013 Apr 15;447(1-2):139-49. IF 2,44
10. *Rampichová M, Buzgo M, Chvojka J, Prosecká E, Kofroňová O, Amler E.* Cell penetration to nanofibrous scaffolds: Forcespinning®, an alternative approach for fabricating 3D nanofibers. *Cell adhesion and Migration,* 2013 Jan 1;8(1). IF 2,521
11. *Amler E, Filová E, Buzgo M, Prosecká E, Rampichová M, Nečas A, Nooeaid P, Boccaccini AR*. Functionalized nanofibers as drug delivery systems for osteochondral regeneration - a review. *Nanomedicine (Lond),*2014 May 9;(7):1083-94. IF 5,055

12. *Plencner M, East B, Tonar Z, M, Otáhal M, Prosecká E, Rampichová M, Krejčí T, Litvinec A, Buzgo M, Míčková A, Nečas A, Hoch J, Amler E.* Abdominal closure reinforcement by using polypropylene mesh functionalized with poly-ε-caprolactone nanofibers and growth factors for prevention of incisional hernia formation. *International Journal of Nanomedicine*, 2014:9 3263–3277. IF 4,2

Acknowledgements

This study has been supported by the Academy of Sciences of the Czech Republic (institutional research plans AV0Z50390703 and AV0Z50390512), the Grant Agency of the Czech Republic (grant P304/10/1307), the Grant Agency of Charles University (grant No. 119209, 330611, 384311, 648112, 626012), and the Grant Agency of the Czech Ministry of Health (project No. NT12156). It has also received support from the European Regional Development Fund (project No. ED2.1.00/03.0076, project No. CZ.1.05/1.1.00/02.0090 – “NTIS - New Technologies for Information Society”, European Centre of Excellence, project No. CZ.1.05/1.1.00/02.0068 - “CEITEC-Central European Institute of Technology”), the Charles University Research Fund (project No. P36), and the University Centre for Energy Efficient Buildings support (CZ.1.05/2.1.00/03.0091).